MECHANISTIC STUDIES TO DETERMINE THE CATALYTIC ROLES OF ACTIVE SITE RESIDUES IN PHOSPHITE DEHYDROGENASE

BY

JOHN EDMOND HUNG

DISSERTATION

Submitted in partial fulfillment of the requirements
for the degree of Doctor of Philosophy in Chemistry
in the Graduate College of the
University of Illinois at Urbana-Champaign, 2013

Urbana, Illinois

Doctoral Committee:

Professor Wilfred A. van der Donk, Chair
Professor John A. Gerlt
Professor William W. Metcalf
Professor Satish K. Nair

ABSTRACT

Phosphite dehydrogenase (PTDH) catalyzes the oxidation of phosphite to phosphate with the concurrent reduction of NAD^+ to NADH. The mechanism of the reaction resembles a phosphoryl transfer reaction. A nucleophilic displacement reaction occurs on the phosphoryl group, with water or hydroxide attacking the phosphorus atom and hydride acting as the leaving group. Given the inherently poor nature of the hydride leaving group, PTDH presents a case of an enzyme catalyzing unusual chemistry.

Although PTDH activity was initially believed to be unique to the enzyme from *Pseudomonas stutzeri*, searches of the protein databases have uncovered genes with high sequence identity to the original PTDH. When diverse members of this family were expressed and the purified proteins characterized, it was revealed that several orthologs of PTDH were able to catalyze the PTDH reaction with similar catalytic parameters. Sequence alignments of the PTDH orthologs showed that numerous enzyme residues are conserved amongst the PTDH family. In conjunction with the recently solved X-ray crystal structure of PTDH, several conserved residues that are present in the active site were identified and studied by mutagenesis experiments.

Arg301 is conserved among known PTDHs and is in good position in the active site to act as the catalytic base in the reaction. Arg301 is important for efficient catalysis, as the Arg301Ala mutant displayed an approximately 100-fold decrease in k_{cat}, and an approximately 700-fold increase in $K_{m,phosphite}$. Chemical rescue and pH dependence experiments suggested that Arg301 acts as a positively charged residue in electrostatic activation of the reaction, rather than acting as the base. In addition, inhibition experiments indicated that binding of the sulfite competitive inhibitor in mutants of Arg301 was greatly decreased, suggesting that Arg301 plays an important

role in substrate binding. The crystal structures of the Arg301Ala and Arg301Lys mutants of PTDH have been solved, and they are consistent with these proposed roles.

In proteins, methionine residues are most commonly associated with hydrophobic interactions and steric effects. However, in the crystal structure of PTDH ternary complex, the sulfur of the conserved Met53 appears to interact with an oxygen atom on the sulfite competitive inhibitor. Mutagenesis experiments showed that Met53 is important for catalysis; mutations of this residue resulted in significantly decreased k_{cat}, without changing K_m for phosphite. A computational quantum mechanics/molecular mechanics (QM/MM) model was developed by the Mulholland Laboratory (University of Bristol, UK), which proposed that the side chain of Met53 stabilizes the transition state for hydride transfer during the PTDH reaction through an $n \rightarrow \pi^*$ interaction between the Met53 sulfur and the His292 imidazolium. This hypothesis was supported by the experimental data, which indicated that mutation of Met53 affects the rate-limiting hydride transfer step in the reaction.

In addition, a library of PTDH mutants was generated in an attempt to generate a PTDH capable of accepting thiophosphite as an alternative substrate through directed evolution. Several preliminary hits in this assay are currently being investigated. Successful mutation could allow for future analysis of the stereochemistry of the PTDH reaction. Attempts have also been made to determine if PTDH uses a covalent catalysis mechanism during phosphoryl transfer by detecting a phosphohistidine adduct using mass spectrometry.

ACKNOWLEDGEMENTS

There are a great number of people that I would like to thank for their contributions to both my work and my personal life during my graduate studies. It is difficult to convey how important their assistance and support has been to not only getting my work done, but also to retaining my sanity over these long years. It has been a quite a journey, but the perseverance and hard work of my family, friends, and colleagues has helped drag me to the end, through hurdles that I may not have otherwise overcome. I would just like to say that it has been greatly appreciated and I couldn't have done this without all of you.

I would first like to thank my advisor, Professor Wilfred van der Donk, for his guidance and support of my research. His advice over the years has provided not only insightful research direction, but has been essential towards my development as both a scientist and as a person. I could not have asked for a better mentor. I would also like to thank my committee members, Professor John Gerlt, Professor William Metcalf, and Professor Satish Nair. My discussions with them over the years have consistently challenged me to become a better scientist, and have led to new insights in my research.

I would like to thank the members of the van der Donk laboratory, past and present, for making the lab an enjoyable place to work. First and foremost, thanks are due to Xiao Yang. She has put up with me beyond what is reasonable to ask of anyone, and has been a great friend and scientific resource as well. I appreciate it more than I can convey in words. Six other first-year students joined the van der Donk group along with me, and I have to say that it has been a pleasure growing with all of them. Thank you to Noah Bindman, Patrick Knerr, Neha Garg, Yanxiang Shi, Ayşe Ökesli, and Min Zeng for your friendship over the years. I would also like to thank many former lab members, including Drs. Trent Oman, Heather Cooke, Leigh Anne

Furgerson-Ihnken, Lisa Cooper, Nicholas Llewellyn, Juan Velasquez, John Whitteck, and Ian Gut, for being great resources and always helping me when I needed it. Thank you to all the current members of the lab, especially Dr. Gabrielle Thibodeaux, Dr. Huan Wang, Dr. Rebecca Splain, Xiao Yang, Spencer Peck, Manuel Ortega, Chantal Garcia de Gonzalo, Subha Mukherjee, Xi Ling Zhao, and Emily Ulrich. It has been enjoyable working with all of you, and I know that the lab is in good hands for the future. Thanks especially to the two undergraduate students I have had the pleasure of working with, Claire Creed and Katarzyna Dubiel. It has been a great experience teaching and mentoring you both, and thank you both for your help.

Thank you to many members of other labs, including Dr. Vinayak Agarwal, Kyle Dunbar, Tucker Maxson, Jonathan Chekan, Joel Cioni, Paul Gormisky, and Iulia Strambeanu, for your assistance and advice over the years. Thanks also to my undergraduate research advisor, Professor TJ Kappock, for his continued encouragement and advice starting from the very beginning of my scientific career. I also have to thank our collaborators at the University of Bristol, Professor Adrian Mulholland and Dr. Kara Ranaghan, who were able to develop a computational model for PTDH catalysis. Special thanks are due to Martha Freeland, Nan Holda, and the Organic-Chemical Biology office for their invaluable work keeping things running and taking care of the graduate students.

Finally, I would like to thank my family for their support throughout all of my time in school – it has helped to drive me through this process. My cats, Eppie and Millie, for always being there for me (sometimes with warm comfort, sometimes with a painfully sharp claw). And of course, I have to thank my friends, especially Paul Gormisky (thanks for all the nights at Crane Alley), Pat and Noah, Samantha Bindman, Jeremy and Deborah Kemmerer, Diana Haas, Callie

Kindt, Kasia and Adam Catherman, and Michael Evans and Jess Kline. I couldn't have done this without all of you.

CHAPTER 1: INTRODUCTION

1.1 The Reaction Catalyzed by Phosphite Dehydrogenase

Phosphite dehydrogenase (PTDH) endows microorganisms with the ability to grow using phosphite as the sole source of phosphorus (*1*). This enzyme was first discovered in *Pseudomonas stutzeri* WM88, an organism that was identified as an efficient oxidizer of reduced phosphorus compounds, with the ability to grow on both phosphite and hypophosphite (*2, 3*). PTDH catalyzes the oxidation of phosphite to phosphate with the concurrent reduction of NAD^+ to NADH (Scheme 1.1). The reaction resembles a phosphoryl transfer process in which water or hydroxide acts as the phosphoryl acceptor and hydride acts as the phosphoryl donor. Thus, this reaction presents an unusual example of an enzyme catalyzing a nucleophilic displacement reaction with a hydride leaving group. Indeed, deuterium-labeling studies have confirmed that the hydride group is transferred directly from phosphite to NADH (*4*). Although at first glance the reaction would appear to be an unfavorable process, analysis of the thermodynamics of the reaction indicates it is actually 15 kcal/mol exergonic (*4*).

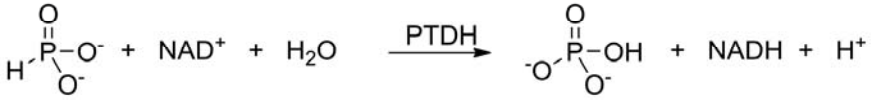

Scheme 1.1

Given the unusual nature of this reaction, significant experimental effort has been put into understanding how the enzyme catalyzes this chemistry (*4-8*). The enzyme follows an ordered kinetic mechanism with NAD^+ binding before phosphite (*1*). Kinetic isotope effect (KIE) studies with deuterium-labeled phosphite and pre-steady state kinetic studies have shown that hydride transfer is fully rate-limiting for the PTDH reaction (*6, 9*). PTDH shares ~25-40% sequence identity with the family of D-hydroxy acid dehydrogenases (DHDHs) (*10*), including several residues that have well defined roles in these enzymes. Site-directed mutagenesis studies on these amino acids have provided some insights into the mechanism of phosphite oxidation (*5, 6*), but many questions still remain. Recent reports have shown that a number of organisms encode enzymes with PTDH activity (*7, 11-13*). Analysis of their amino acid sequences suggests that PTDHs consist of their own branch of the DHDH family and has allowed the investigation of residues that are conserved among PTDHs but not the DHDHs (see Chapter 2).

1.2 Variants of PTDH as a Cofactor Regeneration System

PTDH has been adapted for use in cofactor regeneration strategies to recycle catalytic pools of NADH (*14*). NADH and its phosphorylated analog NADPH are commonly used as stoichiometric hydride donors in biotechnology (*15*), and although the enzymes that utilize these cofactors are highly efficient and selective, the cofactors are quite expensive. As of this writing, the cost of NADH is $80/mmol while NADPH is $4500/mmol (Sigma Aldrich). Although other NADH-regeneration systems are available (*16, 17*), PTDH is uniquely useful due to the high thermodynamic driving force behind the reaction and the inexpensive sacrificial reductant utilized, phosphite ($17.70/mol, Sigma Aldrich).

Variants of PTDH have been engineered with relaxed cofactor specificity (*18*), using homology models to rationally design an enzyme capable of accepting NADP as a substrate. In addition, directed evolution studies via error-prone polymerase chain reaction (PCR) have developed mutants with increased activity (*19*) and greatly increased thermostability (*20*), yielding an enzyme with a half-life of nearly six days at 45 °C. This variant is the most versatile for cofactor regeneration, and is termed 17X-PTDH due to its 17 amino acid mutations from the wild-type. 17X-PTDH contains 12 mutations that result in considerably increased thermostability with minimal change in activity, and 4 additional mutations that increase its activity. An additional E175A mutation confers on the enzyme the ability to utilize both NAD^+ and NADP. The kinetic isotope effects, pH dependence, and pre-steady state kinetics observed with 17X-PTDH are all very similar to those observed with wild-type (wt) PTDH (*9*), suggesting that these two proteins use the same mechanism of catalysis.

In addition to general cofactor regeneration, other uses for PTDH have been developed and reported in the literature. PTDH with dual cofactor specificity has been fused to flavin monooxygenases and the resulting self-sufficient biocatalysts have been demonstrated to have excellent activities for enantioselective catalysis (*21-24*). PTDH has also found use in fluorescence assays to quantify phosphite concentrations in plants (*25*).

1.3 Previous Insights into the PTDH Mechanism

In an effort to identify how PTDH achieves catalysis, several highly conserved residues that are shared between members of the DHDH family and PTDH were identified, and their roles in the PTDH reaction studied through mutagenesis (*5, 6, 9*). One residue of particular interest is His292 (PTDH numbering); in the DHDHs, this conserved histidine is proposed to act as a

catalytic base that deprotonates the alcohol substrate and as an acid that protonates the carbonyl in the reverse reaction (*26*). In PTDH, mutation of this residue completely abolished activity, and covalent modification of the residue with diethylpyrocarbonate (DEPC) led to complete inactivation of the wild-type (wt) enzyme (*5*). Given its catalytic importance, His292 was proposed to be the active site base that deprotonates the water nucleophile in the PTDH reaction. However, no direct experimental evidence has been obtained to confirm this hypothesis. Two other conserved residues that act in DHDH catalysis (*27, 28*), Glu266 and Arg237, were reported to play roles in PTDH by helping to position His292 and modulate its pK_a, and by binding the phosphite substrate, respectively (*5*).

The pH rate profile provided further insight into catalysis. For wt-PTDH, the pH rate profile for log($k_{cat}/K_{m,phosphite}$) shows a bell-shaped curve indicating that for optimal catalysis one group (on the protein or the substrate) must be deprotonated and another group must be protonated (*6*). The pK_a values deduced from the curve are 6.8 and 7.8, respectively. The lower pK_a corresponds well to the second acid dissociation constant of phosphorous acid (the conjugate acid of phosphite) suggesting that the enzyme may utilize the dianionic form of the substrate. The higher pK_a would then correspond to an enzyme residue that must be protonated. The pH dependence of DEPC inactivation tentatively suggests that this limb corresponds to His292 (*29*), but if so it could not be the catalytic base that deprotonates the water nucleophile. One scenario that would still allow His292 to serve as base involves binding of dianionic phosphite to PTDH with a protonated His292, followed by proton transfer from His292 to phosphite in the ternary complex because of perturbed pK_a values in the ternary complex (Figure 1.1). An alternative interpretation of the data is that phosphite must be protonated and His292 deprotonated for substrate binding. In this interpretation, the minor, monoprotonated form of the substrate at the optimal pH of 7.25

would bind to the minor form of the enzyme with a deprotonated His (Figure 1.1). Such a reverse protonation scenario would result in an identical pH-rate profile because both of these two protonation states of the substrate and enzyme would have maximum occupancy at pH 7.25, falling off at both higher and lower pH values (*6*). Because the pK_a values of the acidic and basic limbs of the PTDH pH rate profile have less than 2 pH units in separation, it is difficult to differentiate between normal and reverse protonation states (*30*).

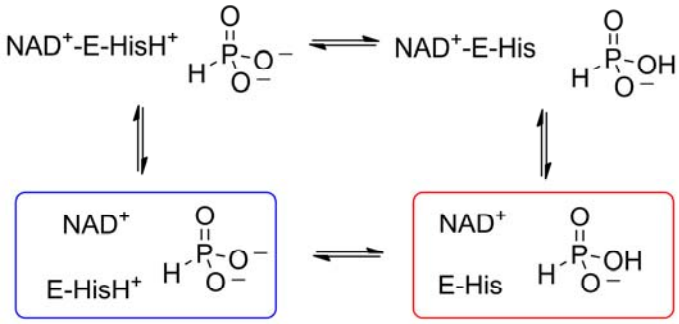

Figure 1.1. Possible protonation states of phosphite and His292 in PTDH. The two substrates bind to the enzyme in an ordered mechanism with NAD^+ binding first (*1*). Based on the pH-rate profile, dianionic phosphite could bind to the NAD^+-PTDH complex containing a protonated His292 (blue). If this is the active complex, a residue other than His292 must function as base to deprotonate the water nucleophile. Alternatively, the pK_a values of phosphite and the His could be perturbed in the ternary complex such that a proton transfer takes place from the protonated His to the phosphite to generate a monoprotonated phosphite as the actual electrophile (red). This form of the ternary complex could also be accessed if monoanionic phosphite binds to the NAD^+-PTDH complex in which the His is unprotonated (reverse protonation based on their pK_a values). Reprinted with permission from (*7*).

The mechanism of phosphoryl transfer for the PTDH reaction is also unverified. Four potential mechanisms have been discussed (*8*). One possibility is a concerted S_N2-like mechanism in which water or hydroxide attacks the phosphorus of phosphite and the hydride leaving group is transferred to NAD^+ (Figure 1.2A). However, the solvent isotope effect (SIE) and substrate kinetic isotope effect (KIE) are not multiplicative, suggesting that a multi-step mechanism is operational instead (*6*).

Alternatively, an associative mechanism is possible in which the nucleophile attacks prior to hydride group departure, resulting in a pentavalent phosphorane intermediate (Figure 1.2B). A dissociative mechanism could also take place in which the hydride group leaves prior to attack by the nucleophile, forming a trivalent metaphosphate intermediate (Figure 1.2C). The viability of the metaphosphate moiety as a stable intermediate in solution has been debated (*31, 32*), though the species has been putatively observed in the crystal structure of fructose 1,6 bisphosphatase (*33*). Finally, a covalent catalysis mechanism is possible in which a catalytic residue attacks phosphite to form a covalent intermediate (Figure 1.2D, see Appendix A). Like the mechanisms in panels A-C, the first step of a covalent mechanism could be concerted (as shown in panel D), associative, or dissociative. In addition to the uncertain mechanism of phosphoryl transfer, the timing of deprotonation of the water nucleophile is unresolved and could occur before, during or after nucleophilic attack.

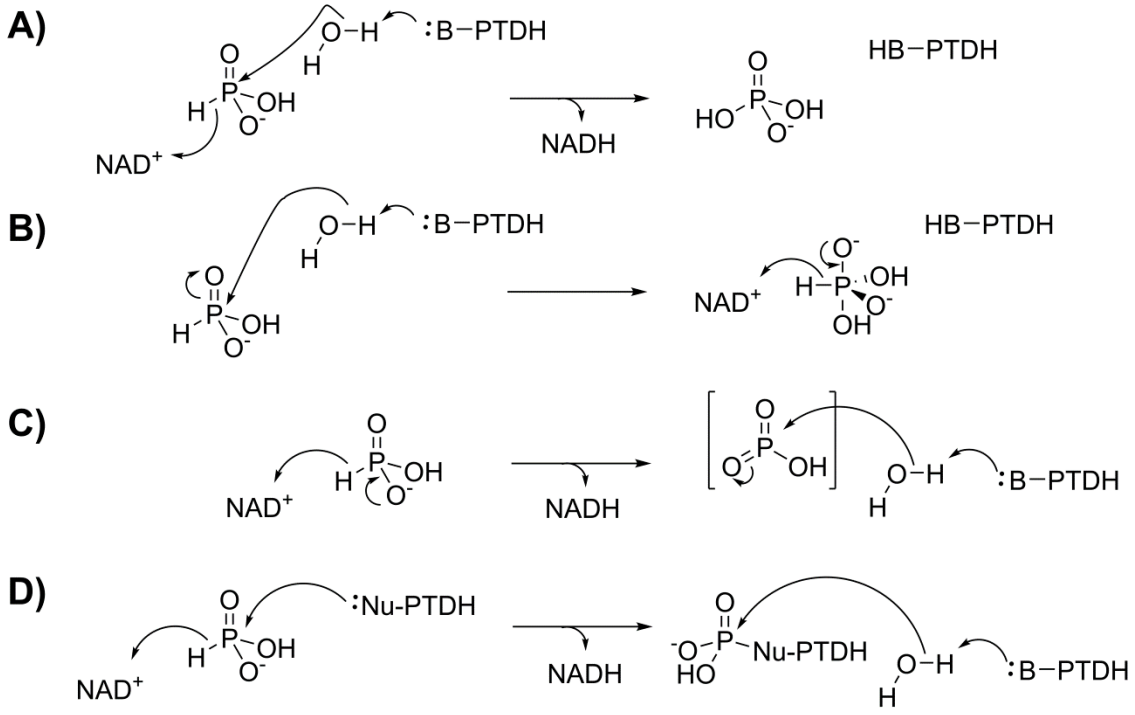

Figure 1.2. Potential mechanisms of phosphoryl transfer by PTDH: A) concerted, B) associative, C) dissociative, and D) covalent catalysis

1.4 The PTDH Crystal Structure

The crystal structures of several thermostable PTDH variants have recently been solved (*34*). A co-crystal structure of TS-PTDH with NAD^+ and sulfite, which is a competitive inhibitor for phosphite (*4*), is available, which depicts the ternary structure of the enzyme (Figure 1.3, PDB: 4E5K). TS-PTDH differs from 17X-PTDH only through the lack of the E175A mutation that allows 17X-PTDH to use both NAD^+ and NADP. The X-ray structures of 17X-PTDH and TS-PTDH show very similar positions of active site residues (*34*), and it is very likely that they proceed through the same mechanism of catalysis.

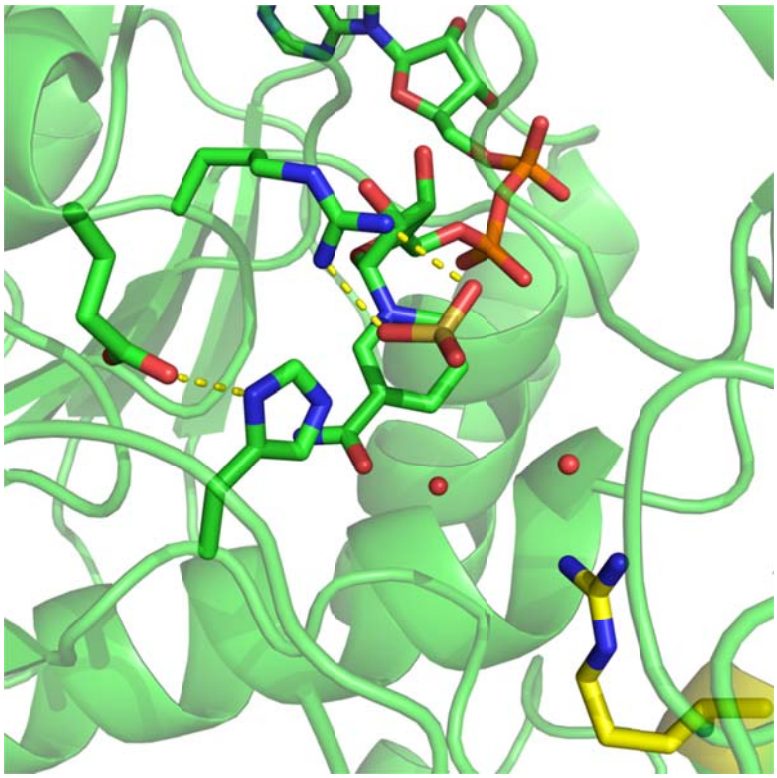

Figure 1.3. Depiction of the active site of TS-PTDH with NAD^+ and sulfite bound. Also shown are the conserved active site residues His292, Glu266, and Arg237. Shown in yellow is the newly identified residue Arg301 (see Chapter 2).

In the crystal structure of the enzyme active site, His292, Glu266, and Arg237 are located in close proximity to sulfite. The X-ray structure supports the roles of the residues that were designated by the mutagenesis studies. Arg237 indeed appears to be playing a role to bind

phosphite, while His292 is in good distance and orientation to a crystallographic water molecule that would allow it to act as a base. Glu266 is hydrogen bonded to the Nδ1 nitrogen of the His292 imidazole, and appears to play a stabilizing role. The 16 mutations from wt-PTDH were revealed to be far from the PTDH active site, and they are unlikely to play direct roles in catalysis (*34*).

The crystal structure also revealed that another residue, Arg301, is within hydrogen bonding distance of a water molecule adjacent to sulfite, in a position that would allow it to act as a base. Although arginine is not typically associated with acid-base chemistry in enzymes given its high solution pK_a, there are reports of arginine residues acting as bases in the literature (*35-44*). Arg301 is not conserved amongst the DHDH family and hence it was not investigated in previous studies, but it is conserved in putative PTDH proteins. Given its potentially important role in the PTDH reaction, the role of the Arg301 residue in catalysis was extensively tested (see Chapter 2).

In the following chapters of this thesis, further insights into PTDH catalysis will be discussed. Chapter 2 presents the discovery of newly-identified PTDHs from other organisms and the investigations of the role of Arg301. Chapter 3 will discuss the catalytic role of Met53, another active site residue that is conserved in PTDHs. The function of Met53 was studied collaboratively by computational and experimental methods. Chapter 4 will address efforts to mutate PTDH to accept thiophosphite as an alternate substrate through directed evolution. Finally, Appendix A will discuss the possibility that the PTDH reaction progresses through a covalent catalysis mechanism.

1.5 References

1. Costas, A. M., White, A. K., and Metcalf, W. W. (2001) Purification and characterization of a novel phosphorus-oxidizing enzyme from Pseudomonas stutzeri WM88, *J. Biol. Chem. 276*, 17429-17436.
2. Metcalf, W. W., and Wolfe, R. S. (1998) Molecular genetic analysis of phosphite and hypophosphite oxidation by Pseudomonas stutzeri WM88, *J. Bacteriol. 180*, 5547-5558.
3. White, A. K., and Metcalf, W. W. (2004) The htx and ptx operons of Pseudomonas stutzeri WM88 are new members of the pho regulon, *J. Bacteriol. 186*, 5876-5882.
4. Vrtis, J. M., White, A., Metcalf, W. W., and van der Donk, W. A. (2001) Phosphite dehydrogenase: an unusual phosphoryl transfer reaction, *J. Am. Chem. Soc. 123*, 2672-2673.
5. Woodyer, R., Wheatley, J., Relyea, H., Rimkus, S., and van der Donk, W. A. (2005) Site-directed mutagenesis of active site residues of phosphite dehydrogenase, *Biochemistry 44*, 4765-4774.
6. Relyea, H. A., Vrtis, J. M., Woodyer, R., Rimkus, S. A., and van der Donk, W. A. (2005) Inhibition and pH dependence of phosphite dehydrogenase, *Biochemistry 44*, 6640-6649.
7. Hung, J. E., Fogle, E. J., Christman, H. D., Johannes, T. W., Zhao, H. M., Metcalf, W. W., and van der Donk, W. A. (2012) Investigation of the role of Arg301 identified in the X-ray structure of phosphite dehydrogenase, *Biochemistry 51*, 4254-4262.
8. Relyea, H. A., and van der Donk, W. A. (2005) Mechanism and applications of phosphite dehydrogenase, *Bioorg. Chem. 33*, 171-189.

9. Fogle, E. J., and van der Donk, W. A. (2007) Pre-steady-state studies of phosphite dehydrogenase demonstrate that hydride transfer is fully rate limiting, *Biochemistry 46*, 13101-13108.

10. Grant, G. A. (1989) A new family of 2-hydroxyacid dehydrogenases, *Biochem. Biophys. Res. Commun. 165*, 1371-1374.

11. Liu, D.-F., Ding, H.-T., Du, Y.-Q., Zhao, Y.-H., and Jia, X.-M. (2012) Cloning, expression, and characterization of a wide-pH-range stable phosphite dehydrogenase from *Pseudomonas* sp. K in *Escherichia coli*, *Appl. Biochem. Biotech. 166*, 1301-1313.

12. Martínez, A., Osburne, M. S., Sharma, A. K., DeLong, E. F., and Chisholm, S. W. (2012) Phosphite utilization by the marine picocyanobacterium Prochlorococcus MIT9301, *Environ. Microbiol. 14*, 1363-1377.

13. Hirota, R., Yamane, S., Fujibuchi, T., Motomura, K., Ishida, T., Ikeda, T., and Kuroda, A. (2012) Isolation and characterization of a soluble and thermostable phosphite dehydrogenase from Ralstonia sp. strain 4506, *J. Biosci. Bioeng. 113*, 445-450.

14. Vrtis, J. M., White, A., Metcalf, W. W., and van der Donk, W. A. (2002) Phosphite dehydrogenase, a new versatile cofactor regeneration enzyme, *Angew. Chem., Int. Ed. Engl. 41*, 3257-3259.

15. Faber, K. (2000) *Biotransformations in Organic Chemistry - A Textbook*, 4th ed., Springer-Verlag, Berlin.

16. Chenault, H. K., and Whitesides, G. M. (1987) Regeneration of nicotinamide cofactors for use in organic synthesis, *Appl. Biochem. Biotech. 14*, 147-197.

17. Wichmann, R., Wandrey, C., Bueckmann, A. F., and Kula, M. R. (1981) Continuous enzymic transformation in an enzyme membrane reactor with simultaneous NAD(H) regeneration, *Biotechnol. Bioeng. 23*, 2789-2802.

18. Woodyer, R., van der Donk, W. A., and Zhao, H. (2003) Relaxing the nicotinamide cofactor specificity of phosphite dehydrogenase by rational design, *Biochemistry 42*, 11604-11614.

19. Woodyer, R., van der Donk, W. A., and Zhao, H. (2006) Optimizing a biocatalyst for improved NAD(P)H regeneration: Directed evolution of phosphite dehydrogenase, *Comb. Chem. High Throughput Screen. 9*, 237-245.

20. Johannes, T. W., Woodyer, R. D., and Zhao, H. M. (2005) Directed evolution of a thermostable phosphite dehydrogenase for NAD(P)H regeneration, *Appl. Environ. Microbiol. 71*, 5728-5734.

21. Torres Pazmino, D. E., Snajdrova, R., Baas, B. J., Ghobrial, M., Mihovilovic, M. D., and Fraaije, M. W. (2008) Self-sufficient Baeyer-Villiger monooxygenases: effective coenzyme regeneration for biooxygenation by fusion engineering, *Angew. Chem. Int. Ed. Engl. 47*, 2275-2278.

22. Rioz-Martinez, A., Kopacz, M., de Gonzalo, G., Torres Pazmino, D. E., Gotor, V., and Fraaije, M. W. (2011) Exploring the biocatalytic scope of a bacterial flavin-containing monooxygenase, *Org. Biomol. Chem. 9*, 1337-1341.

23. Torres Pazmino, D. E., Riebel, A., de Lange, J., Rudroff, F., Mihovilovic, M. D., and Fraaije, M. W. (2009) Efficient biooxidations catalyzed by a new generation of self-sufficient Baeyer-Villiger monooxygenases, *Chembiochem 10*, 2595-2598.

24. Mascotti, M., Juri Ayub, M., Dudek, H., Sanz, M., and Fraaije, M. (2013) Cloning, overexpression and biocatalytic exploration of a novel Baeyer-Villiger monooxygenase from Aspergillus fumigatus Af293, *AMB Express 3*, 33.

25. Berkowitz, O., Jost, R., Pearse, S. J., Lambers, H., Finnegan, P. M., Hardy, G. E. S. J., and O'Brien, P. A. (2011) An enzymatic fluorescent assay for the quantification of phosphite in a microtiter plate format, *Anal. Biochem. 412*, 74-78.

26. Taguchi, H., and Ohta, T. (1993) Histidine 296 is essential for the catalysis in Lactobacillus plantarum D-lactate dehydrogenase, *J. Biol. Chem. 268*, 18030-18034.

27. Taguchi, H., Ohta, T., and Matsuzawa, H. (1997) Involvement of Glu-264 and Arg-235 in the essential interaction between the catalytic imidazole and substrate for the D-lactate dehydrogenase catalysis, *J. Biochem. 122*, 802-809.

28. Taguchi, H., and Ohta, T. (1994) Essential role of arginine 235 in the substrate-binding of Lactobacillus plantarum D-lactate dehydrogenase, *J. Biochem. 115*, 930-936.

29. Relyea, H. A. (2006) Kinetic Analysis and pH Dependence of the Phosphite Dehydrogenase Reaction, PhD Dissertation, University of Illinois, Urbana.

30. Cleland, W. W. (1977) Determining the chemical mechanisms of enzyme-catalyzed reactions by kinetic studies, *Adv. Enzymol. 45*, 273-387.

31. Knowles, J. R. (1980) Enzyme-catalyzed phosphoryl transfer reactions, *Annu. Rev. Biochem. 49*, 877-919.

32. Cleland, W. W., and Hengge, A. C. (1995) Mechanisms of phosphoryl and acyl transfer, *FASEB J. 9*, 1585-1594.

33. Choe, J.-Y., Iancu, C. V., Fromm, H. J., and Honzatko, R. B. (2003) Metaphosphate in the active site of fructose-1,6-bisphosphatase, *J. Biol. Chem. 278*, 16015-16020.

34. Zou, Y., Zhang, H., Brunzelle, J. S., Johannes, T. W., Woodyer, R. D., Hung, J. E., Nair, N., van der Donk, W. A., Zhao, H., and Nair, S. K. (2012) Crystal structures of phosphite dehydrogenase provide insights into nicotinamide cofactor regeneration, *Biochemistry 51*, 4263-4270.

35. Guillén Schlippe, Y. V., and Hedstrom, L. (2005) Is Arg418 the catalytic base required for the hydrolysis step of the IMP dehydrogenase reaction?, *Biochemistry 44*, 11700-11707.

36. Guillén Schlippe, Y. V., and Hedstrom, L. (2005) A twisted base? The role of arginine in enzyme-catalyzed proton abstractions, *Arch. Biochem. Biophys. 433*, 266-278.

37. Hedstrom, L., and Gan, L. (2006) IMP dehydrogenase: structural schizophrenia and an unusual base, *Curr. Opin. Chem. Biol. 10*, 520-525.

38. Bossi, R. T., Negri, A., Tedeschi, G., and Mattevi, A. (2002) Structure of FAD-bound L-aspartate oxidase: insight into substrate specificity and catalysis, *Biochemistry 41*, 3018-3024.

39. Tedeschi, G., Ronchi, S., Simonic, T., Treu, C., Mattevi, A., and Negri, A. (2001) Probing the active site of L-aspartate oxidase by site-directed mutagenesis: role of basic residues in fumarate reduction, *Biochemistry 40*, 4738-4744.

40. Charnock, S. J., Brown, I. E., Turkenburg, J. P., Black, G. W., and Davies, G. J. (2002) Convergent evolution sheds light on the anti-beta -elimination mechanism common to family 1 and 10 polysaccharide lyases, *Proc. Natl. Acad. Sci. U. S. A. 99*, 12067-12072.

41. Mowat, C. G., Moysey, R., Miles, C. S., Leys, D., Doherty, M. K., Taylor, P., Walkinshaw, M. D., Reid, G. A., and Chapman, S. K. (2001) Kinetic and crystallographic

analysis of the key active site acid/base arginine in a soluble fumarate reductase, *Biochemistry 40*, 12292-12298.

42. Doherty, M. K., Pealing, S. L., Miles, C. S., Moysey, R., Taylor, P., Walkinshaw, M. D., Reid, G. A., and Chapman, S. K. (2000) Identification of the active site acid/base catalyst in a bacterial fumarate reductase: a kinetic and crystallographic study, *Biochemistry 39*, 10695-10701.

43. Scavetta, R. D., Herron, S. R., Hotchkiss, A. T., Kita, N., Keen, N. T., Benen, J. A., Kester, H. C., Visser, J., and Jurnak, F. (1999) Structure of a plant cell wall fragment complexed to pectate lyase C, *Plant Cell 11*, 1081-1092.

44. Sanchez-Torres, P., Visser, J., and Benen, J. A. (2003) Identification of amino acid residues critical for catalysis and stability in Aspergillus niger family 1 pectin lyase A, *Biochem. J. 370*, 331-337.

CHAPTER 2: IDENTIFICATION AND CHARACTERIZATION OF THE CATALYTIC RESIDUE ARG301 IN PTDH

2.1 Introduction

The recently published crystal structure of the ternary complex for the thermostable phosphite dehydrogenase variant from *Pseudomonas stutzeri* WM88 (TS-PTDH, PDB: 4E5K) (*1*), has allowed for preliminary identification of the residues in the PTDH active site pocket that may be catalytically important. Several conserved residues that were previously studied based on the homology of PTDH to the greater family of NAD^+-dependent D-hydroxyacid dehydrogenases (DHDHs) (*2*) are indeed present in the active site. These include the previously investigated His292, Glu266, and Arg237 residues (*3*), which are highly conserved and thought to play important roles in DHDH catalysis (*4-6*). The hypothesized roles of these residues in PTDH were discussed in detail in Chapter 1.

In addition to these previously characterized residues, the crystal structure uncovered additional active site residues that are not conserved in the DHDH family and that had not been investigated thus far (Figure 2.1). As discussed herein, more PTDHs have recently been identified (*7-10*), and it appears that the PTDHs are a distinct subfamily of the greater DHDH

This chapter contains material adapted with permission from:

Hung, J. E., Fogle, E. J., Christman, H. D., Johannes, T. W., Zhao, H. M., Metcalf, W. W., and van der Donk, W. A. (2012) Investigation of the Role of Arg301 Identified in the X-ray Structure of Phosphite Dehydrogenase, *Biochemistry 51*, 4254-4262. Copyright 2012 American Chemical Society.

And adapted from:

Hung, J.E., Fogle, E. J., Garg, N., Chekan, J. R., Nair, S. K., and van der Donk, W. A. Chemical Rescue and Inhibition Studies to Determine the Role of Arg301 in Phosphite Dehydrogenase, *Submitted*.

family. Indeed, many of these newly identified active site residues are conserved among the PTDH family but not within the DHDHs, and as such these residues may play important roles in catalysis.

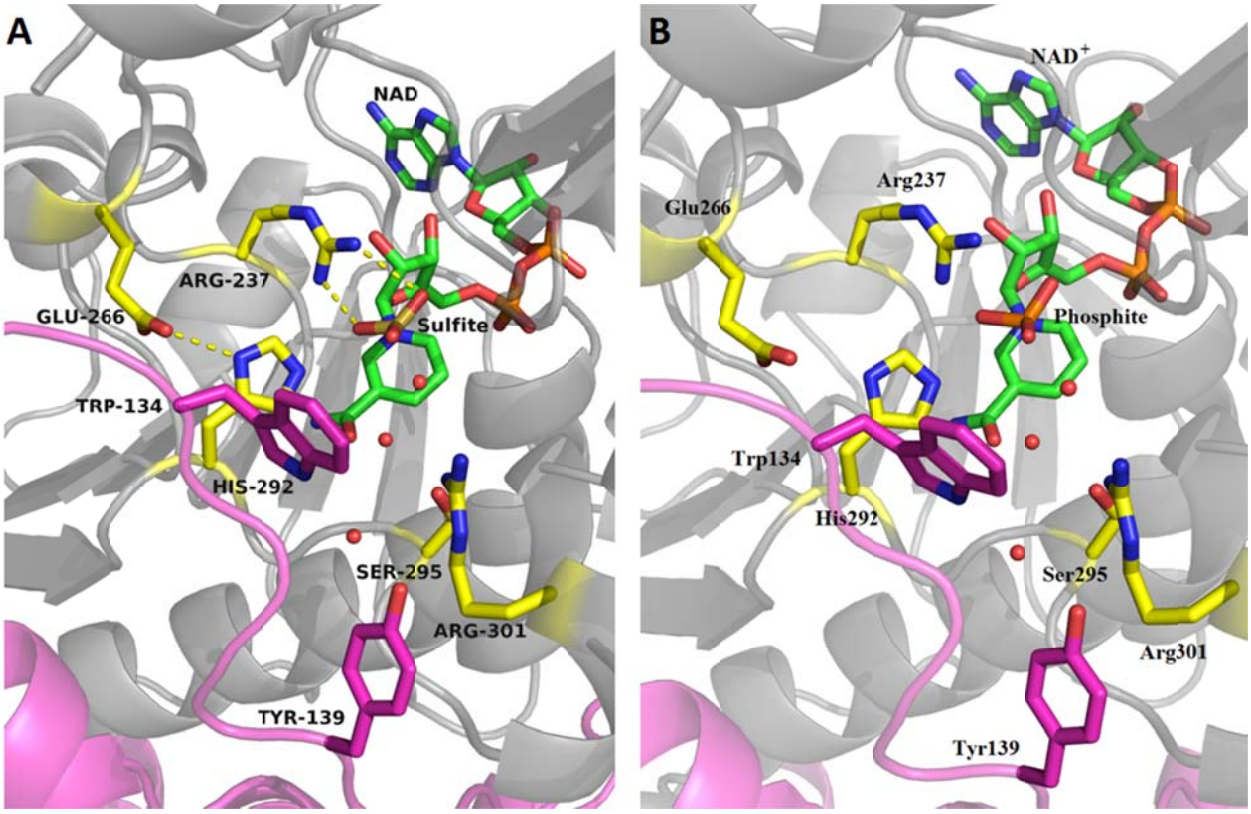

Figure 2.1. (A) A representation of the active site of TS-PTDH (see Chapter 1) containing NAD^+ and sulfite inhibitor. (B) The active site of TS-PTDH containing NAD^+, with phosphite modeled in place of sulfite. The hydride group and the proton on monoprotonated phosphite are not shown. In PTDH, His292 is the likely catalytic base, Glu266 is hydrogen bonded to His292, and Arg237 plays a role in phosphite binding (*3, 11*). $Trp134^B$, $Tyr139^B$ and Ser295 are hydrogen bonded to Arg301; residues in pink are from monomer B whereas all other residues come from monomer A. Note that the sulfite-NAD^+-PTDH complex may not be an exact representation of the active form of the ternary complex with phosphite, and must be used with caution. Adapted with permission from (*7*).

One of these residues is Arg301, which is in good orientation and distance in the active site crystal structure to deprotonate a water molecule that is adjacent to sulfite (Figure 2.2). As

discussed below, mutation to the Arg301Ala mutant was strongly deleterious to catalysis, with k_{cat} decreasing ~100-fold and K_m for phosphite greatly increasing. Given its important contribution to catalysis and its location in the crystal structure, Arg301 may act as the catalytic base to deprotonate the water nucleophile. Although arginine is not typically considered in acid-base chemistry due to the high solution pK_a of its side chain, there have been several recent reports in the literature where arginine residues are believed to act as bases in enzymatic reactions (*12-21*).

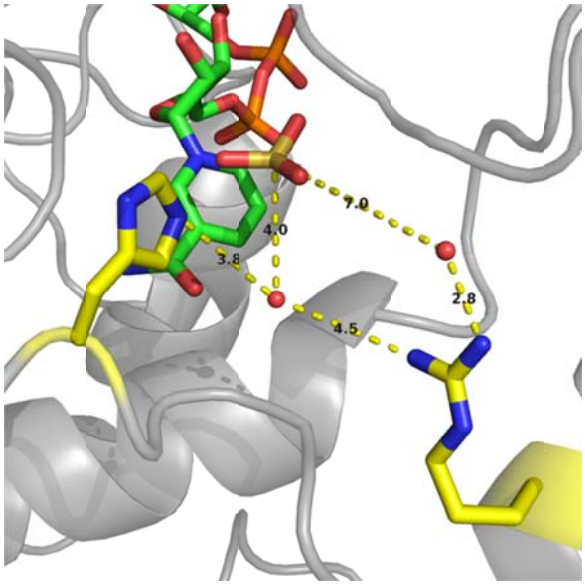

Figure 2.2. The crystal structure of the TS-PTDH ternary complex with NAD^+ and the competitive inhibitor sulfite, depicting the potential active site bases His292 and Arg301.

Alternatively, it is possible that Arg301 is instead positively charged and plays a role in electrostatic catalysis. Arg301 resides near the surface of the enzyme on the dimer interface, so it may also play a role in substrate binding or contribute towards oligomerization of the enzyme to its active dimer form. Herein, the discovery of the PTDHs as a distinct family of enzymes is detailed, and attempts to characterize the role of Arg301 through steady-state kinetics, pH rate

profiles, isotope effects, X-ray crystallography, chemical rescue experiments, and inhibition experiments are reported.

2.2 Results and Discussion

2.2.1 Identification and Characterization of PTDH Orthologs

Several uncharacterized proteins from different bacteria were selected to test for PTDH activity based on the level of their sequence identity (44-56%) to wild type (wt) PTDH from *P. stutzeri* in a BLAST survey (Table 2.1).

Table 2.1. Pairwise sequence identities of PTDH orthologs with confirmed activity.

	R. metallidurans	*Nostoc* sp. 7120	*P. stutzeri*	*N. punctiforme*	*A. faecalis*	*M. extorquens*
R. metallidurans	100%					
Nostoc sp. 7120	39.4%	100%				
P. stutzeri	43.7%	52.7%	100%			
N. punctiforme	38.8%	71.5%	52.4%	100%		
A. faecalis	41.9%	56.3%	51.4%	56.4%	100%	
M. extorquens	50.2%	49.4%	55.6%	50.2%	49.2%	100%

These proteins were heterologously expressed in *E. coli*, purified, and assayed for PTDH activity with phosphite and NAD^+ (Table 2.2). The enzymes from *Nostoc* sp. 7120, *Pseudomonas stutzeri, Nostoc punctiforme,* and *Ralstonia metallidurans* were characterized by Harry Christman in the Metcalf group (*7*). Characterization of the PTDH from *Alcaligenes faecalis* was reported previously (*22*). The enzyme from *Methylobacterium extorquens* was characterized in my work. NADH formation was observed spectrophotometrically and phosphate

production was verified by malachite green assay (*23*). Each of the proteins tested were found to catalyze the same chemical reaction as the PTDH from *P. stutzeri.*

Table 2.2. Kinetic characterization of PTDH orthologs at 30 °C. PT refers to phosphite. Error bars in parentheses were obtained from fits to the Michaelis-Menten equation. Enzyme from *M. extorquens* contained an N-terminal His_6-tag whereas the other enzymes did not. Reprinted with permission from (*7*).

	P. stutzeri	*R.. metallidurans*	*Nostoc* sp. 7120	*N. punctiforme*	*M. extorquens*
$K_{m,NAD}$ (μM)	52.2 (3.3)	4.5 (0.9)	10.3 (1.4)	19.4 (1.6)	40.5 (11.1)
$K_{m,PT}$ (μM)	81.1 (1.6)	54.9 (6.8)	20.2 (1.6)	25.4 (1.2)	237 (36)
k_{cat} (s^{-1})	6.57 (0.03)	6.83 (0.43)	2.41 (0.03)	3.36 (0.03)	5.10 (0.14)

The increase in available PTDH protein sequences suggests that a substantial branch of the DHDH family is likely composed of phosphite dehydrogenases (Figure 2.3, Table 2.3). Four of these enzymes were found to catalyze phosphite oxidation to complement the previously characterized enzymes from *P. stutzeri* (*2*) and *A. faecalis* (*22*). In addition, recent reports in the literature have documented several other microorganisms that also encode proteins that exhibit PTDH activity (*8-10*). Analysis of the kinetic parameters of these enzymes illustrates that they all have similar k_{cat} values despite a high degree of sequence diversity (39-72% pairwise identity, Table 2.1). The similar kinetic parameters and the fact that the enzymes catalyze the same chemical reaction suggest that the PTDH orthologs utilize the same mechanism as the PTDH from *P. stutzeri*.

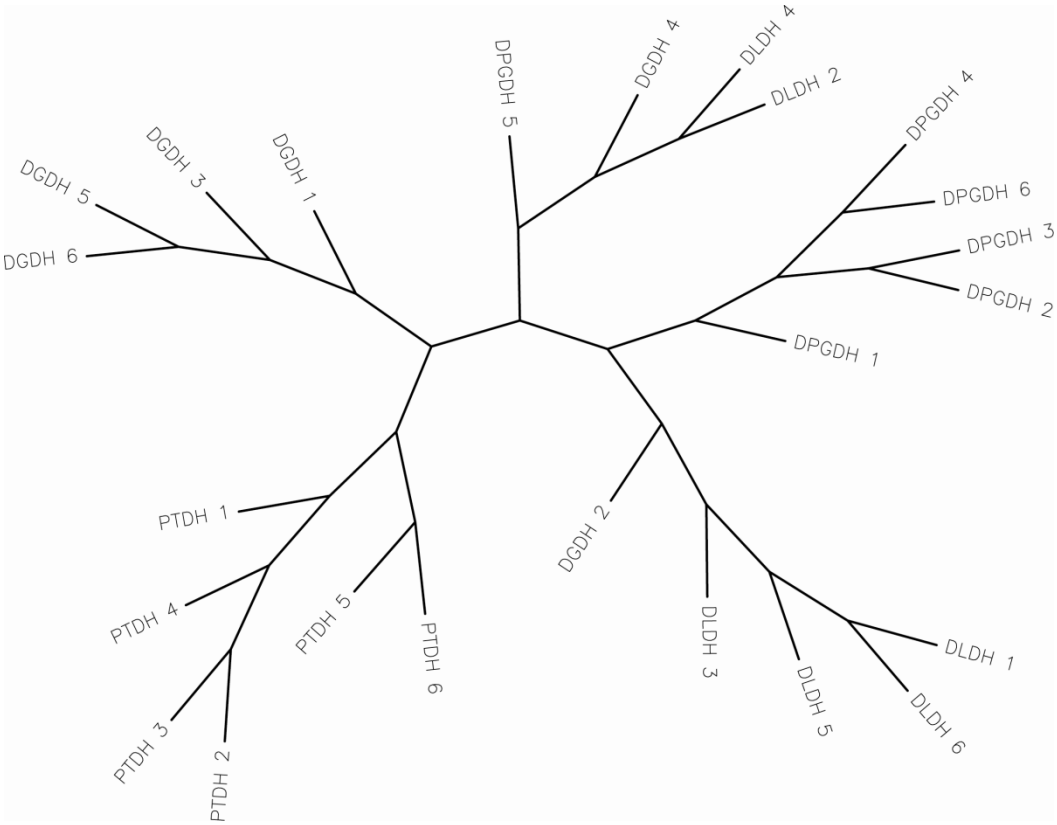

Figure 2.3. PHYLIP unrooted tree for PTDH orthologs and various DHDHs. Abbreviations used are explained in Table 2.3.

Table 2.3. Designations for PTDH orthologs and various DHDHs. DGDH, D-glycerate dehydrogenase; DPGDH, D-3-phosphoglycerate dehydrogenase; DLDH, D-lactate dehydrogenase.

Label	Strain	Accession Number
PTDH 1	*Pseudomonas stutzeri* WM88	AAC71709
PTDH 2	*Nostoc punctiforme* PCC 73102	YP_001866684.1
PTDH 3	*Nostoc* sp. 7120	NP_478512
PTDH 4	*Alcaligenes faecalis*	AAT12779.1
PTDH 5	*Methylobacterium extorquens* AM1	ACS43224
PTDH 6	*Ralstonia metallidurans* CH34	YP_585134.1
DLDH 1	*Lactobacillus helveticus*	P30901
DLDH 2	*Corynebacterium glutamicum* ATCC 13032	YP_225194
DLDH 3	*Aquifex aeolicus* VF5	NP_213499
DLDH 4	*Saccharomyces cervisiae* S288c	NM_001180234
DLDH 5	*E. coli* K-12	NP_415898
DLDH 6	*Staphylococcus aureus* subsp. aureus COL	YP_187328
DGDH 1	*Hyphomicrobium methylovorum*	P36234
DGDH 2	*Methylobacterium extorquens* AM1	Q59516
DGDH 3	*Coleus blu*	Q65CJ7
DGDH 4	*Rhizobium etli*	AC035311
DGDH 5	*Homo sapiens*	NP_036335
DGDH 6	*Thermococcus litoralis*	BAB40320
DPGDH 1	*E. coli*	P08328
DPGDH 2	*Homo sapiens*	NM_006623
DPGDH 3	*Mus musculus*	NM_016966
DPGDH 4	*Aphanothece halophytica*	BAF91727
DPGDH 5	*Mycobacterium tuberculosis* H37Rv	NP_215242
DPGDH 6	*Arabidopsis thaliana*	NP_001031061

The residues Arg237, Glu266, and His292 are highly conserved among the DHDH family and have been shown to be important for catalysis in PTDH (*3, 11*). With more than one PTDH now identified experimentally, a sequence alignment was performed to determine if any other residues are conserved among this enzyme family. Based on this alignment, Arg301, Ser295, Tyr139 and Trp134 were found to be fully conserved among PTDHs but not among the DHDH family (Figure 2.4). Furthermore, all four residues are near the phosphite binding site (Figure 2.1) in the X-ray structure. Several other conserved residues were observed, but in the crystal structure of PTDH these residues are distant from the enzyme active site (*1*). Another conserved residue that is present in the active site, Met53, is discussed in Chapter 3.

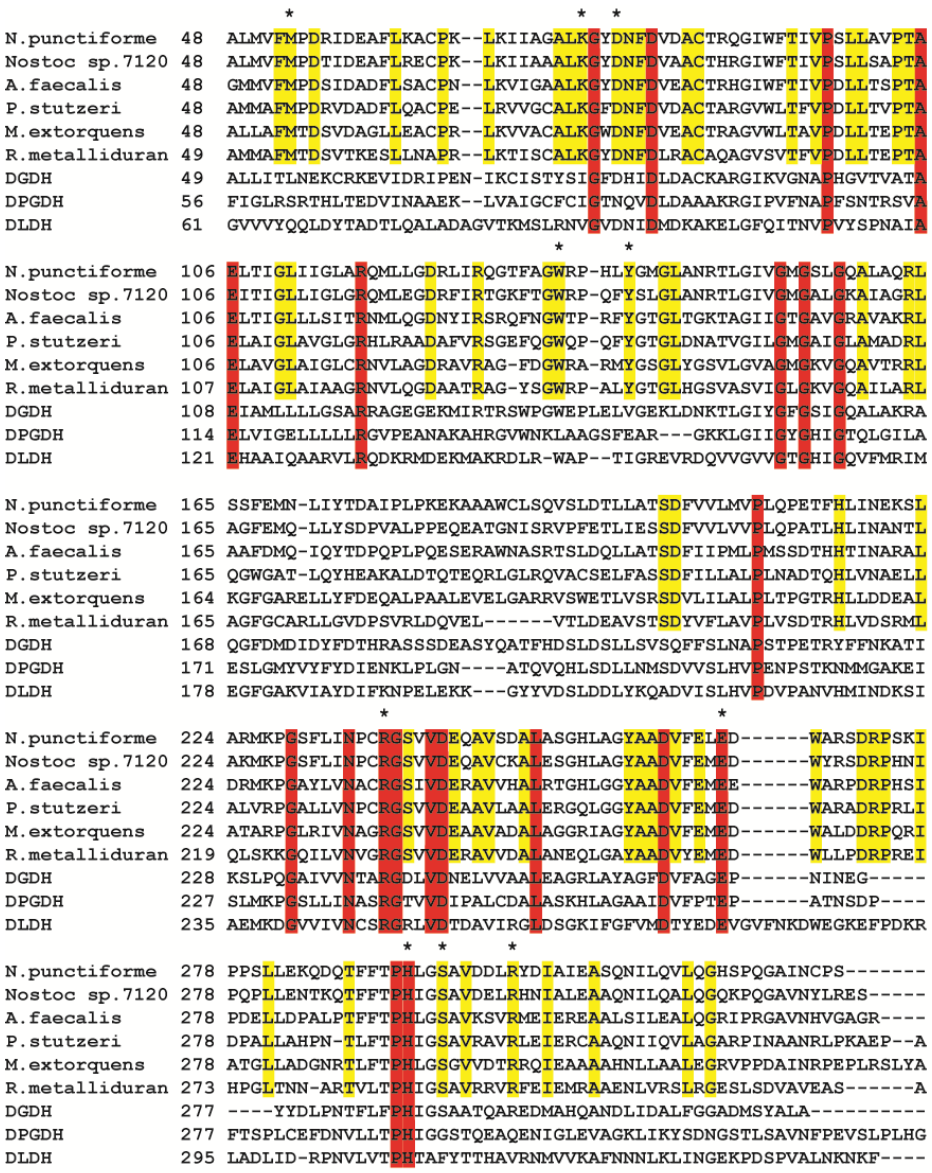

Figure 2.4. Partial sequence alignment of several previously-investigated D-hydroxy acid dehydrogenases with enzymes with confirmed PTDH activity (*7, 22*). Numbering is based on PTDH from *P. stutzeri* WM88. Residues within the active site that may be important for catalysis are denoted by an asterisk. Highlighted in red are residues that are completely conserved among both DHDHs and PTDHs. Highlighted in yellow are residues that are completely conserved only among PTDHs. The important catalytic residues Arg237, Glu266 and His292 are conserved among both groups (*5, 24, 25*). Residues Ser295, Tyr139, Trp134, Arg301, identified at or near the active site in the crystal structure (*1*), are only conserved among PTDHs. Lys76 was previously believed to be important for binding phosphite but the X-ray structure shows instead it interacts with the pyrophosphate of NAD^+ (*1*). Abbreviations (% identity with wt-PTDH, accession number): *Nostoc punctiforme* PCC 73102 (54%, YP_001866684.1); *Nostoc* sp. 7120 (54%, NP_478512); *Alcaligenes faecalis* (53%, AAT12779.1); *Methylobacterium extorquens* AM1 (56%, ACS43224); *Ralstonia metallidurans* CH34 (47%, YP_585134.1); DGDH, D-glycerate dehydrogenase (*Hyphomicrobium methylovorum*, 27%, P36234) (*26*); DPGDH, D-3-phosphoglycerate dehydrogenase (*E. coli*, 24%, P08328) (*27*); and DLDH, D-lactate dehydrogenase (*Lactobacillus helveticus*, 26%, P30901) (*28*).

2.2.2 Steady State Assays of PTDH Active Site Mutants

To investigate the importance of Arg301, Ser295, Tyr139, and Trp134 for catalysis, site-directed mutagenesis was performed to generate the following mutants, all in the 17X-PTDH background: Arg301Lys, Arg301Ala, Ser295Ala, Tyr139Phe, Trp134Phe, and Trp134Ala. All mutants were successfully expressed in *E. coli* as N-terminal His_6-tagged fusion proteins and purified by immobilized Ni^{2+} affinity chromatography.

Steady state kinetic assays were used to determine the effect of each mutation on enzyme activity (Table 2.4). Overall, the values of k_{cat} for all mutants except Arg301Ala are very similar to the parent PTDH. The k_{cat} of the R301A mutant was reduced about 100-fold, but the k_{cat} of the R301K mutant was actually slightly increased compared to 17X-PTDH. $K_{m,Phosphite}$ was greatly increased for both Arg301 mutants, with a particularly large increase (almost 700-fold) for R301A. $K_{m,NAD}$ was also increased 10-fold for the R301A mutant with a more modest increase (3-fold) for R301K. Use of a full matrix of varying phosphite and NAD^+ concentrations allowed determination of the dissociation constant for NAD, $K_{ia,NAD}$, using the equation (see Materials and Methods) (*29*) for an ordered, sequential mechanism in which NAD^+ binds prior to phosphite (*2*) (Figure 2.5). Mutations of Arg301 did not substantially increase $K_{ia,NAD}$ (Table 2.4), perhaps not unexpected given the large distance between Arg301 and the cofactor in the crystal structure (*1*). In the X-ray structure, Arg301 participates in the dimer interface for 17X-PTDH (Figure 2.1). To ensure that the data obtained with the Arg301Ala mutant were not a consequence of disruption of the oligomerization state of the protein, gel filtration experiments were performed, which showed that the Arg301Ala mutant remains a dimer.

Table 2.4. Steady State Parameters of 17X-PTDH Mutants.[a]

	k_{cat} (s^{-1})	$K_{m, PT}$ (mM)	$K_{m, NAD}$ (mM)	$K_{ia, NAD}$ (mM)	$k_{cat}/K_{m, PT}$ ($M^{-1}s^{-1}$)	$^{D}k_{cat}$	$^{D}(k_{cat}/K_{m,PT})$
17X-PTDH[b]	3.27 (0.24)	0.028 (0.007)	0.022 (0.006)	1.0 (0.3)	1.2 (0.3) x 10^5	2.3 (0.1)	2.1 (0.2)
R301K[b]	4.50 (0.72)	1.1 (0.1)	0.074 (0.007)	0.97 (0.14)	4,000 (800)	1.9 (0.1)	2.2 (0.5)
R301A[b]	0.041 (0.007)	19 (1)	0.22 (0.02)	0.48 (0.07)	2.1 (0.4)	2.7 (0.1)	2.1 (0.2)
S295A[c]	2.53 (0.22)	0.10 (0.02)	0.25 (0.03)	nd[d]	2.5 (0.5) x 10^4	Nd	Nd
W134F[c]	2.96 (0.10)	0.24 (0.01)	0.10 (0.01)	nd	1.2 (0.1) x 10^4	2.2 (0.1)	2.7 (0.2)
W134A[c]	1.73 (0.14)	1.9 (0.1)	0.19 (0.02)	nd	900 (90)	2.2 (0.1)	2.1 (0.2)
Y139F[c]	3.68 (0.37)	0.039 (0.002)	0.036 (0.002)	nd	9.4 (1.1) x 10^4	nd	nd

[a] All assays were performed at 25 °C, pH 7.25 in 100 mM MOPS. PT refers to phosphite. k_{cat} values were obtained for three batches of each enzyme and the average is presented here (see Materials and Methods). [b] The values were determined by varying the concentrations of both substrates, determining the initial rates, and fitting all data to the equation shown in the Materials and Methods section. [c] The values were determined by holding one substrate at saturating concentration and varying the concentration of the other substrate. Initial rates were fit to the Michaelis Menten equation. The errors given in parentheses are obtained from the fits of the experimental data to the respective equations (see Materials and Methods). [d] nd—not determined. Reprinted with permission from (*7*).

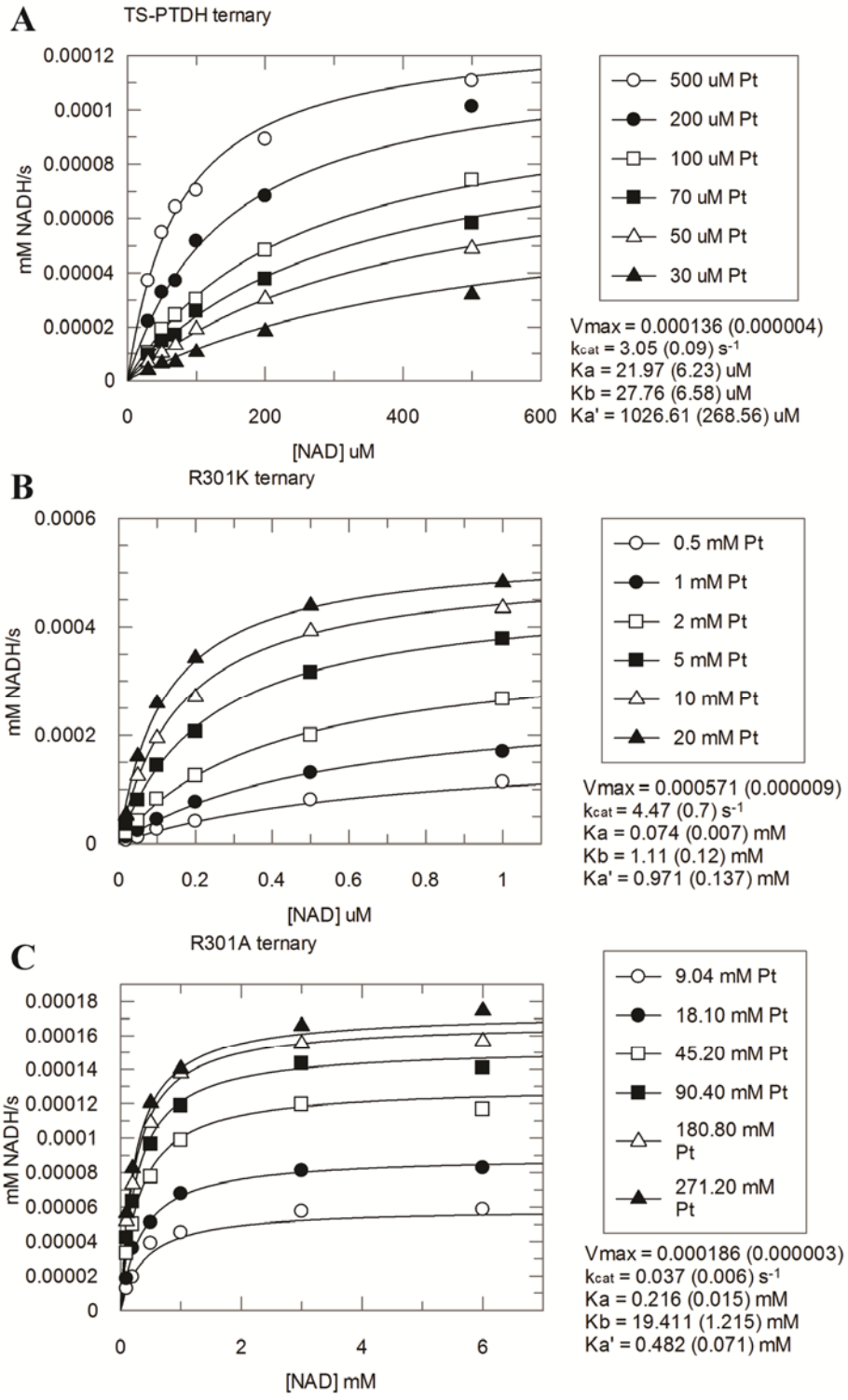

Figure 2.5. Steady-state kinetic assays of 17X-PTDH and Arg301 mutants fit simultaneously to the appropriate equation for a two-substrate reaction with NAD^+ binding first and phosphite binding second (*30*). (A) 17X-PTDH (B) R301K, and (C) R301A. Pt stands for phosphite, uM stands for μM, Ka stands for the $K_{m,NAD}$, Kb stands for $K_{m,Phosphite}$, and Ka' stands for $K_{ia,NAD}$ (which is $K_{d,NAD}$).

The Ser295Ala, Trp134Phe, Trp134Ala, and Tyr139Phe mutants had only slightly reduced k_{cat} values compared to 17X-PTDH. As these conservative mutations removed the functional groups on the side chains of the residues, the mutagenesis studies suggest that these residues do not play an important role in catalysis. Mutations of Trp134 did affect the K_m values for phosphite, with the Trp134Ala mutant exhibiting a 40-fold increase in $K_{m,Phosphite}$. The Trp134Phe mutant had a similar effect on $K_{m,Phosphite}$, although it was smaller in magnitude. It is likely that the residues play roles in optimizing catalytic efficiency, perhaps by helping position Arg301 to which they are hydrogen bonded in the wt enzyme (*1*). Kinetic isotope effect (KIE) experiments performed with selected mutants yielded normal $^{D}k_{cat}$ and $^{D}k_{cat}/K_{m,Phosphite}$ values, which were similar in magnitude to those observed with 17X-PTDH. These results suggests that hydride transfer remains rate-limiting at pH 7.25, as has been previously shown for wild-type PTDH and a series of mutants with a wide range of catalytic activities (*31*).

Arg301 is fully conserved among all confirmed PTDH enzymes, and in the crystal structure it is located with its side chain pointed towards sulfite in the active site, with a total distance of 7.0 Å between the terminal nitrogen of the guanidine and sulfur atom. Given the results of the mutagenesis studies, it is clear that Arg301 plays an important role in PTDH catalysis, though its exact role is unclear from the steady state kinetics data. The magnitude of the reduction in k_{cat} of the Arg301Ala mutant and the observation that the Arg301Lys mutant retained a comparable k_{cat} to 17X-PTDH are similar to the findings with mutants of inosine monophosphate dehydrogenase for which a role of an Arg as active site base to deprotonate a water molecule has been proposed (*12-14, 32, 33*). Indeed, a water molecule is present between the Arg301 side chain and sulfite, and it is in good orientation and distance to act as a nucleophile onto the substrate. Arginine is not commonly considered in the acid-base chemistry of proteins owing to its relatively high

solution phase pK_a, but several recent reports have documented enzymes in which arginine have been proposed to act as a base (*12-21*). However, the observed phenotype of the Arg301Ala mutant may also be attributed to removal of an important electrostatic effect (i.e. if Arg301 is positively charged as expected based on its pK_a). To further characterize the catalytic role of Arg301, pH dependence experiments were performed.

2.2.3 pH Rate Profiles of 17X-PTDH Mutants

The pH dependence of the steady-state kinetic constants was determined for 17X-PTDH-R301A and 17X-PTDH-R301K, the mutants with the most interesting phenotypes. Like wt-PTDH (*11*), the pH rate profile for 17X-PTDH is pH independent for log(k_{cat}) (Figure 2.6A) and displays a bell-shaped curve for log($k_{cat}/K_{m,Phosphite}$) (Figure 2.6B) with extracted pK_a values of 6.53 ± 0.10 and 7.90 ± 0.08 from a fit to the appropriate equation (see Materials and Methods). The pH rate profile for R301K was overall similar to that of 17X-PTDH. The log(k_{cat}) profile is pH independent in the range of pH 7-9, but it appears that a deprotonation event with a pK_a of 5.93 ± 0.03 may affect k_{cat}. This pK_a is close to the limits of the pH range in which this mutant is stable (Figure 2.6C), and the data cannot completely rule out that the observed decrease in activity may be the result of loss of activity that is not associated with a defined ionizable residue. The mutant displays a bell shaped curve for log($k_{cat}/K_{m,Phosphite}$), with extracted pK_a values of 6.62 ± 0.05 and 8.37 ± 0.07 for the two proton transitions (Figure 2.6D).

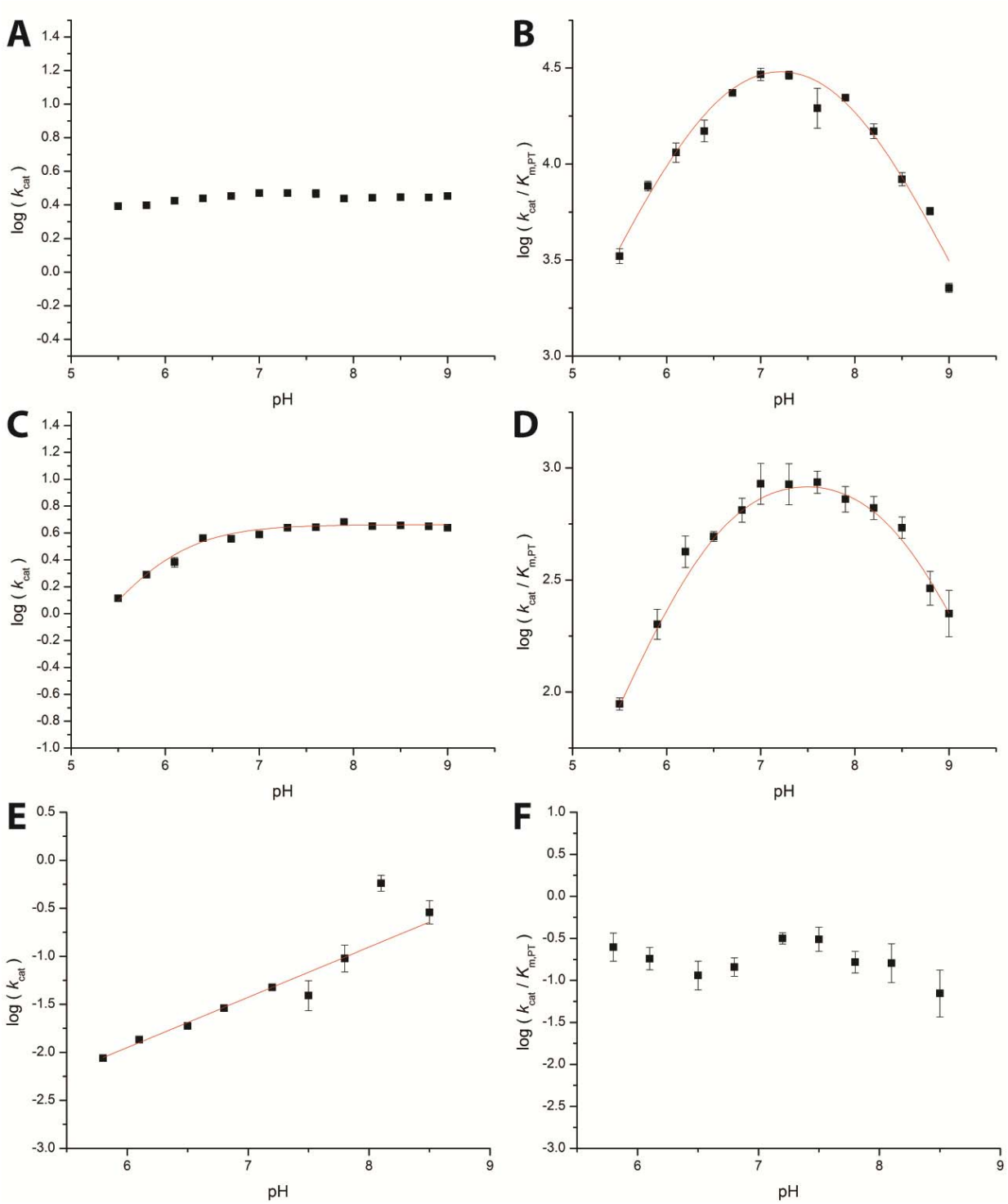

Figure 2.6. pH rate profiles of log(k_{cat}) and log($k_{cat}/K_{m,Phosphite}$) for 17X-PTDH (panels A and B, respectively), 17X-PTDH-R301K (panels C and D), and 17X-PTDH-R301A (panels E and F). When error bars are not visible, they were smaller than the font size used for the data point. Reprinted with permission from (*7*).

In contrast to the plots for $k_{cat}/K_{m,Phosphite}$ and k_{cat} of 17X-PTDH and R301K, the pH dependence of the kinetic parameters of R301A was very different. The plot of log(k_{cat}) versus pH was nearly linear with a slope of 0.6 (Figure 2.6E) and may suggest specific base catalysis by hydroxide. Slopes less than 1 have been reported previously (*34-37*) and a number of reasons can be offered including a decreased activity coefficient of hydroxide in the active site environment, a partial contribution of an uncatalyzed reaction (i.e. with water as nucleophile), or the superposition of titration curves of multiple different ionizable residues with a hydroxide ion dependent specific base mechanism. In contrast, log($k_{cat}/K_{m,Phosphite}$) was essentially pH independent (Figure 2.6F). This latter finding is the result of offsetting effects on k_{cat} and $K_{m,Phosphite}$ (Table 2.6). The former increases with pH resulting in improved catalysis, but the latter also increases with pH, resulting in less efficient catalysis at low substrate concentrations. The same findings were obtained in three different buffer systems: a universal buffer of constant ionic strength (*38*), a broad-range Tris-maleate buffer, and MOPS, the standard PTDH assay buffer (Table 2.5). The data in Figure 2.5 were obtained in the universal buffer.

Table 2.5. Steady-state kinetic constants for 17X-PTDH and the R301A mutant in different buffers at pH 7.25. Assays were performed at optimal pH of 7.25, 25 °C in different buffers. NAD^+ concentrations were held at saturating values. PT refers to phosphite. High K_m values in 'Universal' buffer increased the error. nd = not determined. Errors given in parenthesis are determined from the fit to the Michaelis-Menten equation.

	Buffer	k_{cat} (s^{-1})	$K_{m,PT}$ (mM)	$k_{cat}/K_{m,PT}$ ($M^{-1}s^{-1}$)	$^{D}k_{cat}$	$^{D}k_{cat}/K_{m,PT}$
17X-PTDH	MOPS	3.26 (0.15)	0.050 (0.005)	5.9 (0.6) x 10^4	2.16 (0.15)	1.78 (0.2)
R301A	MOPS	0.038 (0.001)	28 (1)	1.4 (0.1)	2.67 (0.09)	2.06 (0.22)
17X-PTDH	Universal	2.71 (0.09)	0.090 (0.01)	3.0 (0.1) x 10^5	nd	nd
R301A	Universal	0.038 (0.001)	650 (45)	0.059 (0.004)	4.32 (0.30)	2.35 (0.44)
17X-PTDH	Tris maleate	2.93 (0.04)	0.37 (0.02)	8.0 (0.4) x 10^3	2.01 (0.05)	2.05 (0.19)
R301A	Tris maleate	0.039 (0.001)	49 (3)	0.79 (0.21)	2.20 (0.1)	2.71 (0.79)

If Arg301 indeed is the active site base, the observation that its pK_a is not seen in the pH-rate plots for 17X-PTDH (Figure 2.6) can have several explanations. One is that the rate constant for water deprotonation is not in the rate equation (i.e. it takes place after the rate determining step, which for 17X-PTDH is hydride transfer based on KIEs and pre-steady kinetic state measurements). Such a model would imply a dissociative reaction in which hydride transfer occurs prior to attack by the nucleophile. Alternatively, the nucleophile could be water and deprotonation could occur after hydride transfer. There is no evidence for either scenario and both models appear unlikely, but there is also no direct evidence against these possibilities. Another possible scenario in which Arg301 would not show up in the pH-rate plots for 17X-PTDH is that its pK_a is above 9 and outside the pH range we experimentally investigated. If so, then only a very small fraction of the enzyme would contain a deprotonated Arg that could

accept the proton from water. But, as pointed out previously for other biological catalysts (*13, 39, 40*), this would not preclude catalysis. Again, at present we have no evidence that this is the case for PTDH.

For $\log(k_{cat}/K_{m,Phosphite})$ of the R301A mutant, both the basic and acidic limbs of the pH rate profile disappeared, yielding a pH-independent profile. As the pK_a of phosphite (corresponding to the acidic limb of the profile) should not have been altered by the mutation of Arg301, these results argue that either the acidic limb observed with wt-PTDH is not associated with substrate, or more likely that a change in mechanism has occurred for the mutant. To address this possibility, the KIEs for the R301A mutant were determined over the pH range. 17X-PTDH displays KIEs that do not change significantly over the pH range. In contrast, substrate deuterium KIEs obtained at three pH values in Tris-maleate buffer for R301A showed that $^{D}k_{cat}$ increased as the pH was raised (Table 2.6). This result is consistent with a change in mechanism over the pH range, with the chemical step of the reaction becoming more rate limiting in a basic environment. The pH dependence of $^{D}(k_{cat}/K_{m,Phosphite})$ of 17X-PTDH-R301A was also very different from that of the parent enzyme, displaying a substantially larger value at low pH than at high pH, indicating that commitment to catalysis is much smaller at low pH. This stronger selection against deuterium labeled phosphite could be a consequence of a slower chemical step or an increase in the dissociation rate of the substrate. As the maximum KIE for a P–H/P–D bond is calculated to be approximately 5.0 (*41*), it is also possible that the KIEs for the mutant are approaching the intrinsic KIE at the pH extremes. The observed changes in the kinetic mechanism as a function of pH could have many causes (e.g. different chemical mechanism, different relative rate constants, different order of addition, etc.) that were not further

investigated, as such studies on a mutant with very different properties than wt-PTDH would not provide much insight into the physiological reaction.

Table 2.6. KIEs of 17X-PTDH-R301A at different pH values. All assays were performed at 25 °C in 100 mM Tris maleate buffer of varying pH. PT refers to phosphite. Errors, given in parentheses, are from fits of the data to the Michaelis Menten equation. Similar changes in the KIEs as the pH was varied were also observed in MOPS and the Universal buffer.

	k_{cat} (s^{-1})	$K_{m,\ PT}$ (mM)	k_{cat}/K_m ($M^{-1}s^{-1}$)	$^{D}(k_{cat})$	$^{D}(k_{cat}/K_m)$
pH 5.5	0.005 (0.001)	5.2 (1.0)	0.90 (0.18)	1.3 (0.1)	7.4 (1.6)
pH 7.3	0.039 (0.001)	49 (3)	0.79 (0.21)	2.2 (0.1)	2.7 (0.8)
pH 8.3	0.25 (0.02)	920 (190)	0.28 (0.06)	6.0 (0.6)	2.1 (0.6)

Overall, the large changes in the K_m values for both substrates as well as the drastically different pH dependence of both k_{cat} and $k_{cat}/K_{m,Phosphite}$ suggest that the R301A mutant is severely disrupted and that its mechanism of catalysis may not be representative for the parent enzyme. Therefore, the pH dependence data of R301A do not directly support Arg301 acting as a base in catalysis.

An electrostatic role of Arg301 appears to be supported by the data obtained for 17X-PTDH-R301K. This mutant shows a more modest increase in $K_{m,Phosphite}$ and has a slightly improved k_{cat} compared to 17X-PTDH. Furthermore, the pH-rate profiles are very similar with the only substantial change being a shift of the basic pK_a in the bell shaped curve for $\log(k_{cat}/K_{m,Phosphite})$ to a higher value (from 7.9 to 8.4). If this pK_a indeed represents His292 (*11, 42*), its pK_a could be raised because of a weaker electrostatic destabilization of the imidazolium group of His292 by a protonated Lys than by a protonated Arg. Collectively, the steady state kinetic parameters and the pH rate profiles suggest that lysine is capable of playing a similar catalytic role as arginine, and these observations are more readily explained by an electrostatic interaction than by a role as

base. These positively charged residues may also be important for orienting the phosphite substrate for efficient catalysis.

2.2.4 X-Ray Crystallography of Arg301Ala and Arg301Lys Mutants of 17X-PTDH

Crystals were obtained that contained NAD^+ and that diffracted to 2.35 Å and 2.65 Å for the R301A and R301K (Figure 2.7A) mutants, respectively. The R301A crystal was grown by Neha Garg whereas I grew the R301K crystal. The crystals were diffracted and the structures solved by Jonathan Chekan and Professor Satish Nair as reported in (*43*). Superposition of the mutant structures with the crystal structure of the parent 17X-PTDH containing NAD^+ (*1*) revealed that the overall structure of the mutants was unchanged, with the exception of the appearance of a solvent-accessible channel into the substrate binding pocket caused by the mutation of Arg301 (Figure 2.7B). This effect is more pronounced for R301A than R301K. Unfortunately, the side chain of Lys301 exhibits poor electron density in the latter mutant indicating that the Lys does not occupy a well-defined position in the crystal. Attempts to co-crystallize the PTDH mutants with sulfite inhibitor did not yield crystals containing sulfite nor did attempts to soak the ligand into the crystals generate structures that contained sulfite.

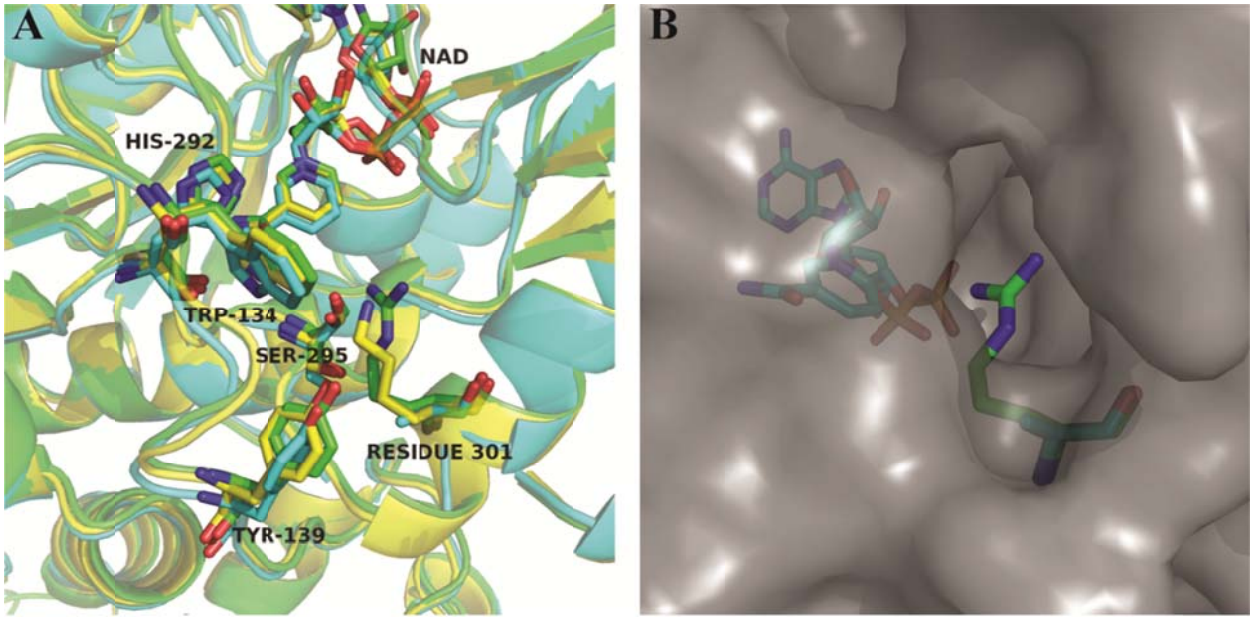

Figure 2.7. (A) Overlay of the crystal structures of 17X-PTDH (green), the R301A mutant (blue), and the R301K mutant (yellow) with NAD^+ bound. Residue 301 is shown with the immediately adjacent residues Trp134, Tyr139, and Ser295, which hydrogen bond to Arg301 in the 17X-PTDH structure. Also shown is the essential residue His292. Note that Lys301 is not well defined in the electron density of the R301K structure and that the best fit is shown here. (B) Surface model of the R301A mutant (grey) overlaid with Arg301 from 17X-PTDH (green) and Ala301 from R301A (blue) in sticks, showing the presence of a solvent-accessible channel into the substrate-binding pocket.

Comparison of the crystal structure of the R301A mutant with that of 17X-PTDH indicates that the mutant has a solvent-exposed phosphite binding site that is covered by the side chain of Arg301 in the parent PTDH. This observation provides a possible explanation for the greatly increased values of $K_{m,Phosphite}$ and $K_{is,sulfite}$ (see below) for the mutant, and indicates that Arg301 may be playing a role to bind phosphite in the active site.

2.2.5 Chemical Rescue Experiments on the Arg301Ala Mutant

The multifaceted but incompletely understood role of Arg301 combined with the solvent exposed active site in the R301A mutant prompted attempts of chemical rescue experiments (*32, 44*) to better define the function of Arg301. The poor activity of the R301A mutant could indeed be markedly improved by addition of exogenous guanidine, methylguanidine, acetamidine,

aminoguanidine, ethylguanidine, or *N*-guanylurea (Table 2.7). Rescue was not observed with nitroguanidine, hydroxyurea, urea, thiourea, imidazole or with primary amines such as methylamine, ethylamine, and butylamine (all tested at concentrations of 20 – 100 mM depending on aqueous solubility limits). The failure for reagents other than guanidine derivatives to rescue mutations of Arg residues has been observed previously for other enzymes (*32, 45*). For each successful reagent, the $k_{cat,apparent}$ (the maximal activity at each concentration of rescue reagent under saturating concentrations of both substrates) of the reaction increased in a hyperbolic fashion as the concentration of rescue reagent was increased (Figure 2.8). At saturating substrate concentrations, the addition of a saturating concentration of rescue agent led to a 10- to 30-fold increase in k_{rescue} ($k_{cat,apparent}$ under conditions of saturating rescue reagent) compared to k_{cat} for the R301A mutant without any rescue reagent, yielding about 40% of wild-type activity with the most effective reagent, aminoguanidine (Table 2.7). Whereas k_{cat} could be restored, the high $K_{m,Phosphite}$ observed with the R301A mutant was not significantly decreased towards wild type values in the presence of saturating rescue reagent. The activity of the parent 17X-PTDH was unaffected at the highest concentrations of rescue reagent used, suggesting that the absence of the Arg301 side chain in the mutant is necessary for the small molecules to affect activity. The stability of the engineered 17X-PTDH towards guanidinium derivatives may be related to its engineered increased thermostability compared to wt PTDH. The observed saturation kinetics with respect to rescue agent for the R301A mutant combined with the unperturbed kinetics of the parent 17X-PTDH in the presence of rescue agent strongly suggest that the observed improvement in catalysis by R301A imparted by the rescue reagents involves a quaternary complex (enzyme, NAD^+, phosphite, and rescue agent).

Table 2.7. Steady State Constants for Chemical Rescue of Activity on R301A

	k_{rescue} (s^{-1})	$K_{m,\ phosphite}$ (mM)	k_{rescue} / $K_{m,\ phosphite}$ ($M^{-1}s^{-1}$)	K_R (mM)	$\log(k_{rescue} / K_R^{Base})$	pK_a [a]	$^D k_{cat}$	$^D k_{cat}/K_m$
R301A + guanidine	1.23 (0.05)	30 (3)	41 (4)	17.9 (2.9)	8.13 (0.07)	13.6	1.79 (0.07)	2.3 (0.1)
R301A + methylguanidine	0.68 (0.04)	130 (30)	5.2 (1.1)	54.5 (9.5)	7.20 (0.08)	13.4	1.35 (0.14)	1.6 (0.5)
R301A + acetamidine	0.86 (0.08)	130 (20)	6.7 (1.1)	63.0 (14.9)	6.33 (0.11)	12.5	1.50 (0.13)	1.8 (0.6)
R301A + aminoguanidine	1.35 (0.04)	7.4 (0.5)	180 (13)	31.5 (1.7)	5.33 (0.03)	11.0	2.10 (0.05)	3.1 (0.3)
R301A + ethylguanidine	0.52 (0.13)	nd	nd	439 (194)	6.09 (0.22)	13.3	nd	nd
R301A + *N*-guanylurea	0.42 (0.07)	nd	nd	116 (36.3)	-2.85 (0.15)	3.9	nd	nd

The errors given in parentheses were obtained from fits of the experimental data to the appropriate equations. na = not applicable. nd = not determined. [a]Data from reference (*46*).

Although the R301K mutant possesses slightly higher activity than the parent enzyme, amine bases failed to affect the activity of the R301A mutant. It is possible that the amines tested could not attain the correct orientation in the active site cleft introduced by the mutation of Arg301 as reported for other examples of unsuccessful rescue of an Arg mutation by alkylamines (*47*).

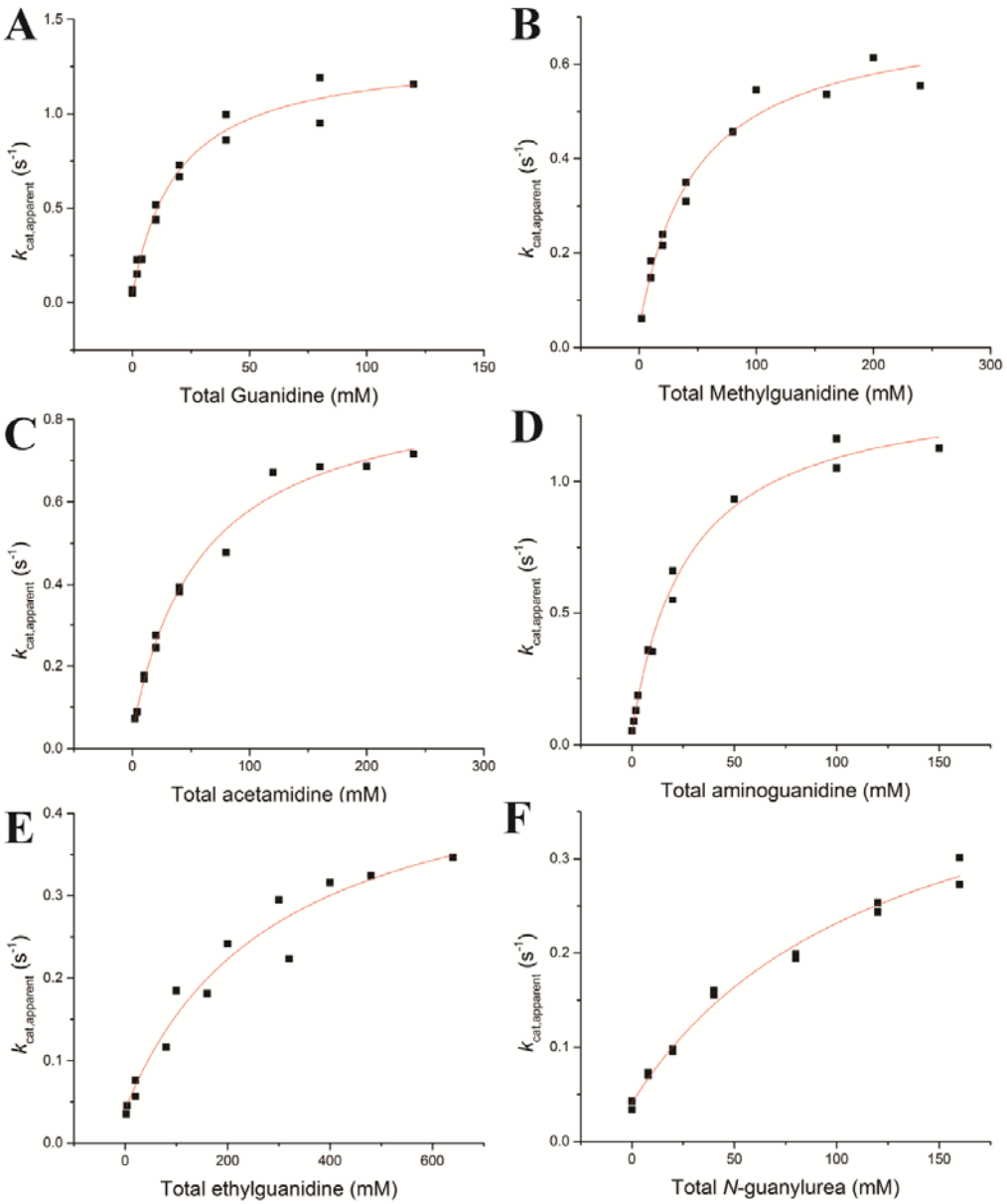

Figure 2.8. Chemical rescue plots of 17X-PTDH-R301A with (A) guanidine, (B) methylguanidine, (C) acetamidine, (D) aminoguanidine, (E) ethylguanidine, and (F) *N*-guanylurea. The values of $k_{cat,apparent}$ at each concentration of rescue reagent were determined by varying the concentration of phosphite and keeping the concentration of NAD^+ fixed at 4 mM (saturated).

The K_R value, which represents the concentration of rescue reagent that gives half maximal rate enhancement, was adjusted to the concentration of rescue reagent in the deprotonated state at the assay pH, K_R^{Base}, and a linear correlation was observed between the efficiency of R301A

rescue and the pK_a of the conjugate acid of the rescue reagent (Figure 2.9A). When fit to equation 2.5 (see Materials and Methods) by linear regression, a value of the Brønsted parameter β of 1.03 ± 0.09 was obtained. The β value near one suggests that transfer of a proton to the guanidine group is complete in the transition state of the rate determining step. When the apparent outlier point was removed (ethylguanidine, pK_a =13.3), a slightly better linear correlation is observed, but the Brønsted parameter does not change significantly (β = 1.05 ± 0.09) (Figure 2.9B). Because correlation between the Taft steric parameters (*48*) of the rescue reagents and rescue activity was poor, the steric contribution was ignored.

Two scenarios can account for the observed β value. First, the deprotonated rescue reagent may act as a general base with complete proton transfer in the transition state of the rate determining step. Alternatively, a pre-equilibrium protonation step prior to the rate limiting step may take place, and the resulting protonated, positively-charged group is important for the rate limiting step. The definition of the Brønsted coefficient allows for both interpretations (*49*), making it difficult to differentiate directly from the rescue data (*50*).

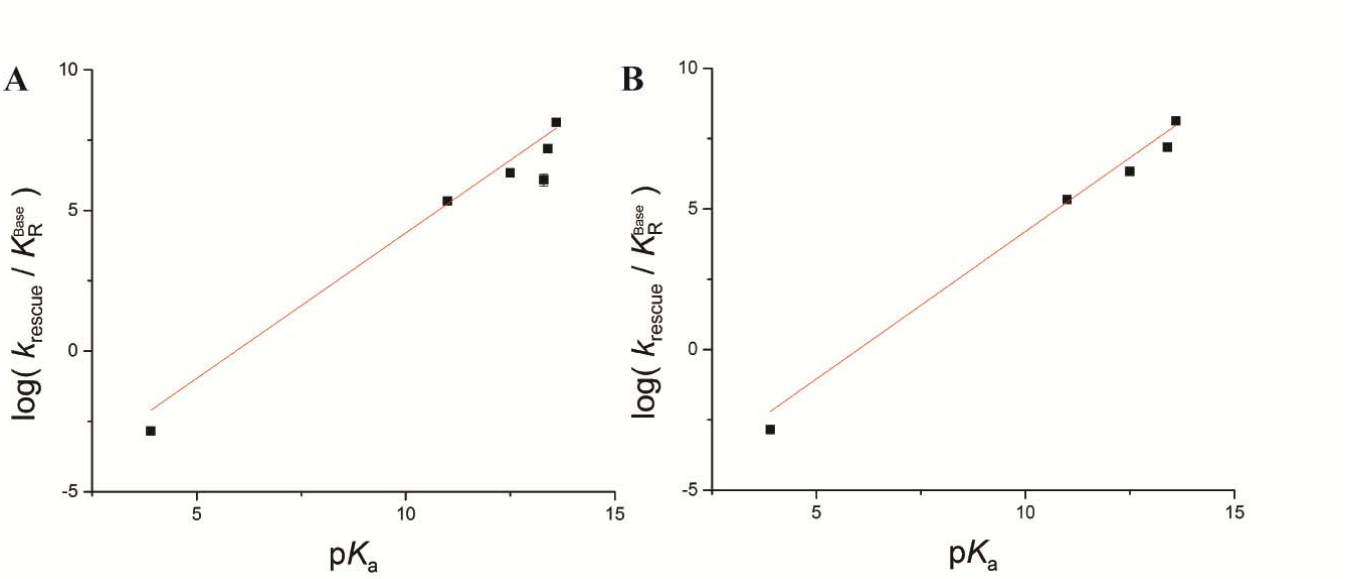

Figure 2.9. Chemical rescue plots for R301A-PTDH. (A) Brønsted plot depicting the observed rates of phosphite oxidation by R301A in the presence of various rescue reagents at pH 7.25 as a function of their pK_a. $\beta = 1.03 \pm 0.09$ ($r^2 = 0.96$). (B) Chemical rescue plot for R301A-PTDH with the data point for ethylguanidine (pK_a = 13.3) removed. $\beta = 1.05 \pm 0.09$ ($r^2 = 0.97$).

2.2.6 Isotope Effect Studies on Chemical Rescue of the Arg301Ala Mutant

Substrate kinetic isotope effects (KIEs) were determined for the assays with R301A in the presence of saturating conditions of rescue agent to determine whether the chemical step remained rate limiting. Although some variation was observed in the KIEs of the R301A mutant when rescue reagents were added (Table 2.7), moderate KIEs were detected on both $^{D}k_{cat}$ and $^{D}(k_{cat}/K_m)$. Hence, chemistry is at least partially rate limited under rescue conditions. Taking into account the experimental errors, the KIEs for the rescue experiments are all quite close to those observed with 17X-PTDH.

The KIEs suggest that the chemical step remains rate-limiting, as is the case in the parent 17X-PTDH (*31*). We reasoned that if a large β value indeed represented full proton transfer to the guanidine group in the transition state of the rate limiting step (i.e. a late transition state with respect to proton transfer), that perhaps increasing the barrier for the chemical step by using

deuterium labeled phosphite might result in a different value for β (note that the site of labeling is not the hydrogen that ends up on the guanidinium group, hence the isotope effect is not on the proton transfer step itself). However, a Brønsted plot using deuterium labeled phosphite resulted in a β value of 1.05 ± 0.07, which is within error of the value obtained for the protiated reagent. Hence, the rather modest change in energy barrier with deuterium-labeled phosphite did not appreciably change the timing of the proton transfer event.

The solvent isotope effect (SIE) on k_{cat} for the wt enzyme is rather small (1.55 ± 0.07) (*11*). In addition, the SIE and substrate KIE are not multiplicative, suggesting that deprotonation of the water nucleophile and hydride transfer are not in the same step (*11*), or that solvent labeling may affect more than just the water deprotonation step (i.e. that the observed SIE is only partially due to the deprotonation step and hence that the isotope effect on water deprotonation is less than 1.55). Such a small isotope effect would not be inconsistent with Arg301 acting as the active site base because a β value of 1 implies a very late transition state (where there is effectively full bond formation between the guanidine nitrogen and the proton), which in turn would be expected to have a small KIE. Of course, SIEs are well known to be difficult to interpret because of the many properties of the enzyme that are affected in D_2O compared to H_2O (*49*). Nevertheless, we also determined the SIE on the reaction catalyzed by the R301A mutant. If Arg were the base that deprotonates the water nucleophile, its removal might be expected to greatly affect the SIE, either because deprotonation would become more important in determining the overall rate (larger SIE), or because the reaction might require specific base catalysis (expected inverse SIE). The observed value of 1.77, which is close to that observed with the wt enzyme, does not provide strong evidence for either. Hence, although not definitive, the SIE studies do not provide evidence for a role of Arg301 as an active site base.

2.2.7 pH Dependence of Chemical Rescue

As discussed above, the observed large slope of the Brønsted plot can be indicative of two different scenarios. Either a neutral guanidine group is completely protonated in the transition state of the rate determining step or the guanidine group needs to already be protonated in a step prior to the rate determining step. As has been noted previously (*32*), in the former case, one would expect the rate at low concentrations of rescue agent to be linearly dependent on the concentration of the unprotonated rescue reagent, whereas in the latter case, one would expect the overall rate to be dependent on the concentration of protonated rescue reagent. Thus, in favorable cases, one can distinguish between these two scenarios by determining the pH dependence of the chemical rescue rates in a pH window where the concentration of the unprotonated reagent varies strongly with pH but the concentration of the protonated reagent does not. For instance, when raising the pH from 7 to 8, the concentration of protonated aminoguanidine (pK_a = 11.0) does not change substantially, whereas the concentration of neutral aminoguanidine increases approximately 10-fold (Table 2.8). Hence, if neutral aminoguanidine were the reagent that is responsible for rescue, the observed rate under conditions where phosphite and NAD^+ are saturating should be directly linear with the concentration of neutral aminoguanidine at low concentrations, and should increase roughly 10-fold in going from pH 7 to 8 (and 3.2-fold going from pH 7.0 to 7.5, Table 2.8). In contrast, if protonated aminoguanidine were the active rescue reagent, then the observed rate under these same conditions should be nearly the same at pH 7 and 8. For PTDH, a complication is that at low concentrations of rescue agent, background catalysis by R301A is significant, and hence its pH dependence, discussed in section 2.2.3, must also be corrected for using equation 2.4 (see Materials and Methods).

Another complication is that the K_m of phosphite for R301A is strongly pH dependent (Table 2.6). Indeed, we found that at pH 8.0 the K_m value was 300 ± 35 mM, and hence very high (i.e. molar) phosphite concentrations were needed to saturate the enzyme. In the presence of rescue agent, the K_m for phosphite decreases somewhat, but in the low millimolar range of rescue reagent, where $k_{cat,apparent}$ would be linear with the concentration of rescue agent, the $K_{m,Phosphite}$ was still larger than 150 mM. Hence all experiments were performed with 1 M phosphite.

Table 2.8. Expected proportion of aminoguanidine (pK_a = 11.0) in unprotonated and protonated states at pH 7.0, pH 7.5, and pH 8.0.

	Unprotonated (RNH_2)	Protonated (RNH_3^+)
pH 7.0	0.01%	99.99%
pH 7.5	0.03%	99.97%
pH 8.0	0.10%	99.90%
Ratio of concentrations of reagent (pH 7.5 : pH 7)	3.2	1.0
Ratio of concentrations of reagent (pH 8 : pH 7)	10	1.0

The chemical rescue experiments were performed at pH 7.0, 7.5, and 8.0 with aminoguanidine as the most efficient rescue agent. Over the pH range, the k_{rescue} value remained mostly unchanged, though a slight decrease in K_R was observed as the pH increased. At pH 7.0, k_{rescue} = 1.17 ± 0.05 s^{-1} and K_R = 64.5 ± 8.81 mM, at pH 7.5, k_{rescue} = 0.91 ± 0.07 s^{-1} and K_R = 22.7 ± 6.2 mM, and at pH 8.0, k_{rescue} = 1.12 ± 0.06 s^{-1} and K_R = 9.9 ± 2.3 mM. At low concentrations of rescue reagent (i.e. K_R >> [rescue agent]), equation 2.4 (Materials and Methods) simplifies and $k_{cat,apparent}$ corresponds to (k_{rescue}/K_R)[rescue agent] + $k_{cat,R301A}$. At each pH value, a linear increase in $k_{cat,apparent}$ was observed as the concentration of aminoguanidine was increased (Figure 2.10A). As expected, after correction of the pH dependence of the background activity by R301A, the

lines nearly intersect in the absence of aminoguanidine (Figure 2.10B). The slope of the line at pH 8.0 is significantly larger than at pH 7.0 with a ratio of 3.72 ± 0.31, and the ratio of the slopes of the lines at pH 7.5 and pH 7.0 is 1.23 ± 0.10. Both of these ratios are, however, significantly smaller than those expected if the unprotonated compound were the active rescue agent (expected ratios of 10 and 3.2, respectively, see dashed lines of Figure 2.10B). Conversely, they are also larger than 1.0 (expected if the protonated aminoguanidine were the active rescue agent). The experiment was repeated with a different batch of enzyme and reagents, but these experiments resulted in similar ratios of slopes of 3.0 ± 0.1 (pH 8.0: pH 7.0) and 1.6 ± 0.1 (pH 7.5 : pH 7.0). Similar results were also observed when the pH dependence of chemical rescue was performed with guanidine instead of aminoguanidine. Hence, the experimental pH dependence of rescue activity was not definitive with respect to the protonation state of aminoguanidine that is required for rescue. It may be that the pH dependence of the background reaction combined with the strong pH dependence of K_m for phosphite are in part responsible for the inconclusive outcome of these experiments.

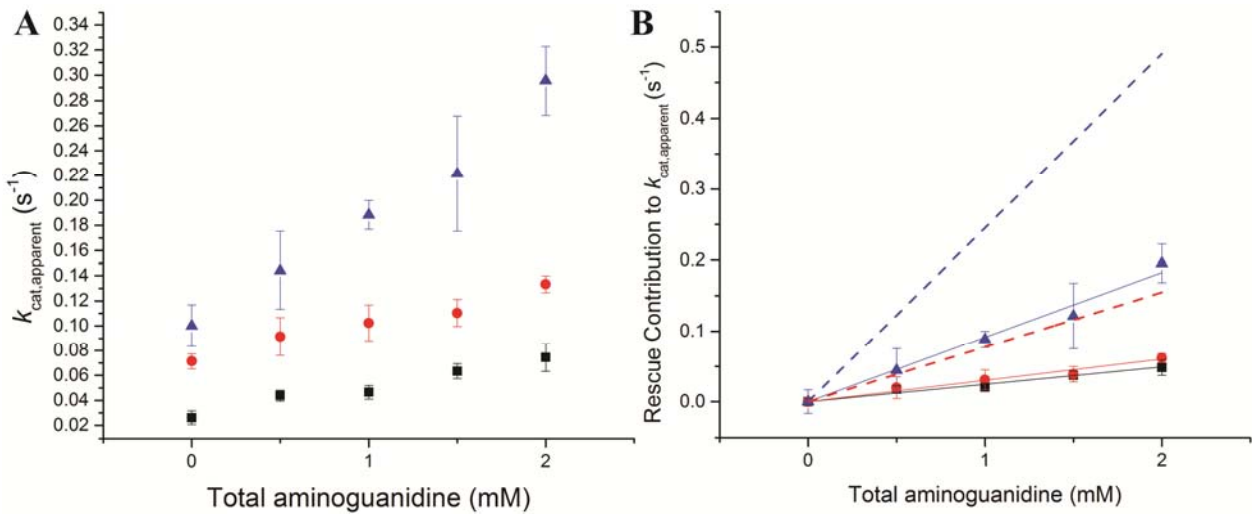

Figure 2.10. pH dependence of chemical rescue for R301A-PTDH. Dependence of the rate of chemical rescue on the concentration of aminoguanidine at pH 7.0 (black squares), pH 7.5 (red circles), and pH 8.0 (blue triangles) (A) prior to correction for the background activity of R301A without rescue agent at each pH and (B) corrected for the pH-dependence of $k_{cat,R301A}$. Also shown is the expected activity at pH 7.5 (red dashed line) and pH 8.0 (blue dashed line) based on the observed activity at pH 7.0 if the active reagent were the unprotonated aminoguanidine. Experiments were performed in duplicate; when error bars are not visible, the error was smaller than the marker.

2.2.8 Sulfite Inhibition Experiments

K_m values of substrates can greatly deviate from their corresponding K_d values because the K_m term typically contains many more microscopic rate constants than the K_d term. On the other hand, the inhibition constants of competitive inhibitors (K_{is}) can provide a direct reflection of the influence of mutations on binding events. Inhibition experiments were therefore performed with R301A to determine the K_{is} value for sulfite (Table 2.9). Similarly to the large increases in $K_{m,Phosphite}$ that were observed for the mutant compared to the parent 17X-PTDH (Table 2.4), the K_{is} value also greatly increased. A K_{is} of 0.31 ± 0.05 μM was observed for 17X-PTDH (Figure 2.11) whereas the K_{is} increased to 132.6 ± 19.3 μM for R301A, corresponding to a more than 400-fold increase. This effect is comparable in magnitude with the nearly 700-fold increase in $K_{m,Phosphite}$. When saturating concentrations of aminoguanidine rescue reagent were added to the

reaction with the R301A mutant, the K_{is} value of 77.8 ± 8.4 μM was only slightly decreased compared to the value in the absence of rescue agent. Thus, addition of the rescue reagent fails to substantially recover inhibitor binding, just as it is unable to recover $K_{m,phosphite}$. The K_{is} for R301K was 0.608 ± 0.051 μM, considerably lower than that of R301A-PTDH but still slightly increased from 17X-PTDH.

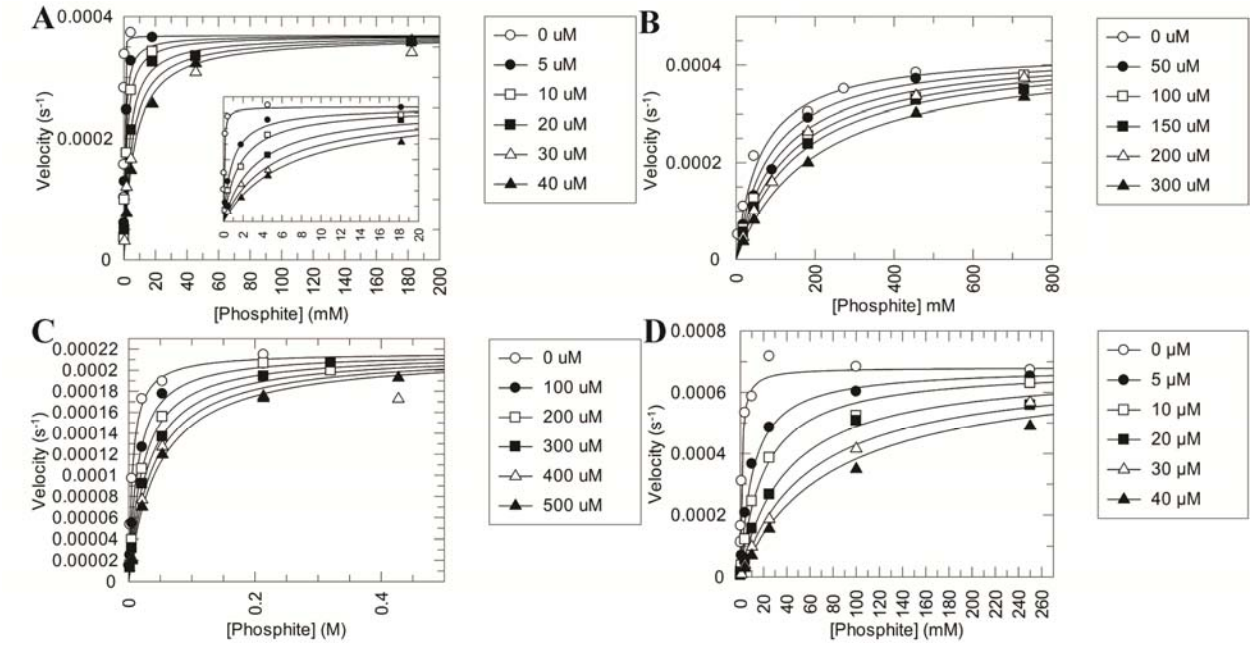

Figure 2.11. Inhibition of PTDH activity by sulfite for (A)17X-PTDH, (B) R301A-PTDH, (C) R301A-PTDH + saturating aminoguanidine, and (D) R301K-PTDH. The different symbols indicate the concentration of sulfite added.

Overall, the large increase in the dissociation constant for sulfite indicates that Arg301 plays a role in inhibitor binding, and likely phosphite binding. This observation is consistent with the crystal structure of the R301A mutant, which shows that a cavity into the phosphite binding region of the active site is formed (Figure 2.7B). The smaller increase in the inhibition constant for sulfite for R301K is consistent with the smaller increase of $K_{m,Phosphite}$ in this mutant, and suggests that the Arg301Lys mutation may be able to regain some of the phosphite binding lost

in the R301A mutant by blocking the channel into the active site, which is again consistent with the placement of the residue in the active site (Figure 2.7A).

In addition to the sulfite dissociation constants, the K_d for phosphite itself can be calculated from $^{D}(V/K)$, ^{D}V and $K_{m,Phosphite}$ using the method of Klinman and Matthews (*51*). The K_d for phosphite so determined is 23 ± 6 μM for 17X-PTDH and 12.6 ± 1.5 mM for R301A, again showing a large decrease in affinity for the substrate in the mutant. Collectively, these findings along with the X-ray structures illustrate that proper positioning of the side chain of Arg301 is very important for efficient capturing of phosphite (*52*), which cannot be recapitulated by the rescue agents for the R301A variant.

Table 2.9. Sulfite inhibition constants for Arg301 mutants of 17X-PTDH

	K_{is} (μM)
17X-PTDH	0.31 (0.05)
R301A	130 (20)
R301A + aminoguanidine	78 (8)
R301K	0.61 (0.05)

2.3 Conclusions

The studies presented here indicate that PTDH activity is not unique to the enzyme from *P. stutzeri,* but that the PTDHs are instead a distinct branch of the greater DHDH family. The reaction catalyzed by PTDHs has a very strong thermodynamic driving force and it has been speculated that perhaps the rather moderate values of k_{cat} were the result of a "young" enzyme that had relatively recently evolved from a progenitor in the DHDH family (*11*). The strong

sequence diversity suggests that instead phosphite oxidation is likely an old activity, and the very similar catalytic parameters, combined with the inability to increase k_{cat} substantially by directed evolution (*53*), suggest that the rates of phosphite oxidation by PTDHs may be limited by a relatively high intrinsic barrier.

With the recently determined crystal structure of TS-PTDH (*1*) and the sequences of additional PTDH orthologs with moderate sequence homology to the enzyme from *P. stutzeri*, several previously unidentified conserved residues near the active site have been revealed. These amino acids include Ser295, Tyr139, Trp134, and Arg301, which are conserved among the known members of the PTDH family but not the greater DHDH family. While mutations to Ser295, Tyr139, and Trp134 have minimal effect on k_{cat} of the reaction, the Arg301Ala mutant exhibits ~ 100-fold reduced k_{cat} and greatly increased K_m for phosphite, indicating that it plays an important role in the reaction.

From its position in the crystal structure, Arg301 could be playing a number of roles in catalysis. It is in good position and orientation relative to a water molecule in the active site that would allow it to act as the catalytic base to deprotonate the water nucleophile that attacks phosphite. Alternatively, it could act as a positively charged residue to promote electrostatic catalysis. Initial studies to probe the mechanism of catalysis with a pH rate profile of R301A proved inconclusive, as KIE experiments showed the mechanism of R301A changes over the pH range. However, the pH rate profile of the R301K mutant exhibited a shift in the basic limb of the $\log(k_{cat}/K_{m,Phosphite})$, suggesting that Arg301 may act in electrostatic catalysis by destabilizing the His292 imidazolium.

The crystal structure of the R301A mutant exhibits a solvent-exposed phosphite binding site that is covered by the side chain of Arg301 in the wild type structure. The appearance of a cleft

into the active site prompted the attempt of chemical rescue studies, which showed that exogenous guanidinium analogs were able to enhance activity of the R301A mutant. Brønsted linear free energy analysis with the rescue reagents yielded a high β value, which could be attributed to a high degree of proton transfer to the rescue reagent in the transition state of the rate limiting step of the reaction (if Arg301 acts as a base). Alternatively, a pre-equilibrium protonation event of Arg301 could occur, which would again result in the group be fully protonated at the transition state of the rate-determining step.

Although the pH dependence of rescue unfortunately did not conclusively resolve whether the rescue reagent is in the protonated or unprotonated state, a protonated aminoguanidine as the active rescue agent (and hence a protonated Arg side chain in the wild type enzyme) is the most straightforward interpretation of all the current data. The essentially complete proton transfer indicated by the β value, the very small SIE for the wt enzyme, and the previous finding that the SIE and substrate KIE on k_{cat} were not multiplicative for the wt enzyme (*11*), suggesting that deprotonation of the water nucleophile and hydride transfer are not in the same step, are all in agreement with a protonation of the guanidine prior to the rate limiting step. In addition, if Arg were the base that deprotonates the water nucleophile, its removal might be expected to greatly affect the SIE, either because deprotonation would become more important in determining the overall rate (larger SIE), or because the reaction might require specific base catalysis (inverse SIE expected). The observed SIE of 1.77, which is close to that observed with the wt enzyme, does not provide strong evidence for either. Hence, although not definitive, I tentatively conclude that Arg301 is protonated during catalysis and is not the active site base.

The importance of the protonated side chain for catalysis is obvious, given the large decrease in k_{cat} upon its removal in R301A, and the fact that addition of exogenous guanidine analogs can

recover activity. The purpose of Arg301 in catalysis may be to properly orient phosphite for efficient hydride transfer, to activate the water molecule for deprotonation, or to activate the phosphite electrophile electrostatically. The pH profiles also indicate that it is possible that Arg301 decreases the pK_a of the imidazolium group of His292 such that it can serve as the base. Inhibition experiments showed that the R301A mutant binds the sulfite inhibitor poorly, which correlates with the high K_m and K_d for phosphite of the mutant. Addition of rescue reagent was unable to improve sulfite binding, indicating that Arg301 is important for the binding of the phosphite substrate, and this role may be independent of its electrostatic role in catalysis.

Overall, these studies suggest that Arg301 is not the catalytic base in the PTDH reaction. It is likely that His292 instead plays this role. The orientation of His292 in the enzyme active site is consistent with a role as a base (*1*), and His292 mutations completely abolish activity (*3*), as does covalent modification of the His residues by DEPC (*3*). Unfortunately, previous attempts to rescue activity of mutants of His292 by Dr. Emily Fogle were unsuccessful (*43*).

2.4 Materials and Methods

2.4.1 Materials

All chemicals were obtained from Sigma or Aldrich and used without further purification. The development of 17X-PTDH is reported in (*54*); in the reference this mutant is called 12X-PTDH, but it actually contains 17 mutations. In the crystal structure of 17X-PTDH, all mutated residues are distant from the active site, with the exception of E175A, which disrupts an interaction with the ribose group of NAD^+ to allow NADP to be used as a substrate (*1*).

2.4.2 General methods

The concentration of NAD^+ stock solutions were determined by the absorbance at 260 nm (ε = 18,000 M^{-1} cm^{-1}). The concentration of stock solutions of phosphite was determined by running the PTDH reaction to completion in the presence of excess NAD^+. The maximum absorbance at 340 nm was then measured, which represents the concentration of NADH formed (ε = 6.2 mM^{-1} cm^{-1}) and is equivalent to the concentration of phosphite consumed. Tris buffer was made from Tris base and adjusted to the correct pH with 5 M HCl; MOPS and MES buffers were made by adjusting the pH using 5 M NaOH.

2.4.3 Cloning of the ptxD Gene from Methylobacterium extorquens AM1

M. extorquens AM1 (ATCC 14718) was purchased (ATCC #14718) and grown in nutrient broth at 30 °C for 48 h. The culture was then pelleted and the genomic DNA extracted using an Ultra Clean Microbial Genomic DNA Kit (MO-BIO). The gene from *M. extorquens* was then amplified from the purified genomic DNA using the following primers: 5'-GCCAGTTCCATATGAGAGCCAAGG-3' and 5'-CTCACACTCGAGTCACGGATGTCG-3'. The primers contain *Nde*I and *Xho*I restriction sites (underlined) which were used to incorporate the gene into pET28a. (JEH-5-13, JEH-5-18).

2.4.4 Preparation of 17X-PTDH Mutant Constructs

All mutants were generated in the 17X-PTDH background using the pET15b plasmid unless noted otherwise. The mutants were prepared by the polymerase chain reaction (PCR) using QuikChange mutagenesis (Agilent). The following primers were used to incorporate the mutations (along with their reverse complement strands, which are not listed): R301K: 5'- GTG

CGC GCG GTG AAA CTG GAG ATT GAA C -3'; S295A: 5'-CCG CAC ATA GGG GCG GCA GTG CGC GCG-3'; Y139F: 5'-C TGG CAA CCA CGG TTC TTC GGC ACG GG-3'; W134F: 5'-GC AAG TTC CGG GGC TTC CAA CCA CGG TTC TAC-3'; W134A: 5'-GC AAG TTC CGG GGC GCG CAA CCA CGG TTC TAC-3'. The mutated codon is underlined in each case. The R301A mutant was prepared by Tyler Johannes in the Zhao group, as detailed in (*7*). Once the mutant genes were constructed, they were sequenced in their entirety to ensure that the desired mutation was incorporated and no other mutations were generated. (JEH-4-32, JEH-4-55, JEH-4-73, JEH-4-93, JEH-5-85).

2.4.5 Overexpression and Purification of PTDH Mutants

To obtain mutants of 17X-PTDH, chemically competent *E. coli* BL21 (DE3) cells were transformed with plasmids containing the desired gene in pRW2 vector and plated on a LB agar plate containing 100 μg/mL ampicillin. A single colony was picked and used to inoculate an overnight culture (50 mL). The cells were harvested by centrifugation, resuspended in 1 L of LB/ampicillin and grown at 37 °C to $OD_{600\ nm}$ = 0.6. IPTG was added to the culture (0.3 mM final concentration), which was incubated at 18 °C for 16-20 h. Cells were then pelleted by centrifugation (8,000 × *g*, 30 min), resuspended in 20 mM Tris pH 7.6, 0.5 M NaCl, 10% glycerol (v/v), and stored at −80 °C. The resuspended pellet was then thawed on ice and lysed using an Avestin Emulsiflex-C3 Homogenizer (15 kPsi, 6 passes). The insoluble lysate was removed by centrifugation (15,000 × *g*, 30 min), and the soluble lysate was passed through a 0.44 μm filter. The enzyme was purified via FPLC (Äkta) by immobilized metal affinity chromatography with a HisTrap HP Ni^{2+}-affinity column (GE Life Sciences). The column was washed with 5 CV of buffer A, followed by a gradient to 40% buffer B over 5 CV, and another

gradient of 2 CV to 100% buffer B (buffer A: 20 mM Tris pH 7.6, 100 mM NaCl, 10 mM imidazole, 10% glycerol (v/v); buffer B: 20 mM Tris pH 7.6, 100 mM NaCl, 500 mM imidazole, 10% glycerol (v/v)). Fractions containing 17X-PTDH mutants were identified by activity assay and analyzed by SDS-PAGE. The fractions that showed only PTDH by SDS-PAGE were pooled and concentrated using centrifugal filtration (Amicon membrane, 30 kDa molecular weight cutoff; Millipore), followed by buffer exchange or dialysis to 20 mM MOPS pH 7.6, 100 mM KCl, 10% glycerol. Protein purity was >95% based on FPLC analysis and SDS-PAGE analysis. Specific activities for several independent purifications of each mutant were found to be comparable, further suggesting that the enzyme was highly pure. The k_{cat} values shown in Table 1 are the average of three independent measurements. The protein solution was then flash frozen and stored at −80 °C. Protein concentrations were determined in triplicate using the calculated extinction coefficient for 17X-PTDH, 28,000 M^{-1} cm^{-1} (*31*). For Trp134 mutants, the extinction coefficient was calculated to be 21,000 M^{-1} cm^{-1} (ExPASy ProtParam tool). For comparison, protein concentrations for a stock solution of 17X-PTDH were also determined by the method of Bradford (*55*), using Coomassie Plus reagent (Thermo Scientific) and bovine serum albumin (BSA) to generate a standard curve. Measurements were taken at 595 nm and compared to the standard curve to determine protein concentration, using the calculated molar mass of 17X-PTDH. Experimental measurements were obtained in triplicate in each case. Concentrations of 22.4 ± 1.3 μM and 22.7 ± 0.1 μM were determined by absorbance at A280 using the calculated extinction coefficient and the Bradford method, respectively. The concentrations determined by each method were within experimental error of one another. The PTDH from *M. extorquens* was purified using the same method.

2.4.6 Steady State Kinetic Assays

Initial rates were determined using a Cary 4000 UV-vis spectrophotometer (Agilent) to monitor the rate of formation of NADH using its absorbance at 340 nm (ε = 6.2 mM^{-1} cm^{-1}). Typical reactions were performed in 100 mM MOPS at pH 7.25. For 17X-PTDH, R301K, and R301A, a full set of kinetic data was collected varying both the phosphite and NAD^+ concentrations (Figure 2.5). For 17X-PTDH the following concentrations were used for both substrates: 0.03, 0.05, 0.07, 0.10, 0.20 and 0.50 mM and 0.0910 ± 0.0004 μM enzyme. For R301K, the NAD^+ concentrations used were 0.02, 0.05, 0.10, 0.20, 0.50 and 1.0 mM and the phosphite concentrations used were 0.50, 1.0, 2.0, 5.0, 10.0 and 20.0 mM, with 0.126 ± 0.001 μM enzyme. For R301A, the NAD^+ concentrations were 0.1, 0.2, 0.5, 1.0, 3.0 and 6.0 mM, and the phosphite concentrations 9.0, 18, 45, 90, 181 and 271 mM, using 4.976 ± 0.022 μM enzyme. For the other mutants, NAD^+ was held at saturating concentrations of 4 mM (> 16 × $K_{m,NAD}$) while the phosphite concentration was varied, or NAD^+ concentrations were varied while phosphite was held at a saturating concentration of 2.2 mM for S295A (21 × $K_{m,Phosphite}$), 9.0 mM for W134F (26 x $K_{m,Phosphite}$), 46.5 mM for W134A (24 × $K_{m,Phosphite}$), and 5.0 mM for Y139F (128 × $K_{m,Phosphite}$). Enzyme concentrations were 0.259 ± 0.001 μM for S295A; 0.147 ± 0.001 μM for Y139F; 0.233 ± 0.001 μM for W134A; and 0.215 ± 0.001 μM for W134F. Error bars on k_{cat} were obtained from three independently purified batches of protein.

For the kinetic assays, reaction mixtures were allowed to equilibrate at 25 °C in a controlled temperature block, which was verified using a thermocouple inserted into the cuvette, and the reaction was initiated by addition of enzyme. Assays on the 17X-PTDH mutants were performed with the His_6-affinity tag attached. The His-tag has been shown not to have a significant effect on the kinetic parameters of the enzyme in a previous study (*56*). Assays for PTDH orthologs

were performed at 30 °C. Initial rates were obtained over the course of one minute. The data were fit to the Michaelis-Menten equation using OriginPro 8 (OriginLab) for the orthologs and the mutants of Ser295, Trp134, and Tyr139 or using the equation for an ordered, sequential, two-substrate mechanism (equation 2.1) (*30*) using GraFit 7 (*57*) for 17X-PTDH, R301A, and R301K. In this equation, A represents the first substrate to bind (NAD^+), and B represents the second substrate (phosphite). K_A and K_B are $K_{m,NAD}$ and $K_{m,Phosphite}$, respectively. K_{ia} represents the dissociation constant for NAD^+. (JEH-6-58, JEH-6-59, JEH-6-61, JEH-6-65, JEH-6-78, JEH-6-93).

$$v = \frac{V_{max}[\mathrm{A}][\mathrm{B}]}{K_{ia}K_B + K_B[\mathrm{A}] + K_A[\mathrm{B}] + [\mathrm{A}][\mathrm{B}]} \quad (\mathrm{eq.}\ 2.1)$$

2.4.7 Kinetic Isotope Effects

Deuterium-labeled phosphite was prepared as reported previously *(11)* by mixing phosphorous acid with deuterium oxide at 50 °C for 6 h. The solution was then concentrated by rotary evaporator and the residue redissolved in deuterium oxide. This procedure was repeated until only deuterium-labeled phosphite was observed by ^{31}P NMR spectroscopy (500 MHz Varian, H_3PO_4 used as external reference, δ = 0 ppm): δ 3.71 (t, $J_{P\text{-}D}$ = 88 Hz). The solution was then neutralized using aqueous NaOH and lyophilized to obtain solid deuterium labeled sodium phosphite. Kinetic isotope effects (KIEs) were determined by holding NAD^+ at saturating conditions (>10 × K_m) and obtaining initial rates with varying concentrations of either deuterated or protiated phosphite. The pH of the assay mix prior to enzyme addition was verified prior to initiation of the assay. (JEH-3-11, JEH-3-13, JEH-3-60, JEH-4-08, JEH-4-16, JEH-4-25).

2.4.8 pH Rate Profiles of 17X-PTDH Mutants

Solutions containing 100 mM Tris, 50 mM MES, and 50 mM acetic acid, generating a universal buffer of constant ionic strength (*38*), were prepared at pH 5.5, 5.8, 6.1, 6.4, 6.7, 7.0, 7.3, 7.6, 7.9, 8.2, 8.5, 8.8 and 9.0. NAD^+ was dissolved in buffer of desired pH and phosphite stock solutions were adjusted to the pH of the assay. Experiments were also performed in 100 mM Tris maleate, a broad range buffer, as well as in 100 mM MOPS from pH 6.7 to pH 7.7. NAD^+ was held at saturating conditions (>10 × K_m), whereas phosphite concentrations were varied from 0.05-1500 mM (for 17X-PTDH-R301A), 0.5-500 mM (for 17X-PTDH-R301K), and 0.15-50 mM (for 17X-PTDH). The concentrations of phosphite used at each pH varied according to the $K_{m,Phosphite}$ at that pH, ranging from approximately 0.2 × K_m to >10 × $K_{m,Phosphite}$. Reactions were mixed and allowed to equilibrate for several minutes to adjust the temperature and ensure homogeneity until the baseline absorbance at 340 nm remained constant. Reactions were initiated by addition of 17X-PTDH (0.16 μM final), 17X-PTDH-R301K (0.08 μM final), or 17X-PTDH-R301A (3-6 μM final). Initial rates of NADH formation were monitored at 340 nm using a Cary 4000 spectrophotometer. Kinetic parameters were determined from fits to the Michaelis-Menten equation using OriginPro 8, and pK_a values were determined by fitting logarithmic plots of k_{cat} and k_{cat}/K_m to the equation for curves with one or two proton transitions (equations 2.2 and 2.3, respectively) (*58*), with K_1, K_2, and $(k_{cat}/K)_0$ representing dependent variables that are calculated by fitting of the data. K_1 represents the acid dissociation constant for a proton transition that increases activity upon deprotonation (ascending limb) and K_2 represents the acid dissociation constant for a proton transition that decreases activity upon deprotonation (descending limb); $(k_{cat}/K)_0$ is a pH-independent value. (JEH-3-44, JEH-6-38, JEH-6-43, JEH-6-46)

$$\log\left(\frac{k_{cat}}{K_m}\right) = \log\left(\frac{\left(\frac{k_{cat}}{K_m}\right)_0}{1 + \frac{[H^+]}{K_1}}\right) \quad \text{(eq. 2.2)}$$

$$\log\left(\frac{k_{cat}}{K_m}\right) = \log\left(\frac{\left(\frac{k_{cat}}{K_m}\right)_0}{1 + \frac{[H^+]}{K_1} + \frac{K_2}{[H^+]}}\right) \quad \text{(eq. 2.3)}$$

2.4.9 Gel Filtration Experiments

Gel filtration experiments were performed on a BioSil SEC-250 (BioRad) HPLC gel filtration column using a buffer composed of 100 mM MOPS pH 7.3, 0.4 M sodium phosphite. Albumin, alcohol dehydrogenase, β-amylase, blue dextran, carbonic anhydrase, and cytochrome C standards (Sigma-Aldrich) were used to generate a standard curve. 17X-PTDH-R301A and 17X-PTDH were run on the column with and without 5 mM NAD^+. The retention time was unaffected by the presence of cofactor. The elution time compared to that of the standards was used to determine the oligomerization states of the proteins. (JEH-3-97).

2.4.10 Protein Crystallography of Arg301Ala and Arg301Lys

To remove the His_6-affinity tag, thrombin (MP Biomedicals, 1 U / mg PTDH) was added to the Ni^{2+}-affinity purified protein during overnight dialysis at 4 °C. The cleavage product was purified by FPLC with a Superdex 200 gel filtration column (GE Healthcare) in 20 mM HEPES with 100 mM KCl (pH 7.5). The cleaved protein was determined to be >95% pure by SDS-

PAGE and FPLC analysis and full activity was observed for each His-tag-cleaved mutant by steady-state kinetic assay.

Crystals of both PTDH variants were grown using the hanging drop method. Following gel-filtration, samples of each variant were concentrated to 10 mg/mL and incubated with 10 mM NAD^+ for 30 min and then equilibrated against a reservoir of 0.1 M NaCl, 0.1 M sodium cacodylate pH 5.8, 16% PEG 6000 (w/v) (for R301K) or 0.1 M ammonium acetate, 0.1 M Bis Tris pH 5.5, 17% PEG 10000 (w/v) (for R301A, performed by Neha Garg). Crystallization samples were incubated at 288 K for 5-7 days. Prior to data collection, crystals of each PTDH variant were briefly immersed into a solution composed of the crystallization media supplemented with 20% (v/v) glycerol and vitrified by direct immersion into liquid nitrogen. The crystals were diffracted and the data solved by Jonathan Chekan and Professor Satish Nair; final data collection and crystallographic statistics are detailed in (*43*). (JEH-7-96).

2.4.11 Chemical Rescue Experiments with 17X-PTDH-R301A

The initial rates with and without rescue agent were determined at 25 °C. Typical reactions were conducted in 100 mM MOPS pH 7.25, and contained 1 μM 17X-PTDH-R301A, 4 mM NAD^+ (saturated), a defined concentration of rescue reagent, and varying phosphite concentrations. Control experiments showed that activity above background was only observed when enzyme, NAD^+, phosphite and rescue agent were present. At several different concentrations of rescue reagent, phosphite concentration was varied to obtain a Michaelis-Menten curve from which the maximal activity at each concentration of rescue reagent ($k_{cat,apparent}$) was extracted. The values of $k_{cat,apparent}$ so determined were then plotted against the concentration of rescue reagent and fit to equation 2.4 (*44, 59*) to obtain K_R, the concentration of rescue reagent at which half-maximal

rate was observed, and k_{rescue} ($k_{cat,apparent}$ under conditions of saturating rescue reagent). The purity of the rescue reagent was verified prior to running assays by ^{13}C NMR analysis. The apparent $K_{m,Phosphite}$ was determined by holding the concentration of rescue agent and NAD^+ at saturating conditions (>10 × K_R) and varying the concentration of phosphite. Addition of rescue reagent at this concentration to the reaction catalyzed by the parent 17X-PTDH had no effect on activity. The compounds tested as rescue agents were acetamidine, guanidine, methylguanidine, aminoguanidine, ethylguanidine, nitroguanidine, *N*-guanylurea, methylamine, and ethylamine. Other compounds, including urea, hydroxyurea, thiourea, *n*-butylamine, and imidazole were tested by Dr. Emily Fogle (*43*). A Brønsted plot was constructed by plotting the pK_a values of the conjugate acids of the successful rescue agents against $\log(k_{rescue} / K_R^{Base})$ (Equation 2.5), where K_R^{Base} is the K_R parameter, corrected for free base concentration at pH 7.25 (*32, 44*), and β is the Brønsted coefficient. (JEH-5-87, JEH-5-89, JEH-5-91, JEH-7-53)

$$k_{cat,apparent} = (k_{rescue}[\text{rescue reagent}])/(K_R + [\text{rescue reagent}]) + k_{cat,R301A} \quad \text{(eq. 2.4)}$$

$$\log(k_{rescue} / K_R^{Base}) = \beta(pK_a) + C \quad \text{(eq. 2.5)}$$

2.4.12 pH Dependence of Chemical Rescue

Reactions were performed at 0, 0.5, 1.0, 1.5, or 2.0 mM aminoguanidine sulfate or guanidine HCl in 100 mM MOPS at pH 7.0, 7.5, and 8.0. These concentrations were selected as they are less than ½ K_R and would be within the initial linear region of a square hyperbola for recovery of activity. NAD^+ concentration was held at 4 mM, which was verified to be saturating at each pH value and at all concentrations of rescue reagent used. Phosphite was similarly held at saturating conditions of 1 M. For the pH rate profile of R301A with aminoguanidine, saturating

concentrations of 1 M rescue reagent were utilized at each pH value, and the experiment was performed as detailed in section 2.4.8. (JEH-5-56, JEH-8-10, JEH-8-22, JEH-8-28).

2.4.13 Solvent Isotope Effect Experiments on 17X-PTDH-R301A

All buffers and reagents were prepared in D_2O and adjusted by addition of DCl or NaOD, according to pD = pH-reading + 0.4. Sodium phosphite hexahydrate salt was dissolved in D_2O (25 mL) to create a 0.5 M stock and the pH was adjusted to the desired value. The solution was then lyophilized and resuspended in D_2O, and this procedure was repeated twice. The enzyme was diluted from a stock solution into 100 mM MOPS in D_2O (1:10 dilution of enzyme, 30 min on ice). The reactions were performed in 100 mM MOPS with 4 mM NAD^+ at pD 7.25 and initiated by addition of 4 μM R301A-PTDH. To obtain the solvent isotope effect, the rate constants observed in D_2O were directly compared with those obtained from the reaction performed in H_2O at pH 7.25. Following the reaction, the stock of phosphite in D_2O was analyzed by ^{31}P NMR spectroscopy to verify no ^{2}H-phosphite was formed during the incubation period. (JEH-5-57).

2.4.14 Kinetic Isotope Effects for Chemical Rescue Experiments

Deuterium-labeled phosphite was prepared as reported previously in section 2.4.7. Kinetic isotope effects (KIEs) were determined by holding NAD^+ at saturating conditions of 4 mM and obtaining initial rates with varying concentrations of either deuterated or protiated phosphite. Experiments were performed in 100 mM MOPS (pH 7.25) at 25 °C with saturating amounts (>20 × K_R) of rescue reagent. Apparent Michaelis-Menten constants were obtained from these

data. The ratios of the apparent rate constants k_{cat} and k_{cat}/K_m for labeled and unlabeled phosphite yielded $^{D}k_{cat}$ and $^{D}(k_{cat}/K_m)$, respectively.

The overall isotope effect on the Brønsted rescue plot was determined by holding phosphite or deuterium-labeled phosphite at saturating concentrations (>10 × K_m) and varying the concentration of each rescue reagent. A Brønsted plot was generated for each isotopologue of phosphite and the Brønsted constant, β, was determined as described above. (JEH-7-22, JEH-7-65).

2.4.15 Sulfite Inhibition Studies with 17X-PTDH-R301A

Reactions were performed in 100 mM MOPS (pH 7.25) at saturating concentrations of 4 mM NAD^+. Sodium sulfite was adjusted to the desired concentration by serial dilution from a 0.5 M stock solution. Sulfite concentration was adjusted to 0, 50, 100, 150, 200 or 300 μM for R301A; 0, 50, 100, 300 or 600 μM for R301K; or 0, 0.5, 1, 5, 10 or 20 μM for 17X-PTDH. An experiment was also performed with 17X-PTDH-R301A and saturating concentrations of 300 mM aminoguanidine, with sulfite concentrations of 0, 100, 200, 300, 400 or 500 μM. The reaction was initiated by addition of PTDH (0.1 μM final concentration, or 5 μM for R301A). At each concentration of inhibitor, phosphite concentration was varied. The data was analyzed in GraFit 7.0 (*57*) using the equation for competitive inhibition (Equation 2.6) to fit all of the data, where I is the inhibitor concentration and K_{is} is the dissociation constant for a competitive inhibitor (*29*). (JEH-6-31, JEH-6-34, JEH-6-35, JEH-7-33, JEH-8-20)

$$v = \frac{V_{max}[S]}{K_m\left(1+\frac{[I]}{K_{is}}\right)+[S]} \quad \text{(eq. 2.6)}$$

2.5 References

1. Zou, Y., Zhang, H., Brunzelle, J. S., Johannes, T. W., Woodyer, R. D., Hung, J. E., Nair, N., van der Donk, W. A., Zhao, H., and Nair, S. K. (2012) Crystal structures of phosphite dehydrogenase provide insights into nicotinamide cofactor regeneration, *Biochemistry 51*, 4263-4270.
2. Costas, A. M., White, A. K., and Metcalf, W. W. (2001) Purification and characterization of a novel phosphorus-oxidizing enzyme from Pseudomonas stutzeri WM88, *J. Biol. Chem. 276*, 17429-17436.
3. Woodyer, R., Wheatley, J., Relyea, H., Rimkus, S., and van der Donk, W. A. (2005) Site-directed mutagenesis of active site residues of phosphite dehydrogenase, *Biochemistry 44*, 4765-4774.
4. Taguchi, H., and Ohta, T. (1991) D-lactate dehydrogenase is a member of the D-isomer-specific 2-hydroxyacid dehydrogenase family. Cloning, sequencing, and expression in Escherichia coli of the D-lactate dehydrogenase gene of Lactobacillus plantarum, *J. Biol. Chem. 266*, 12588-12594.
5. Taguchi, H., and Ohta, T. (1993) Histidine 296 is essential for the catalysis in Lactobacillus plantarum D-lactate dehydrogenase, *J. Biol. Chem. 268*, 18030-18034.
6. Goldberg, J. D., Yoshida, T., and Brick, P. (1994) Crystal structure of a NAD-dependent D-glycerate dehydrogenase at 2.4 A resolution, *J. Mol. Biol. 236*, 1123-1140.
7. Hung, J. E., Fogle, E. J., Christman, H. D., Johannes, T. W., Zhao, H. M., Metcalf, W. W., and van der Donk, W. A. (2012) Investigation of the role of Arg301 identified in the X-ray structure of phosphite dehydrogenase, *Biochemistry 51*, 4254-4262.

8. Hirota, R., Yamane, S., Fujibuchi, T., Motomura, K., Ishida, T., Ikeda, T., and Kuroda, A. (2012) Isolation and characterization of a soluble and thermostable phosphite dehydrogenase from Ralstonia sp. strain 4506, *J. Biosci. Bioeng. 113*, 445-450.

9. Liu, D.-F., Ding, H.-T., Du, Y.-Q., Zhao, Y.-H., and Jia, X.-M. (2012) Cloning, expression, and characterization of a wide-pH-range stable phosphite dehydrogenase from *Pseudomonas* sp. K in *Escherichia coli*, *Appl. Biochem. Biotech. 166*, 1301-1313.

10. Martínez, A., Osburne, M. S., Sharma, A. K., DeLong, E. F., and Chisholm, S. W. (2012) Phosphite utilization by the marine picocyanobacterium Prochlorococcus MIT9301, *Environ. Microbiol. 14*, 1363-1377.

11. Relyea, H. A., Vrtis, J. M., Woodyer, R., Rimkus, S. A., and van der Donk, W. A. (2005) Inhibition and pH dependence of phosphite dehydrogenase, *Biochemistry 44*, 6640-6649.

12. Guillén Schlippe, Y. V., and Hedstrom, L. (2005) Is Arg418 the catalytic base required for the hydrolysis step of the IMP dehydrogenase reaction?, *Biochemistry 44*, 11700-11707.

13. Guillén Schlippe, Y. V., and Hedstrom, L. (2005) A twisted base? The role of arginine in enzyme-catalyzed proton abstractions, *Arch. Biochem. Biophys. 433*, 266-278.

14. Hedstrom, L., and Gan, L. (2006) IMP dehydrogenase: structural schizophrenia and an unusual base, *Curr. Opin. Chem. Biol. 10*, 520-525.

15. Bossi, R. T., Negri, A., Tedeschi, G., and Mattevi, A. (2002) Structure of FAD-bound L-aspartate oxidase: insight into substrate specificity and catalysis, *Biochemistry 41*, 3018-3024.

16. Tedeschi, G., Ronchi, S., Simonic, T., Treu, C., Mattevi, A., and Negri, A. (2001) Probing the active site of L-aspartate oxidase by site-directed mutagenesis: role of basic residues in fumarate reduction, *Biochemistry 40*, 4738-4744.

17. Charnock, S. J., Brown, I. E., Turkenburg, J. P., Black, G. W., and Davies, G. J. (2002) Convergent evolution sheds light on the anti-beta -elimination mechanism common to family 1 and 10 polysaccharide lyases, *Proc. Natl. Acad. Sci. U. S. A. 99*, 12067-12072.

18. Mowat, C. G., Moysey, R., Miles, C. S., Leys, D., Doherty, M. K., Taylor, P., Walkinshaw, M. D., Reid, G. A., and Chapman, S. K. (2001) Kinetic and crystallographic analysis of the key active site acid/base arginine in a soluble fumarate reductase, *Biochemistry 40*, 12292-12298.

19. Doherty, M. K., Pealing, S. L., Miles, C. S., Moysey, R., Taylor, P., Walkinshaw, M. D., Reid, G. A., and Chapman, S. K. (2000) Identification of the active site acid/base catalyst in a bacterial fumarate reductase: a kinetic and crystallographic study, *Biochemistry 39*, 10695-10701.

20. Scavetta, R. D., Herron, S. R., Hotchkiss, A. T., Kita, N., Keen, N. T., Benen, J. A., Kester, H. C., Visser, J., and Jurnak, F. (1999) Structure of a plant cell wall fragment complexed to pectate lyase C, *Plant Cell 11*, 1081-1092.

21. Sanchez-Torres, P., Visser, J., and Benen, J. A. (2003) Identification of amino acid residues critical for catalysis and stability in Aspergillus niger family 1 pectin lyase A, *Biochem. J. 370*, 331-337.

22. Wilson, M. M., and Metcalf, W. W. (2005) Genetic diversity and horizontal transfer of genes involved in oxidation of reduced phosphorus compounds by *Alcaligenes faecalis* WM2072, *Appl. Environ. Microbiol. 71*, 290-296.

23. Lanzetta, P. A., Alvarez, L. J., Reinach, P. S., and Candia, O. A. (1979) An improved assay for nanomole amounts of inorganic phosphate, *Anal. Biochem. 100*, 95-97.

24. Taguchi, H., Ohta, T., and Matsuzawa, H. (1997) Involvement of Glu-264 and Arg-235 in the essential interaction between the catalytic imidazole and substrate for the D-lactate dehydrogenase catalysis, *J. Biochem. 122*, 802-809.

25. Taguchi, H., and Ohta, T. (1994) Essential role of arginine 235 in the substrate-binding of Lactobacillus plantarum D-lactate dehydrogenase, *J. Biochem. 115*, 930-936.

26. Yoshida, T., Yamaguchi, K., Hagishita, T., Mitsunaga, T., Miyata, A., Tanabe, T., Toh, H., Ohshiro, T., Shimao, M., and Izumi, Y. (1994) Cloning and expression of the gene for hydroxypyruvate reductase (D-glycerate dehydrogenase from an obligate methylotroph Hyphomicrobium methylovorum GM2, *Eur. J. Biochem. 223*, 727-732.

27. Tobey, K. L., and Grant, G. A. (1986) The nucleotide sequence of the serA gene of Escherichia coli and the amino acid sequence of the encoded protein, D-3-phosphoglycerate dehydrogenase, *J. Biol. Chem. 261*, 12179-12183.

28. Bernard, N., Ferain, T., Garmyn, D., Hols, P., and Delcour, J. (1991) Cloning of the D-lactate dehydrogenase gene from Lactobacillus delbrueckii subsp. bulgaricus by complementation in Escherichia coli, *FEBS Lett. 290*, 61-64.

29. Cook, P. F., and Cleland, W. W. (2007) *Enzyme Kinetics and Mechanism*, Garland Science, New York.

30. Cleland, W. W. (1979) Statistical analysis of enzyme kinetic data, *Methods Enzymol. 63*, 103-138.

31. Fogle, E. J., and van der Donk, W. A. (2007) Pre-steady-state studies of phosphite dehydrogenase demonstrate that hydride transfer is fully rate limiting, *Biochemistry 46*, 13101-13108.

32. Guillén Schlippe, Y. V., and Hedstrom, L. (2005) Guanidine derivatives rescue the Arg418Ala mutation of Tritrichomonas foetus IMP dehydrogenase, *Biochemistry 44*, 16695-16700.

33. Min, D., Josephine, H. R., Li, H., Lakner, C., MacPherson, I. S., Naylor, G. J., Swofford, D., Hedstrom, L., and Yang, W. (2008) An enzymatic atavist revealed in dual pathways for water activation, *PLoS Biol. 6*, e206.

34. Craik, C., Roczniak, S., Largman, C., and Rutter, W. (1987) The catalytic role of the active site aspartic acid in serine proteases, *Science 237*, 909-913.

35. Hamilton, C. S., Spedaliere, C. J., Ginter, J. M., Johnston, M. V., and Mueller, E. G. (2005) The roles of the essential Asp-48 and highly conserved His-43 elucidated by the pH dependence of the pseudouridine synthase TruB, *Arch. Biochem. Biophys. 433*, 322-334.

36. Plapp, B. V. (1995) Site-directed mutagenesis: a tool for studying enzyme catalysis, *Methods Enzymol. 249*, 91-119.

37. Howell, E. E., Villafranca, J. E., Warren, M. S., Oatley, S. J., and Kraut, J. (1986) Functional role of aspartic acid-27 in dihydrofolate reductase revealed by mutagenesis, *Science 231*, 1123-1128.

38. Ellis, K. J., and Morrison, J. F. (1982) Buffers of constant ionic strength for studying pH-dependent processes, *Methods Enzymol. 87*, 405-426.

39. Sims, P. A., Larsen, T. M., Poyner, R. R., Cleland, W. W., and Reed, G. H. (2003) Reverse protonation is the key to general acid-base catalysis in enolase, *Biochemistry 42*, 8298-8306.

40. Bevilacqua, P. C. (2003) Mechanistic considerations for general acid-base catalysis by RNA: revisiting the mechanism of the hairpin ribozyme, *Biochemistry 42*, 2259-2265.

41. Vrtis, J. M., White, A., Metcalf, W. W., and van der Donk, W. A. (2001) Phosphite dehydrogenase: an unusual phosphoryl transfer reaction, *J. Am. Chem. Soc. 123*, 2672-2673.

42. Relyea, H. A. (2006) Kinetic Analysis and pH Dependence of the Phosphite Dehydrogenase Reaction, PhD Dissertation, University of Illinois, Urbana.

43. Hung, J. E., Fogle, E. J., Garg, N., Chekan, J. R., Nair, S. K., and van der Donk, W. A. Chemical rescue and inhibition studies to determine the role of Arg301 in phosphite dehydrogenase, *In preparation*.

44. Toney, M. D., and Kirsch, J. F. (1989) Directed Brønsted analysis of the restoration of activity to a mutant enzyme by exogenous amines, *Science 243*, 1485-1488.

45. Rynkiewicz, M. J., and Seaton, B. A. (1996) Chemical rescue by guanidine derivatives of an arginine-substituted site-directed mutant of Escherichia coli ornithine transcarbamylase, *Biochemistry 35*, 16174-16179.

46. Perrin, D. D. (1965) *Dissociation Constants of Organic Bases in Aqueous Solution*, Butterworths, London.

47. Lehoux, I. E., and Mitra, B. (2000) Role of arginine 277 in (S)-mandelate dehydrogenase from Pseudomonas putida in substrate binding and transition state stabilization, *Biochemistry 39*, 10055-10065.

48. Hansch, C., and Leo, A. (1979) *Substituent constants for correlation analysis in chemistry and biology*, Wiley.

49. Jencks, W. P. (1987) *Catalysis in Chemistry and Enzymology*, Dover, New York.

50. Harpel, M. R., and Hartman, F. C. (1994) Chemical rescue by exogenous amines of a site-directed mutant of ribulose 1,5-bisphosphate carboxylase/oxygenase that lacks a key lysyl residue, *Biochemistry 33*, 5553-5561.

51. Klinman, J. P., and Matthews, R. G. (1985) Calculation of substrate dissociation constants from steady-state isotope effects in enzyme-catalyzed reactions, *J. Am. Chem. Soc. 107*, 1058-1060.

52. Northrop, D. B. (1998) On the meaning of Km and V/K in enzyme kinetics, *J. Chem. Educ. 75*, 1153-1157.

53. Woodyer, R., van der Donk, W. A., and Zhao, H. (2006) Optimizing a biocatalyst for improved NAD(P)H regeneration: Directed evolution of phosphite dehydrogenase, *Comb. Chem. High Throughput Screen. 9*, 237-245.

54. Johannes, T. W., Woodyer, R. D., and Zhao, H. M. (2005) Directed evolution of a thermostable phosphite dehydrogenase for NAD(P)H regeneration, *Appl. Environ. Microbiol. 71*, 5728-5734.

55. Bradford, M. M. (1976) A rapid and sensitive method for the quantitation of microgram quantities of protein utilizing the principle of protein-dye binding, *Anal. Biochem. 72*, 248-254.

56. Woodyer, R., van der Donk, W. A., and Zhao, H. (2003) Relaxing the nicotinamide cofactor specificity of phosphite dehydrogenase by rational design, *Biochemistry 42*, 11604-11614.

57. Leatherbarrow, R. J. (2009) GraFit Version 7, 7.0 ed., Erithacus Software Limited, Horley, UK.

58. Cleland, W. W. (1982) The use of pH studies to determine chemical mechanisms of enzyme-catalyzed reactions, *Methods Enzymol. 87*, 390-405.

59. Goedl, C., and Nidetzky, B. (2008) The phosphate site of trehalose phosphorylase from Schizophyllum commune probed by site-directed mutagenesis and chemical rescue studies, *FEBS J. 275*, 903-913.

CHAPTER 3: THE CATALYTIC ROLE OF MET53 IN THE PTDH REACTION

3.1 Introduction

Met53 was first identified as a potentially important catalytic residue during analysis of the X-ray crystal structures of PTDH from *P. stutzeri* (*1*). When comparing the co-crystal structures of TS-PTDH-NAD (PDB: 4E5N) and TS-PTDH-NAD-sulfite (PDB: 4E5K), the orientation of Met53 was observed to shift upon binding of sulfite, a competitive inhibitor (*2*), resulting in an apparent interaction between the sulfur of the methionine and an oxygen atom from sulfite with a bond distance of 3.1 Å in the ternary structure (Figure 3.1). This interaction was initially characterized as a putative hydrogen bond, as the distance and orientation between lone-pair electrons on the sulfur and the oxygen (if protonated) were appropriate. As such, the methionine residue was suspected of playing a potential catalytic role.

Met53 is fully conserved among all confirmed PTDHs (*3*) (Figure 3.2). While methionine residues are most commonly associated with hydrophobic interactions and steric effects in proteins, methionine has also been reported to act as a hydrogen bond acceptor to the backbone amide NH in proteins (*4*) and it can also act to stabilize residues through non-hydrogen bond interactions with other residues (*5*). In addition, the residue sometimes serves as a ligand for metal ions (*6, 7*). However, examples of methionine playing a direct role in enzyme-mediated catalysis are rare (*8*), and no examples are known where the residue plays a defined catalytic role.

This chapter contains material adapted from:

Ranaghan, K. E., Hung, J. E., Bartlett, G. J., Mooibroek, T. J., Woolfson, D. N., van der Donk, W. A., and Mulholland, A. J. A catalytic role for methionine revealed by a combination of computation and experiments on phosphite dehydrogenase. *Submitted*.

In order to determine the catalytic role of Met53, a multidisciplinary approach was adopted, combining experiments with mechanistic modeling performed by the Mulholland laboratory (University of Bristol, UK). This type of synergistic strategy has become more common in recent years to answer questions about enzyme mechanisms that have been difficult to elucidate through experimentation alone (*9-12*). Met53 was investigated through experiments, including mutagenesis and pH profiles, and computational quantum mechanics/molecular mechanics (QM/MM) modeling in order to determine its catalytic role.

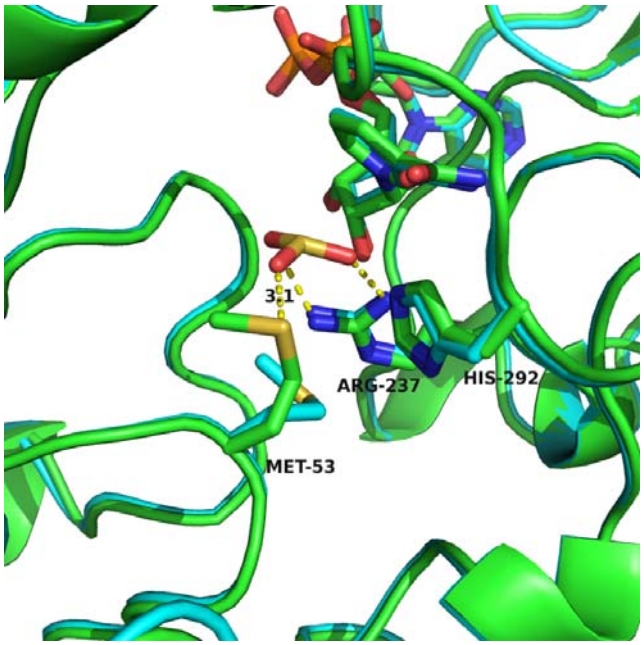

Figure 3.1. A representation of the crystal structures of TS-PTDH with the NAD^+ co-factor and sulfite inhibitor in green and the complex without sulfite in blue. NAD^+ and several key active site residues are shown as sticks: Arg237, His292 and Met53 and their interactions with the sulfite inhibitor are indicated by dotted lines. Arg237 is important for binding of the substrate and His292 is the putative base for the reaction (*13*). When sulfite is present the (Met) sulfur to (sulfite) oxygen distance is 3.1 Å and in the absence of sulfite the side chain of Met53 adopts a different orientation. This figure is adapted from (*14*).

Figure 3.2. Partial sequence alignment of several active PTDH orthologs from different organisms. The orthologs exhibit high sequence diversity, with 39-72% overall pairwise identity (see Chapter 2). The PTDH from *P. stutzeri* corresponds to the wild-type PTDH from which 17X-PTDH was developed. Conserved residues are highlighted in yellow. Highlighted in red is the Met53.

3.2 Results and Discussion

3.2.1 Computational Experiments to Determine the Role of Met53

In order to determine the catalytic role of the Met53 residue in PTDH, a computational QM/MM model was developed by Kara Ranaghan in the Mulholland group (*14*). The reaction was modeled as an associative process in which nucleophilic attack by hydroxide onto phosphite first formed a pentavalent intermediate, which was then followed by hydride transfer to form the NADH and phosphate final products (Figure 3.3). From these models, a putative role of Met53 was hypothesized that was evaluated through experimental efforts (see below).

To summarize, in this scenario His292 acts as the active site base to deprotonate the water nucleophile, leading to the pentavalent phosphorane intermediate. In the next step of the reaction, Met53 acts to stabilize the His292 imidazolium through an n→π* interaction (*15*) in the second transition state (Figure 3.4), offering – 7.9 kcal/mol of stabilization (*14*). In this model, the lone pair electrons (n) of the sulfur atom interact with the antibonding orbitals of the histidine (π*) in a "face-on" interaction to stabilize the complex. Similar n→π* interactions have previously been noted in protein backbones (*15*) and model peptide systems (*16*). Although a hydrogen bonded complex appeared to be present in the crystal structure and gas phase calculations of methylthioethane and the His292 imidazole ring indicated that the hydrogen-bonded complex

would have offered significant stabilizing energy, steric constraints from other active site residues prevented this complex from being seen in the QM/MM simulation (*14*). Gas phase calculations were also performed on a methylselenoethane complex, which resulted in similar results to the methylthioethane. In addition to this n→π* interaction, a C–H–O hydrogen bond is formed between the methyl group of Met53 and the amide oxygen of the NAD^+ cofactor (Figure 3.4). In order to support the computational hypothesis of the role of Met53, experiments were performed, including mutagenesis, pH dependence, and isotope effect studies.

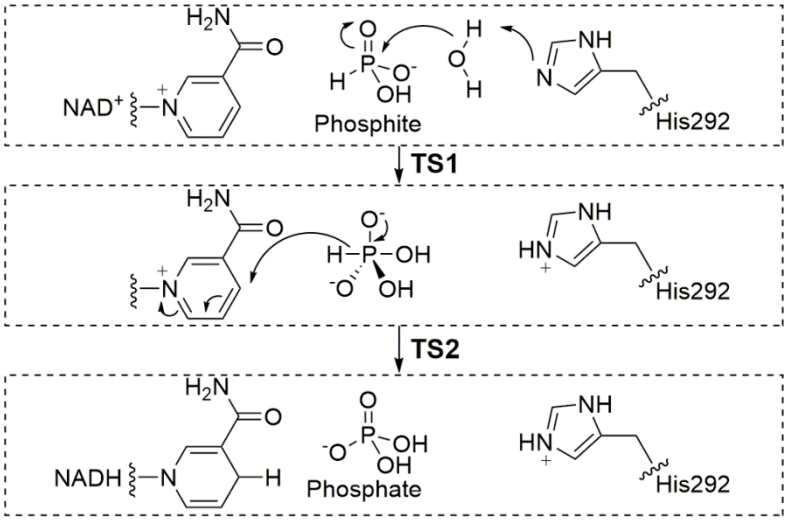

Figure 3.3. An associative mechanism for the nucleophilic displacement reaction catalyzed by PTDH (*17*). TS1 and TS2 are the transition states for the first and second steps. Adapted from (*14*).

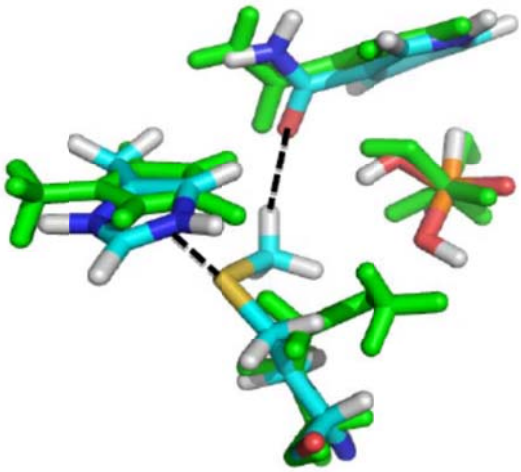

Figure 3.4. Representative structures of the interaction between Met53 and the QM region at the intermediate (green atoms) and at the transition state for the hydride transfer step transition state (atoms colored by type) from AM1-CHARMM27 calculations. The dotted lines indicate interactions between the side chain of Met53 and His292 and between the methyl group of Met53 and the NAD^+ cofactor. Figure made by Kara Ranaghan, reproduced from (*14*).

3.2.2 Incorporation of Non-proteinogenic Amino Acids into 17X-PTDH

Global incorporation into 17X-PTDH of two analogs of methionine, norleucine (Nle) and selenomethionine (SeMet), was accomplished by utilizing the promiscuity of the methionine tRNA synthetase towards substrate analogs (*18*). A methionine-auxotrophic strain of *E. coli* was grown in minimal media in the absence of methionine, but supplemented with the desired analog (*19, 20*). Following overexpression and purification, the proteins were subjected to peptidic digest and analyzed by mass spectrometry to verify incorporation of the methionine analogs (Figure 3.5). The Nle-containing protein (Nle-17X-PTDH) was subjected to in-gel trypsin digest (*21*) and analyzed by electrospray ionization mass spectrometry (ESI-MS), while the SeMet-containing protein (SeMet-17X-PTDH) was digested by GluC and analyzed by matrix-assisted laser desorption ionization mass spectrometry (MALDI-MS). The fragments containing Met53 from the peptidic digests were each predicted to contain three total methionine residues (*22*). In

the mass spectra for each case, ions corresponding to full incorporation of the methionine analog were observed, while the ions corresponding to full or partial incorporation of methionine into the fragments were not observed, indicating that the residue 53 in each of the proteins was fully substituted with the analog. For SeMet-17X-PTDH, the fragments all contain a complex isotopic pattern indicative of selenium incorporation, as selenium has five stable naturally occurring isotopes (*23*). As such, the mass spectrometric analysis suggests that the protein contains full incorporation of SeMet at the Met53 site. When 17X-PTDH was subjected to peptidic digest as a control, ions corresponding to full incorporation of methionine were observed when digested with either protease. Global substitution of Met with its oxygen analog, O-methyl homoserine (also known as methoxinine), was also attempted. However, this incorporation was unsuccessful due to lack of growth of the bacterial culture when supplemented with the amino acid, probably because of the known toxicity of the analog (*24*).

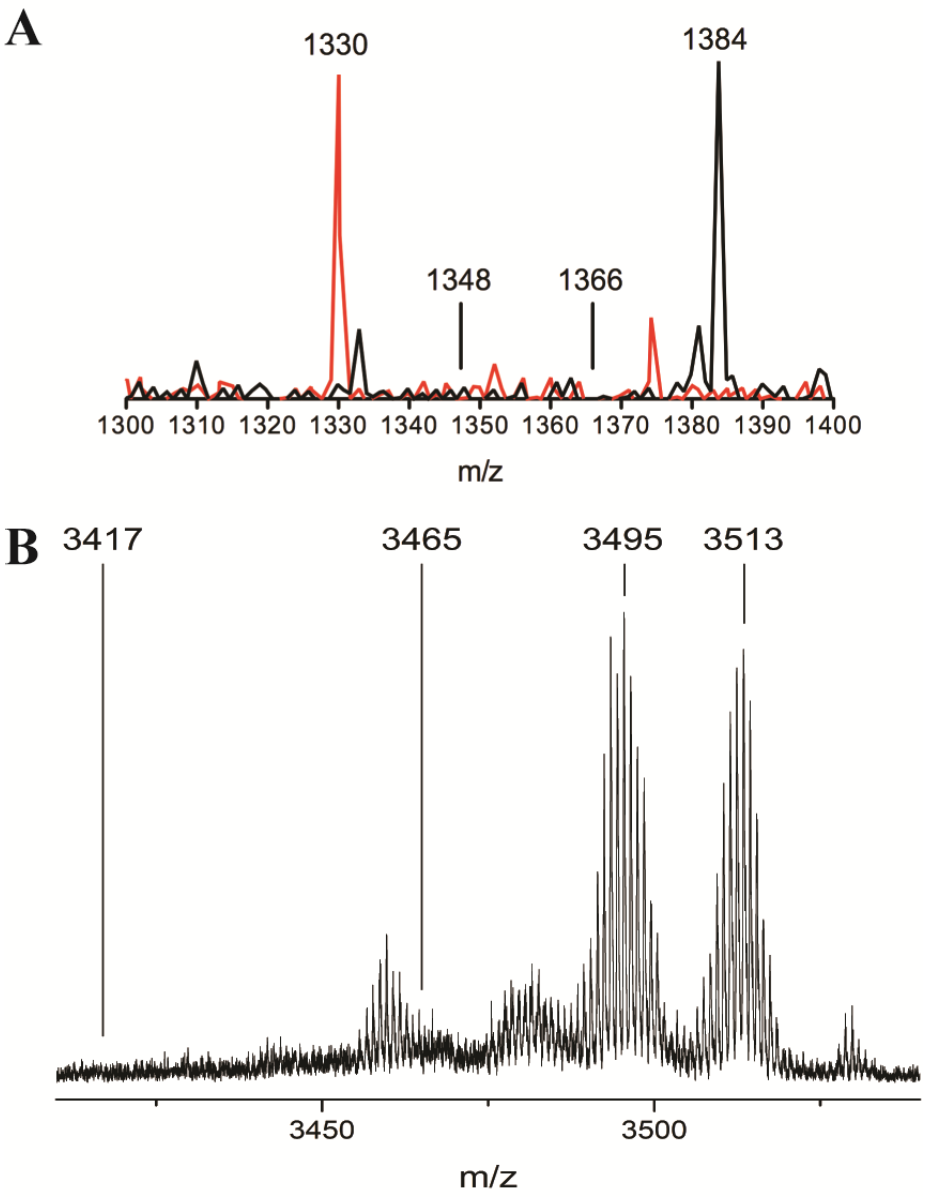

Figure 3.5. MS analysis of trypsin-digested PTDHs. (a) ESI-MS spectrum of Nle-17X-PTDH digested by trypsin indicating the incorporation of 3 norleucines at position X in the peptide fragment 45-DAQAXXAFXPDR-56 (M+H = 1330) (red). Also shown are the expected m/z values of fragments containing 1, 2 or 3 methionines (M+H = 1348, 1366 or 1384). Shown as a control is the peptide fragment from the tryptic digest of 17X-PTDH, which contains 3 methionines (black). The crude spectra were deconvoluted to obtain M+H charge states. (b) MALDI-MS spectrum of SeMet-17X-PTDH digested with GluC. Along with other ions, diagnostic ions were observed that correspond to the peptide fragment 39-ILRRCRDAQAXXAFXPDRVDADFLQACPE-67 containing 3 selenomethionines at position X (M+H =3513 Da). Another ion containing Se is observed at 3495 (M+H – 18) that is a dehydration product, likely formed in the mass spectrometer. No ions are visible corresponding to 1 or 2 incorporated methionines (M+H = 3417, 3465 Da respectively).

3.2.3 Mutagenesis Studies on Met53

The presence of the hydrogen bond between sulfite and Met53 observed in the crystal structure of the ternary complex suggested a possible role for Met53 in catalysis by PTDH, and the residue was therefore targeted in mutagenesis experiments. The Met53 mutants were constructed in the 17X-PTDH background, heterologously expressed in *E. coli* and purified by immobilized metal affinity chromatography. Steady-state kinetic analysis was carried out on the mutants to determine their activity relative to the parent 17X mutant (Table 3.1). Interestingly, while the K_m values for phosphite and NAD^+ exhibited relatively small variation from 17X-PTDH, k_{cat} was reduced ~ 50 to 200-fold for the Met53Ala and Met53Asn mutants. The loss in k_{cat} was more pronounced when larger functional groups were introduced, as the Met53Ala mutation showed a smaller decrease in k_{cat} than the bulkier Met53Asn mutant. In addition, the Met53Leu mutation, which contains a sterically large hydrophobic residue, exhibited a ~ 3750-fold reduced k_{cat}. These observations suggested that packing and/or orientation in the active site was disrupted by the mutations, although this effect was not reflected in the K_m for phosphite, suggesting that binding affinity was not affected. Minimal effect was also observed on $K_{m,NAD}$ in the mutants.

In order to minimize the change to the steric environment of the active site, two non-proteinogenic amino acids that are structural analogs of methionine were globally installed in the place of methionine (as discussed in section 3.2.2): norleucine and selenomethionine, which contain a methylene group and selenium atom in place of the sulfur, respectively. Nle-17X-PTDH displayed only a slightly improved k_{cat} relative to the Met53Ala mutant, suggesting that some interaction with Met53 (e.g. a hydrogen bond or electrostatic interaction) is disrupted, as opposed to only a change in the steric environment of the active site. 17X-PTDH contains eight

total methionine residues which would be substituted, including one in the hexa-histidine tag. In the crystal structure, only Met53 is near the active site so we attribute the change in k_{cat} for Nle-17X-PTDH to the replacement of Met53 with Nle. This conclusion is supported by the kinetic parameters of Nle-17X-PTDH-Met53Ala, which are similar to those observed for the Met53Ala mutant. SeMet-17X-PTDH exhibited a very similar k_{cat} to 17X-PTDH. This observation was consistent with the computational results obtained by our collaborators. When the 4-methyl imidazole/imidazolium (representing His292) was modeled with either methylthioethane (representing Met53) or methylselenoethane (representing SeMet53) in the gas phase, the interaction energies were found to differ by less than 1 kcal/mol from one another (see section 3.2.1) (*14*).

The conformation of the methionine analogs in the active site structure was also considered. In the PTDH crystal structure, Met53 has a gauche-like conformation, with dihedral angles (for the Cβ-Cγ-Sδ-Cε bond) of ~ 74° and ~ 39° for the PTDH-NAD-sulfite ternary complex and the PTDH-NAD binary complex, respectively (Figure 3.6). In the QM/MM model developed by our collaborators, similar gauche-like angles were observed (*14*). These results are consistent with the known conformation of methionine residues in that all rotamers are allowed, with the gauche conformation slightly favored (*25*). While the crystal structure of SeMet-17X-PTDH shows that selenomethionine takes a similar gauche conformation as Met53 (*1*), norleucine would be sterically favored to be in the anti-conformation (*25*). Therefore, we cannot rule out that the different conformational preference of Nle plays a role in reducing k_{cat} by disrupting the active site geometry. However, the comparable activity of Nle-17X-PTDH and the Met53Ala mutant suggests that loss of the side chain sulfur is more important.

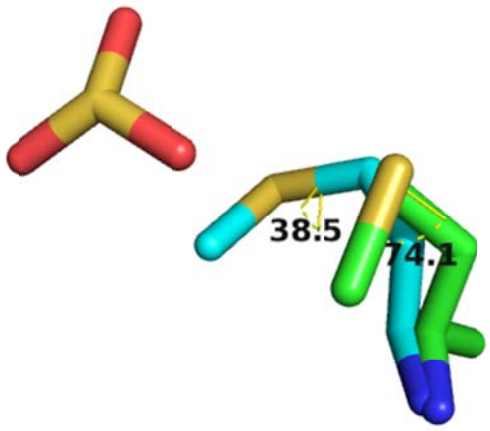

Figure 3.6. The conformation of Met53 in the PTDH crystal structure, with the dihedral/torsion angle for Cβ-Cγ-Sδ-Cε labeled. The PTDH-NAD (blue) and PTDH-NAD-sulfite (green) complexes both exhibit gauche-like conformations with dihedral angles of 38.5° and 74.1°, respectively.

The kinetic isotope effects (KIEs) were analyzed to determine if the rate-limiting step of catalysis was being affected by substitution of Met53. Hydride transfer is fully rate limiting for 17X-PTDH (*26*), as shown by KIE and pre-steady state kinetic measurements. The KIEs for the Met53Ala mutant and Nle-PTDH were also obtained to determine if the rate-limiting step of the reaction changed with the substitution of Met53 (Table 3.1). In each case, $^{D}k_{cat}$ and $^{D}k_{cat}/K_{m,Phosphite}$ are very close in value (e.g. $^{D}k_{cat}$ = 1.9, $^{D}k_{cat}/K_{m}$ = 1.9 for Met53Ala), as would be expected if the chemical step remained fully rate-limiting combined with a small commitment to catalysis (*26*). The observation that hydride transfer remains rate limiting despite a large decrease in k_{cat} has been reported previously for other mutants of PTDH (*3, 26*). The somewhat lower KIEs observed with the Met53 mutants compared to the parent 17X-PTDH suggest that the methionine affects the structure of the transition state of the rate-limiting step or the extent to

which it is rate limiting. This observation is consistent with Met53 playing a stabilizing role in the transition state of the hydride transfer step, as discussed in section 3.2.1.

Table 3.1. Steady-state kinetic parameters and KIEs for Met53 mutants of PTDH. Errors in parentheses were obtained from fitting to the Michaelis Menten equation. PT refers to phosphite. ND = not determined. Adapted from (*14*).

	k_{cat} (s^{-1})	Relative k_{cat}	$K_{m,PT}$ (μM)	$K_{m,NAD}$ (μM)	$k_{cat}/K_{m,PT}$ ($M^{-1}s^{-1}$)	$^{D}k_{cat}$	$^{D}k_{cat}/K_{m}$
17X-PTDH	3.1 (0.1)	1.00	28 (7)	22 (6)	1.1 (0.3) x 10^5	2.3 (0.1)	2.1 (0.2)
M53N	0.016 (0.001)	0.005	17 (1)	64 (1)	920 (70)	ND	ND
M53A	0.059 (0.001)	0.019	100 (10)	17 (1)	590 (30)	1.9 (0.1)	1.9 (0.1)
M53L	0.00081 (0.00005)	0.0003	51 (21)	ND	15 (7)	ND	ND
Nle−17X-PTDH	0.11 (0.01)	0.036	28 (1)	21 (2)	3900 (200)	1.8 (0.1)	1.8 (0.2)
Nle-17X-PTDH-M53A	0.072 (0.003)	0.024	47 (7)	7.8 (0.9)	1500 (200)	ND	ND
SeMet-17X-PTDH	3.3 (0.1)	1.07	110 (10)	ND	3.4 (0.2) x 10^4	ND	ND

3.2.4 pH Rate Profile Studies on Met53Ala

In order to further probe the role of Met53 in the PTDH reaction by experimental means, the pH dependence of the Met53Ala mutant was determined. From the pH dependence of $\log(k_{cat}/K_{m,Phosphite})$, p$K_a$ values of 6.32 ± 0.16 and 7.21 ± 0.04 were extracted for the acidic and basic limbs, respectively (Figure 3.7B). These values are both skewed somewhat from the acidic and basic limb pK_a values of 6.53 ± 0.10 and 7.9 ± 0.08 obtained for 17X-PTDH, see Chapter 2 (*3*). Similar values to 17X-PTDH were obtained for wt-PTDH in a previous study (*27*). These results support that Met53 plays some role in affecting active site protonation states, particularly the protonation of His292 which has been attributed to the basic limb pK_a (*3, 27*). In addition, an

acidic limb pK_a of 4.27 ± 0.02 is observed in the log(k_{cat}) vs. pH plot (Figure 3.7A). Although the original pH profile on k_{cat} was pH independent for both 17X and wt-PTDH (Figure 2.6A), the pH dependence experiments had not been previously attempted at such a low pH values, and hence the limb was not observed. Experiments at low pH over a limited acidic pH range showed that a similar acidic limb pK_a of 4.09 ± 0.02 for k_{cat} is observed in 17X-PTDH (Figure 3.7C), though it is difficult to unambiguously assign this value due to poor buffering capacity at the low pH range. Although this pK_a value is difficult to attribute to a particular residue, it does appear to be present in both the Met53Ala mutant and the parent PTDH, suggesting that Met53 does not play an important role in this protonation event.

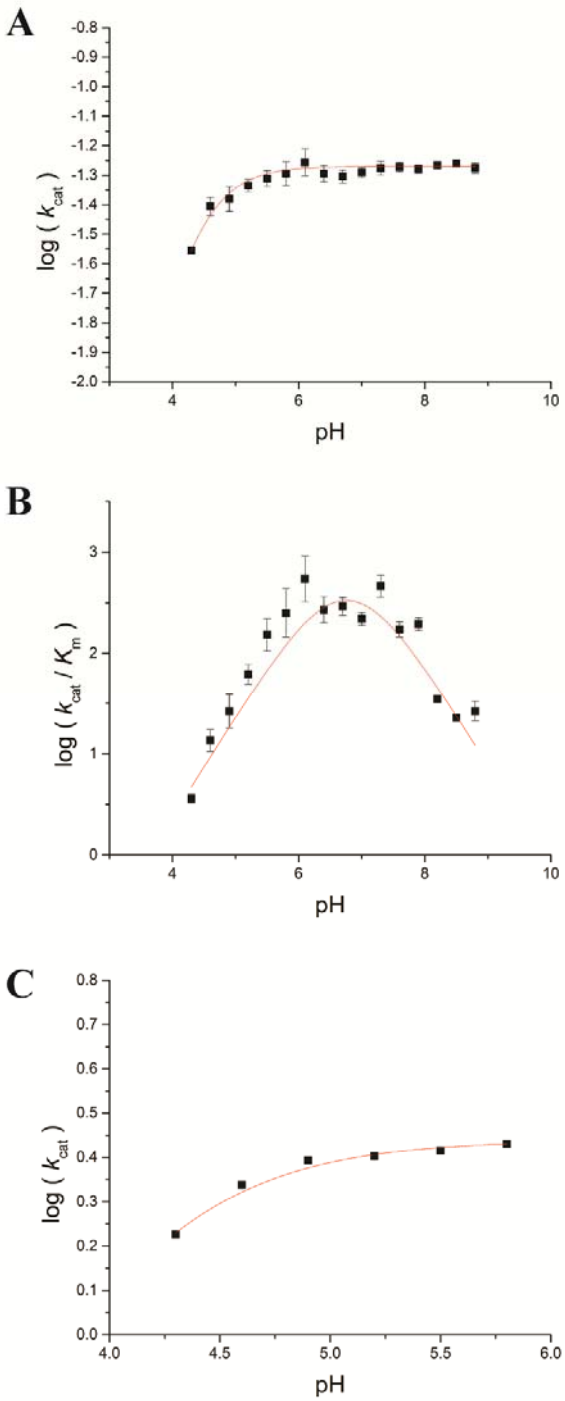

Figure 3.7. The pH dependence of 17X-PTDH-M53A with respect to (a) log(k_{cat}) and (b) log(k_{cat} / $K_{m,Phosphite}$). (c) Also shown is the acidic range of the log(k_{cat}) plot for 17X-PTDH. Error was obtained from fitting to the Michaelis-Menten equation at each pH.

3.3 Conclusions

The experimental results indicate that Met53 plays an important role in PTDH catalysis. Methionine residues are rarely considered to be of direct catalytic importance, but mutational analysis of Met53 has shown it to play a significant role. Met53 is fully conserved among all known PTDHs, and mutation of the residue to other canonical amino acids greatly reduced k_{cat} without significantly altering K_m for either substrate. Computational models performed by Kara Ranaghan in the Mulholland laboratory (*14*) suggested that Met53 directly stabilizes the transition state of the hydride transfer step through an n→π* interaction between the Met53 sulfur and the His292 imidazolium, resulting in 7.9 kcal/mol of stabilization energy.

Overall, this hypothesis is consistent with the experimental results. When norleucine, a structural analog of methionine with a methylene group in place of the sulfur, was substituted, similar loss of activity was observed as with the M53A mutant. In contrast, when selenomethionine was substituted, the selenium atom allowed for full activity to be retained. These observations suggest that the sulfur atom of Met53 (or selenium in SeMet-17X-PTDH) is catalytically important. The lower KIEs observed with the Met53 mutants compared to the parent 17X-PTDH suggest that the methionine affects the structure of the transition state of the rate-limiting step or the extent to which it is rate limiting, again consistent with the computational model. In addition, in the pH rate profile of the M53A mutant, the pK_a of the limb that is attributed to His292 was skewed compared to the profile of 17X-PTDH, suggesting that there may also be an interaction between His292 and Met53 during substrate binding events prior to catalysis.

3.4 Materials and Methods

3.4.1 Materials

All mutants were generated in the 17X-PTDH background (*28*), see Chapter 2. All chemicals were obtained from Sigma or Aldrich and used without further purification unless otherwise noted.

3.4.2 Preparation of PTDH Mutant Constructs

The mutants were prepared by the polymerase chain reaction (PCR) using QuikChange mutagenesis (Agilent). The primers used to incorporate the mutations are provide below, along with their reverse complement strands, which are not shown: M53A: 5'-CG ATG ATG GCG TTC GCG CCC GAT CGG GTC G-3'; M53L: 5'-CG ATG ATG GCG TTC TTG CCC GAT CGG GTC– 3'; M53N: 5'-CAG GCG ATG ATG GCG TTC AAT CCC GAT CGG G-3'; M53L: 5'-CG ATG ATG GCG TTC TTG CCC GAT CGG GTC-3'. The mutated codon is underlined in each case. Once the mutant genes were constructed, they were sequenced in their entirety to ensure that the desired mutation was incorporated and no other mutations were generated. (JEH-4-38, JEH-4-53).

3.4.3 Overexpression and Purification of PTDH Mutants

Chemically competent *E. coli* BL21 (DE3) cells were transformed with plasmids containing the desired gene in pET15b and plated on a LB agar plate containing 100 μg/mL ampicillin. A single colony was picked and used to inoculate an overnight culture (50 mL). The cells were harvested by centrifugation, resuspended in 1 L of LB/ampicillin and grown at 37 °C to $OD_{600\ nm}$ = 0.6.

IPTG was added to the culture (0.3 mM final concentration), which was incubated at 18 °C for 16-20 h. Cells were then pelleted by centrifugation (8,000 × g, 30 min), resuspended in 20 mM Tris pH 7.6, 0.5 M NaCl, 10% glycerol (v/v), and stored at −80 °C. The frozen pellet was then thawed on ice and lysed using an Avestin Emulsiflex-C3 Homogenizer (7500 Psi,6 passes). The insoluble lysate was removed by centrifugation (15,000 × g, 30 min), and the soluble lysate was passed through a 0.44 μm filter. The enzyme was purified via FPLC (Äkta) by immobilized metal affinity chromatography (IMAC) with a HisTrap HP Ni^{2+}-affinity column (GE Life Sciences). The column was washed with 5 column volumes (CV) of buffer A, followed by a gradient to 40% buffer B over 5 CV, and another gradient of 2 CV to 100% buffer B. (Buffer A: 20 mM Tris pH 7.6, 100 mM NaCl, 10 mM imidazole, 10% glycerol (v/v); buffer B: 20 mM Tris pH 7.6, 100 mM NaCl, 500 mM imidazole, 10% glycerol (v/v)). Fractions containing PTDH were identified by activity assay and analyzed by SDS-PAGE. The highly pure fractions were pooled and concentrated using centrifugal filtration (Amicon membrane, 30 kDa molecular weight cutoff; Millipore), followed by buffer exchange or dialysis to 20 mM MOPS pH 7.6, 100 mM KCl, 10% glycerol. The protein solution was then flash frozen and stored at −80 °C. Protein concentration was determined using the calculated extinction coefficient for 17X-PTDH, 28,000 M^{-1} cm^{-1} (*3*). All buffers used for SeMet PTDH preparation were supplemented immediately prior to use with 5 mM dithiothreitol (DTT) to prevent selenomethionine oxidation.

3.4.4 Incorporation of Non-Proteinogenic Amino Acids into PTDH

The method was adapted from (*19*). Methionine-auxotrophic *E. coli* (New England Biolabs, T7 Express Crystal Competent) were transformed with plasmid encoding 17X-PTDH in pET15b (*28*) and plated on a LB agar plate containing 100 μg/mL ampicillin. A single colony was picked

and used to inoculate an overnight culture (50 mL) of M9 medium supplemented with 1 mM $MgSO_4$, 0.1 mM $CaCl_2$, 0.4% glucose, 1 μg/mL thiamine, 20 μg/mL of all proteinogenic amino acids, and 100 μg/mL ampicillin (hereafter called M9aa medium). The culture was grown at 37 ^oC to stationary phase, and used to inoculate a 2 L culture of M9aa supplemented with 100 μg/mL L-Met. The culture was grown at 37 °C to $OD_{600\ nm}$ = 0.6, sedimented (4500 × g, 10 min, 4 °C), and the pellet resuspended in 0.9% NaCl (50 mL). This procedure was repeated three times to ensure complete removal of the original medium. The final pellet was resuspended in 2 L M9aa lacking Met and grown for 20 to 30 min at 37 °C to deplete the remaining methionine within the cells. The cultures were cooled to 4 ^oC, supplemented with L-norleucine or L-selenomethionine (300 μg/mL), induced with IPTG (0.3 mM final concentration), and grown overnight at 18 °C. Protein purification was then performed as detailed above. The purified protein was then analyzed by SDS-PAGE, digested with trypsin (G Biosciences) for Nle-PTDH or GluC (Roche) for SeMet-PTDH (1 U protease per 1 mg PTDH), and analyzed on a Synapt ESI quadrupole ToF Mass Spectrometry System (Waters) equipped with an Acquity Ultra Performance Liquid Chromatography (UPLC) system (Waters) or an ultrafleXtreme MALDI ToF system (Bruker Daltonics). The tryptic digest was performed in gel (*21*), while the GluC digest was performed in solution. GluC was used for the SeMet incorporation due to difficulty resolving the ions of the tryptic digest during mass spectrometry. The mass spectra obtained did not show peaks corresponding to incorporation of methionine in the tryptic peptide 45-DAQAXXAFXPDR-56 or GluC-digested peptide 39-ILRRCRDAQAXXAFXPDRVDADFLQACPE-67, where X refers to norleucine or selenomethionine, respectively (Figure 3.5). This observation indicates complete incorporation of the non-proteinogenic amino acid at the Met53 position. (JEH-4-56, JEH-7-73, JEH-7-100).

3.4.5 Steady-State Kinetic Assays

The concentrations of NAD^+ stock solutions were determined by the absorbance at 260 nm (ε = 18,000 M^{-1} cm^{-1}). The concentration of stock solutions of phosphite was determined by running the PTDH reaction to completion in the presence of excess NAD^+. The maximum absorbance at 340 nm was then measured, which represents the concentration of NADH formed (ε = 6.2 mM^{-1} cm^{-1}) and is equivalent to the concentration of phosphite consumed. Initial rates were determined using a Cary 4000 UV-vis spectrophotometer (Varian) to monitor the rate of formation of NADH using its absorbance at 340 nm (ε = 6.2 mM^{-1} cm^{-1}). Typical reactions were performed in 100 mM MOPS pH 7.25, 0.5-3.0 μM PTDH mutant, and holding either NAD^+ or phosphite at saturating concentrations (20-50x K_M) while varying the concentration of the other substrate. Reaction mixtures were allowed to equilibrate at 25 °C, as verified using a thermocouple, and the reaction was initiated by addition of enzyme. Assays were performed with the His_6-affinity tag attached. The His-tag has been shown not to have a significant effect on kinetics of the enzyme in a previous study (*29*). The data were fit to the Michaelis-Menten equation using OriginPro 8 (OriginLab).

3.4.6 Synthesis of O-methyl Homoserine

Boc-O-methyl-L-homoserine cyclohexyldiammonium salt (2.5 g, 6 mmol, Chem Impex) was dissolved in 47.5% CH_2Cl_2 (5 mL) and 47.5% TFA (5 mL), with 5% H_2O (500 μL) as a cation scavenger. The reaction was stirred at room temperature for 1.5 h. The reaction was then purged with dry N_2 to remove TFA and then evaporated to dryness using a rotary evaporator. Complete deprotection was observed by loss of the t-butyl peak by ^1H NMR spectroscopy. A final yield of

105% was obtained, a 1:1 mixture of o-methyl homoserine and dicylohexylamine as determined by integration of the NMR peaks. ^{1}H NMR (500 MHz, DMSO) δ 3.92 (m, 1H), 3.45 (t, 2 H), 3.22 (s, 3H), 1.44 (d, 2H). LRMS (ESI) calc. $[M+H]^{+}$ for $C_5H_{12}NO_3$ 134.1, found 133.9. (JEH-7-72).

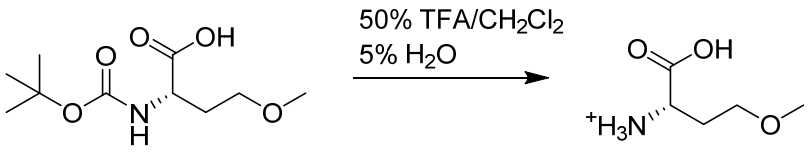

Scheme 3.1

3.4.7 pH rate profile of Met53Ala

Solutions of 100 mM Tris, 50 mM MES, and 50 mM AcOH, generating a universal buffer of constant ionic strength (*30*), were prepared at pH 4.3, 4.6, 4.9, 5.2, 5.5, 5.8, 6.1, 6.4, 6.7, 7.0, 7.3, 7.6, 7.9, 8.2, 8.5, and 8.8. NAD^{+} stock solution was dissolved in buffer of desired pH and phosphite stock solutions were adjusted to the pH of the assay. NAD^{+} was held at presumed saturating conditions of 4 mM, while phosphite concentrations were varied. Reactions were mixed and allowed to equilibrate for several minutes under temperature control at 25° C and to ensure homogeneity until the baseline absorbance at 340 nm remained constant. Reactions were initiated by addition of Met53Ala (1.46 μM final concentration). Initial rates of NADH formation were monitored at 340 nm using a Cary 4000 spectrophotometer. Data were fit to the Michaelis-Menten equation using Origin 8 to obtain kinetic parameters. The data was then fit to Equations 2.2 and 2.3 to extract the pK_a values for only the acidic and both the acidic and basic limbs, respectively. (JEH-5-75).

3.5 References

1. Zou, Y., Zhang, H., Brunzelle, J. S., Johannes, T. W., Woodyer, R. D., Hung, J. E., Nair, N., van der Donk, W. A., Zhao, H., and Nair, S. K. (2012) Crystal structures of phosphite dehydrogenase provide mechanistic insights into nicotinamide co-factor regeneration, *Biochemistry 51*, 4263-4270.
2. Costas, A. M., White, A. K., and Metcalf, W. W. (2001) Purification and characterization of a novel phosphorus-oxidizing enzyme from Pseudomonas stutzeri WM88, *J. Biol. Chem. 276*, 17429-17436.
3. Hung, J. E., Fogle, E. J., Relyea, H. A., Christman, H. D., Johannes, T. W., Zhao, H. M., Metcalf, W. W., and van der Donk, W. A. (2012) Investigation of the role of Arg301 identified in the X-ray structure of phosphite dehydrogenase, *Biochemistry 51*, 4254-4262.
4. Zhou, P., Tian, F., Lv, F., and Shang, Z. (2009) Geometric characteristics of hydrogen bonds involving sulfur atoms in proteins, *Proteins 76*, 151-163.
5. Pal, D., and Chakrabarti, P. (2001) Non-hydrogen bond interactions involving the methionine sulfur atom, *J. Biomol. Struct. Dyn. 19*, 115-128.
6. Reedijk, J. (2012) Plasticity in the copper-thioether bond: Manifestation in blue Cu proteins and in synthetic analogs, *J. Inorg. Biochem. 115*, 182-185.
7. Blackledge, M. J., Guerlesquin, F., and Marion, D. (1995) Novel methionine ligand position in cytochrome c553 and implications for sequence alignment, *Nat. Struct. Mol. Biol. 2*, 532-535.
8. Holliday, G. L., Mitchell, J. B. O., and Thornton, J. M. (2009) Understanding the functional roles of amino acid residues in enzyme catalysis, *J. Mol. Biol. 390*, 560-577.

9. Masgrau, L., Roujeinikova, A., Johannissen, L. O., Hothi, P., Basran, J., Ranaghan, K. E., Mulholland, A. J., Sutcliffe, M. J., Scrutton, N. S., and Leys, D. (2006) Atomic description of an enzyme reaction dominated by proton tunneling, *Science 312*, 237-241.

10. Henzler-Wildman, K. A., Thai, V., Lei, M., Ott, M., Wolf-Watz, M., Fenn, T., Pozharski, E., Wilson, M. A., Petsko, G. A., Karplus, M., Hubner, C. G., and Kern, D. (2007) Intrinsic motions along an enzymatic reaction trajectory, *Nature 450*, 838-844.

11. Lai, C.-L., Landgraf, K. E., Voth, G. A., and Falke, J. J. (2010) Membrane docking geometry and target lipid stoichiometry of membrane-bound PKCα C2 domain: a combined molecular dynamics and experimental study, *J. Mol. Biol. 402*, 301-310.

12. Hammes-Schiffer, S., and Benkovic, S. J. (2006) Relating Protein Motion to Catalysis, *Annu. Rev. Biochem. 75*, 519-541.

13. Vrtis, J. M., White, A. K., Metcalf, W. W., and van der Donk, W. A. (2001) Phosphite dehydrogenase: An unusual phosphoryl transfer reaction, *J. Am. Chem. Soc. 123*, 2672-2673.

14. Ranaghan, K. E., Hung, J. E., Bartlett, G. J., Mooibroek, T. J., Woolfson, D. N., van der Donk, W. A., and Mulholland, A. J. A catalytic role for methionine revealed by a combination of computation and experiments on phosphite dehydrogenase, *Submitted*.

15. Bartlett, G. J., Choudhary, A., Raines, R. T., and Woolfson, D. N. (2010) n ->pi* interactions in proteins, *Nat. Chem. Biol. 6*, 615-620.

16. Tatko, C. D., and Waters, M. L. (2004) Investigation of the nature of the methionine–π interaction in β-hairpin peptide model systems, *Protein Sci. 13*, 2515-2522.

17. Vrtis, J. M., White, A., Metcalf, W. W., and van der Donk, W. A. (2001) Phosphite dehydrogenase: an unusual phosphoryl transfer reaction, *J. Am. Chem. Soc. 123*, 2672-2673.

18. Munier, R., and Cohen, G. N. (1959) Incorporation of structural analogues of amino acid into the bacterial proteins during their synthesis in vivo., *Biochim. Biophys. Acta 31*, 378-391.

19. Cirino, P. C., Tang, Y., Takahashi, K., Tirrell, D. A., and Arnold, F. H. (2003) Global incorporation of norleucine in place of methionine in cytochrome P450 BM-3 heme domain increases peroxygenase activity, *Biotechnol. Bioeng. 83*, 729-734.

20. van Hest, J. C. M., Kiick, K. L., and Tirrell, D. A. (2000) Efficient incorporation of unsaturated methionine analogues into proteins in vivo, *J. Am. Chem. Soc. 122*, 1282-1288.

21. Shevchenko, A., Tomas, H., Havlis, J., Olsen, J. V., and Mann, M. (2007) In-gel digestion for mass spectrometric characterization of proteins and proteomes, *Nat. Prot. 1*, 2856-2860.

22. Gasteiger, E., Gattiker, A., C., H., Ivanyi, I., Appel, R. D., and Bairoch, A. (2003) ExPASy the proteomics server for in-depth protein knowledge and analysis, *Nucleic Acids Res. 31*, 3784-3788.

23. Jham, G. N., Vouros, P., Hanson, R. N., and Giese, R. W. (1981) Selenium-sulfur analogs. Mass spectrometric comparison of substituted selenazoles and thiazoles, *J. Heterocyclic Chem. 18*, 1335-1340.

24. Roblin, R. O., Lampen, J. O., English, J. P., Cole, Q. P., and Vaughan, J. R. (1945) Studies in Chemotherapy VIII. Methionine and purine antagonists and their relation to the sulfonamides., *J. Am. Chem. Soc. 67*, 290-294.

25. Gellman, S. H. (1991) On the role of methionine residues in the sequence-independent recognition of nonpolar protein surfaces, *Biochemistry 30*, 6633-6636.

26. Fogle, E. J., and van der Donk, W. A. (2007) Pre-steady-state studies of phosphite dehydrogenase-demonstrate that hydride transfer is fully rate limiting, *Biochemistry 46*, 13101-13108.

27. Relyea, H. A., Vrtis, J. M., Woodyer, R., Rimkus, S. A., and van der Donk, W. A. (2005) Inhibition and pH dependence of phosphite dehydrogenase, *Biochemistry 44*, 6640-6649.

28. Johannes, T. W., Woodyer, R., and Zhao, H. (2005) Directed evolution of a thermostable phosphite dehydrogenase for NAD(P)H regeneration, *Appl. Environ. Microbiol. 71*, 5728-5734.

29. Woodyer, R., van der Donk, W. A., and Zhao, H. M. (2003) Relaxing the nicotinamide cofactor specificity of phosphite dehydrogenase by rational design, *Biochemistry 42*, 11604-11614.

30. Ellis, K. J., and Morrison, J. F. (1982) Buffers of constant ionic strength for studying pH-dependent processes, *Methods Enzymol. 87*, 405-426.

CHAPTER 4: DIRECTED EVOLUTION OF PTDH TO ACCEPT THIOPHOSPHITE AS A SUBSTRATE

4.1 Introduction

Although significant effort has been put into determining the mechanism of PTDH catalysis (*1-5*), many details about the reaction remain unresolved, including the nature of the transition state of the reaction (i.e. concerted, associative, or dissociative) and the exact identity of the catalytic base. If PTDH were able to accept an alternative substrate, other details about the reaction mechanism could be revealed, particularly details about the stereochemistry of the PTDH reaction. If a chiral substrate (i.e. isotopically labeled thiophosphite) were to be successfully turned over by PTDH, the stereochemistry of the resulting chiral phosphate molecule could be determined (*6-10*), which could expose details about the active site environment (Figure 4.1). However, previous studies have shown that the wild-type PTDH has no activity on phosphite monoesters or thiophosphite (*2*), precluding investigation of the stereochemistry of the reaction.

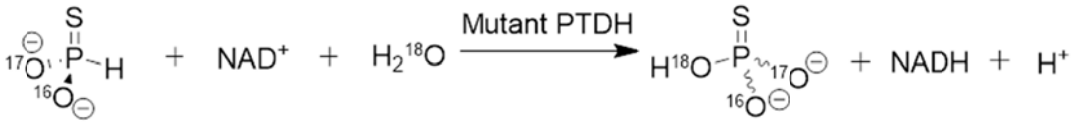

Figure 4.1. Reaction of PTDH with a chiral substrate.

In the literature, several examples of enzymes are reported that utilize phosphate as their natural substrate but that are also capable of accepting thiophosphates (*11*). Indeed, examination of the chirality of phosphoryl transfers by utilizing thiophosphate and phosphate esters is a

common probe of enzyme mechanism (*8-10*). With this in mind, attempts were made to mutate PTDH to accept thiophosphite as an alternative substrate through directed evolution.

PTDH has been successfully engineered multiple times in the past; directed mutation allowed the enzyme to accept the alternative substrate NADP in addition to NAD^+ (*12*), and PTDH has also been engineered to increase thermostability and activity through random mutagenesis (*13-15*). These previous studies have afforded 17X-PTDH (*13*), a highly thermostable PTDH variant that has reduced cofactor specificity towards NADP. Given the high resilience and activity of this mutant, 17X-PTDH was selected as the template for further mutation to accept thiophosphite as a substrate through directed evolution.

4.2 Results and Discussion

4.2.1 Growth of E. coli on Thiophosphate-containing Media

E. coli BW25141 was grown on MOPS minimal media plates with thiophosphate, phosphite or phosphate as the phosphorus source. The experiment was also performed with *E. coli* transformed with a plasmid encoding 17X-PTDH. As expected, growth was observed when phosphate was added, both with and without PTDH. In contrast, growth on phosphite was only seen when the bacteria were transformed with PTDH. Growth was also observed on thiophosphate under both conditions, although the phenotype of the colonies was slightly yellow. The magnitude of growth was comparable among all the plates. A negative control with no phosphorus source added yielded no visible colonies, as expected. This experiment showed that *E. coli* BW25141 can grow using thiophosphate as the sole phosphorus source. As thiophosphate would be the product of thiophosphite when reacted with PTDH, this experiment provided the impetus for further studies.

4.2.2 Synthesis of Thiophosphite

Dibenzyl thiophosphite was successfully synthesized in 73% yield by reacting commercially available dibenzyl phosphite with Lawesson's reagent (Scheme 4.1), in a procedure adapted from (*16*). The resulting compound was then deprotected by treatment with Na metal in NH_3 and the resulting product contained thiophosphite as the sole phosphorus-containing molecule, as determined by ^{31}P NMR spectroscopy (Figure 4.2). However, the dissolved metal reduction reaction resulted in 153% of the expected theoretical yield; this excess yield can likely be attributed to the presence of residual NaOH resulting from quenching of the sodium metal. Attempts to further purify thiophosphite by recrystallization were unsuccessful, and purification through ion exchange chromatography is currently being attempted. Attempts to deprotect dibenzyl thiophosphite via other methods that might result in fewer byproducts, including high pressure hydrogenation and treatment with BBr_3, were unsuccessful. Although the thiophosphite was not fully pure, further studies were attempted as thiophosphite was observed to be the sole contributor of phosphorus according to the ^{31}P NMR analysis.

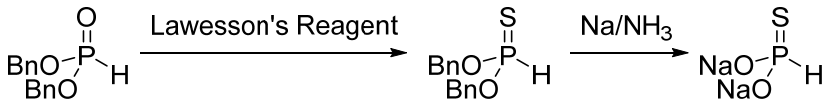

Scheme 4.1

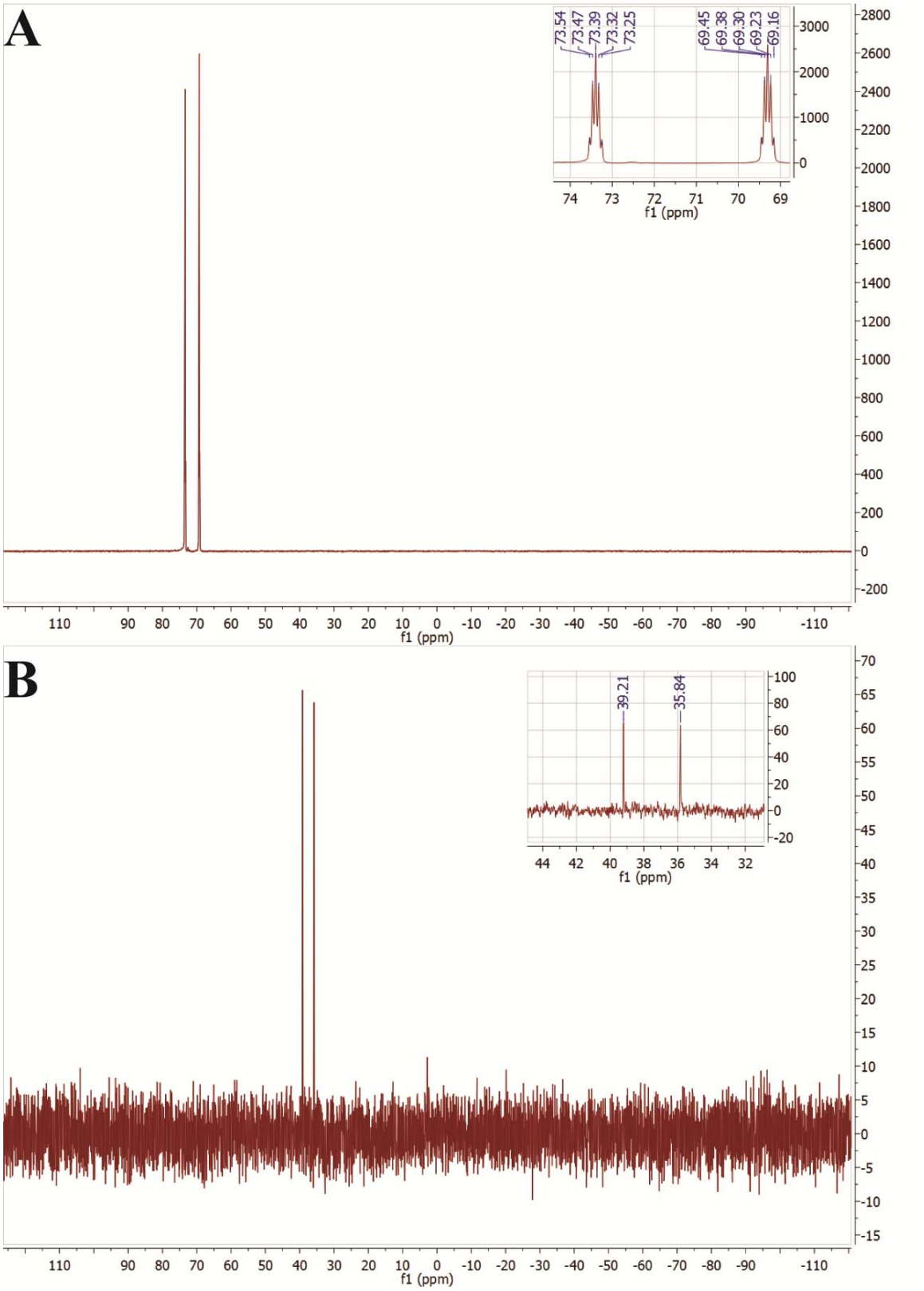

Figure 4.2. ^{31}P NMR analysis of purified (A) dibenzyl thiophosphite and (B) sodium thiophosphite.

4.2.3 Development and Screening of an Error-Prone Library of PTDH Mutants

A library of PTDH mutants was prepared using error-prone PCR. To increase the mutation rate, *Taq* polymerase was used with unbalanced concentrations of dNTPs (*17*) and the addition of $MnCl_2$ (*18*). $MnCl_2$ concentrations were varied between 0.15, 0.30, and 0.60 mM, with the goal of obtaining a library with differing numbers of total mutations per gene. Overall, a total library size of ~ 10^5 mutant PTDHs was successfully obtained.

However, when two individual mutants were sequenced from each experiment with different concentrations of mutagen, the number of mutations obtained was not consistent with what was expected (Table 4.1). Although it has been reported (*13*) that 0.2 mM $MnCl_2$ would introduce 1 to 2 amino acid mutations in a 1000 base pair (bp) plasmid, we observed a different mutation rate. However, these results may simply be a result of insufficient sample size. Alternatively, it is possible that combining $MnCl_2$ with the unbalanced pool of dNTPs increased the mutation rate to an unexpected degree.

Table 4.1. Mutation rate in the PTDH Library

$MnCl_2$ concentration	Number of Mutations
0.15 mM	7
0.15 mM	7
0.30 mM	2
0.30 mM	3
0.60 mM	9
0.60 mM	3

When the mutant PTDH library obtained at each mutagen concentration was screened on minimal media plates with thiophosphite as the sole phosphorus source, dozens of small colonies (>100) were observed. Interestingly, the size of these colonies was considerably smaller than the colonies that were observed for the positive controls with phosphate or phosphite. Unexpectedly, some growth by *E. coli* on the negative control plates that had no phosphorus source added was also observed. However, fewer of these colonies were observed, and their growth phenotype was somewhat smaller than that observed for the thiophosphite plates. In addition, these colonies did not appear to continue growing as incubation time was increased. It is likely that some small amount of phosphorus contamination was present in the media, as has been observed previously (*19*). Interestingly, similar small colonies were observed when *E. coli* containing the parent 17X-PTDH was grown on thiophosphite plates. This observation may be caused by residual phosphorus contamination, or alternatively 17X-PTDH may have slight activity on thiophosphite, though this is not supported by *in vitro* assays (see below) and it has previously been reported that wt-PTDH lacks activity on thiophosphite (*2*).

Several of the mutant colonies that were able to grow on thiophosphite were inoculated into liquid LB culture, grown, and plated again on thiophosphite plates to verify that they indeed had activity. Interestingly, these colonies were also able to grow on phosphite, suggesting that the mutant PTDHs may retain the ability to accept the original substrate. The plasmids of mutants that were able to successfully grow on thiophosphite were extracted, and the mutant PTDH genes were subcloned into pET15b for future analysis, which will be performed by Katarzyna Dubiel.

4.2.4 Test of In Vitro Activity of PTDH Against Thiophosphite

When 17X-PTDH was tested against the partially purified thiophosphite, an apparent increase in the absorbance at 340 nm (corresponding to NADH formation) was observed over time, with a very slow rate. While this appeared at first glance to indicate that 17X-PTDH accepts thiophosphite as a substrate, further analysis suggests that this is not the case. ^{31}P NMR analysis showed that no thiophosphate was being produced, and absorbance scans showed that a peak at 326 nm grew in over time upon mixing of thiophosphite, NAD^+, and PTDH, as opposed to 340 nm. This data suggests that the enzyme is not turning over when thiophosphite is used as the substrate; it is instead likely that some sort of adduct is forming between NAD^+ and thiophosphite. The mutant PTDHs have not yet been tested *in vitro*; it is possible that mutations may allow the enzyme to avoid this phenomenon and turn over thiophosphite.

4.3 Conclusions and Outlook

In this study, I successfully synthesized thiophosphite and created a mutant library of PTDHs through error-prone PCR. This library was then screened for the possibility that *E. coli* was endowed with the ability to grow on thiophosphite as the sole phosphorus source, and it appears that several PTDH mutants may have gained the ability to utilize thiophosphite based on their successful growth on this media. Several of these mutants have been cloned into expression vectors for future analysis by *in vitro* assay.

Although we appear to have successfully generated PTDH mutants that have activity with thiophosphite *in vivo*, further characterization will be needed. In particular, the mutant proteins will need to be purified and tested against thiophosphite *in vitro*. However, in order to perform accurate kinetics assays, the thiophosphite compound will need to be fully purified, or at least

further characterized to determine the exact amount of thiophosphite in the product. These efforts are currently underway and are being attempted by Katarzyna Dubiel. If directed evolution fails to yield a PTDH capable of utilizing thiophosphite, one possible alternative is to test other known PTDH orthologs (*5, 20, 21*) for activity. If mutation of PTDH to accept the alternate substrate is successful, it may be possible to analyze the stereochemistry of the PTDH reaction in future studies by using chiral substrates. Another set of experiments that would reveal important details about the PTDH reaction are heavy atom isotope effects (*22*). Determining the kinetic isotope effect of PTDH when reacted with ^{18}O-labeled phosphite would allow for further insight into the mechanism of phosphoryl transfer.

4.4 Materials and Methods

4.4.1 Materials and General Methods

This study was performed with the assistance of an undergraduate student, Katarzyna Dubiel (referred to as KD in references below). All chemicals were obtained from Sigma or Aldrich and used without further purification. *E. coli* BW25141 was donated by the Metcalf lab (*Δ(araD-araB)567*, *ΔlacZ4787*(::rrnB-3), *Δ(phoB-phoR)580*, λ^-, *galU95*, *ΔuidA3::pir*$^+$, *recA1*, *endA9*(del-ins)*::FRT*, *rph-1*, *Δ(rhaD-rhaB)568*, *hsdR514*). This strain contains a phoBR(-) phenotype to prevent the phosphate starvation response, *ΔaraBAD* to prevent arabinose metabolization, and the encodes the *pir* gene, which allows replication of plasmids with the R6K origin of replication (*15, 23*). pRW2 plasmid containing 17X-PTDH was donated by the Zhao lab. This plasmid contains 17X-PTDH under an arabinose promoter, and uses the R6K origin of replication, making it compatible with *E. coli* BW25141 (*12*). *In vitro* activity experiments were performed as detailed in section 2.4.6.

4.4.2 Synthesis of Thiophosphite

Dibenzyl phosphite (1.66 g) was dissolved in benzene, and Lawesson's reagent was added (1.2 equivalents, 1.53 g). The reaction was heated at 80 °C for 1 h until the Lawesson's reagent (yellow solid) was no longer observed. TLC analysis (CH_2Cl_2) indicated that the product was formed (R_f = 0.95). The reaction mixture was concentrated by rotary evaporator and purified by passing through a silica column (CH_2Cl_2). The resulting crude product was dissolved in toluene and the solvent was removed by evaporation (2x), and the residue was placed on a vacuum line overnight. ^{31}P NMR analysis (400 MHz, $CDCl_3$) showed peaks corresponding to dibenzyl thiophosphite δ71.3 ppm (d,p, J = 695, 12 MHz) (Figure 4.2A). The final yield was 73%. No dibenzyl phosphite starting material was observed in the ^{31}P NMR analysis (δ9.1 ppm, d,p J = 744, 11 MHz).

The deprotection setup was dried by flame under vacuum and purged with nitrogen. About 30 fold excess (~0.45 g) freshly cut Na metal was added to the flask, and NH_3 (10 mL) was condensed into the flask while in an acetone/dry ice bath. The vacuum-dried dibenzyl thiophosphite (0.16 g) was dissolved into dry diethyl ether (5 mL) and added to the reaction. The solution was allowed to stir for 10 min. The reaction was quenched with 20 mL of dry methanol and the flask purged with nitrogen gas to evaporate the NH_3. The sample was then extracted with chloroform and water (20 mL each), and the water layer was lyophilized to dryness. The product contained only peaks corresponding to the sodium salt of thiophosphite when analyzed by ^{31}P NMR spectroscopy (400 MHz, D_2O): δ37.5 (d, J = 582 Hz) (Figure 4.2B). Mass spectrometric analysis (ESI, negative mode) shows ions with expected mass of thiophosphite (m/z = 97). Yield = 153%; the product is likely contaminated by excess NaOH from the methanol quench of excess

sodium and subsequent hydrolysis with water. Attempts to further purify the compound using recrystallization have thus far been unsuccessful. (JEH-7-89, JEH-7-83, JEH-7-84, JEH-7-91).

4.4.3 Growth of E. coli on Thiophosphate

Plates were composed of autoclaved MOPS minimal media (*24*) (Teknova) with 1.6% highly pure Noble agar (Affymetrix), supplemented with 0.2% glucose and 1.0 mM arabinose (sterile filtered). Then each phosphorus source was added (1.0 mM), consisting of phosphite, thiophosphate, phosphate (positive control), or no phosphorus (negative control). Plates were streaked with *E. coli* BW25141, with or without the pRW2 plasmid containing the 17X-PTDH gene. The plates were also supplemented with kanamycin (50 μg/mL) for *E. coli* containing the pRW2 plasmid. Growth was determined after 48 h at 37 °C. (JEH-7-69).

4.4.4 Development of Error-prone PCR Library

The protocol to develop the error-prone PCR library was adapted from (*13, 15*). Error prone PCR was performed by using *Taq* polymerase (Invitrogen) in the presence of Mn^{2+} while varying dNTP concentrations to increase the error rate (*18*). The PTDH gene was amplified from pRW2 plasmid using the following primers: 5'–CGG GAA GAC GTA CGG GGT ATA CAT GT–3' (with *Pci*I restriction site underlined), and 5'–TTT TTG GAT GGA GGA ATT CAT ATG–3' (with *Nde*I restriction site underlined). The typical PCR reaction contained *Taq* buffer, 50 ng template plasmid, 0.5 μM each primer, 6 mM $MgCl_2$, 0.2 mM dATP and dGTP, 1.0 mM dTTP and dCTP, 5 units of *Taq*, and 0.15, 0.30, or 0.60 mM $MnCl_2$ in 50 μL reaction volume. The reaction was cycled 20 times through melting, annealing, and extension temperatures of 95, 55, and 72 °C, respectively. The reaction product was then sequentially digested with *Dpn*I,

*Nde*I, and *Pci*I. The product was run on agarose gel and verified to be the expected ~ 1000 bp, following which the DNA was extracted using a QIAquick Gel Extraction kit (Qiagen). The insert DNA was ligated overnight at 16 °C with *Nde*I and *Pci*I-digested pRW2 plasmid. The resulting ligation product was extracted by butanol (500 µL), dried, and resuspended into sterile water (10 µL). When the library DNA was transformed, a total library size of ~ 10^5 was obtained. (KD-01-57, KD-01-60).

4.4.5 Screening of the Thiophosphite Mutant Library

MOPS minimal media plates were prepared (see section 4.4.3) with 0.5 mg/mL partially purified thiophosphite (see section 4.4.2) as the sole phosphorus source. Aliquots of highly electrocompetent *E. coli* BW25141 were transformed with the error-prone library of PTDH according to standard transformation protocol. Following recovery in SOC media (New England Biolabs), the transformed library cells were sedimented and washed with MOPS minimal media with no phosphorus added (2x) to remove residual phosphorus. The cells were then plated and grown for ~ 48 h at 37 °C. Colonies that successfully grew on the thiophosphite media were used to inoculate a 5 mL LB culture, grown, and the DNA extracted using a Miniprep kit (Qiagen). The plasmid was then digested by *Bam*HI and *Nde*I and the digested insert was ligated into pET15b. (KD-01-73, KD-01-74).

4.5 References

1. Relyea, H. A., and van der Donk, W. A. (2005) Mechanism and applications of phosphite dehydrogenase, *Bioorg. Chem. 33*, 171-189.
2. Relyea, H. A., Vrtis, J. M., Woodyer, R., Rimkus, S. A., and van der Donk, W. A. (2005) Inhibition and pH dependence of phosphite dehydrogenase, *Biochemistry 44*, 6640-6649.
3. Woodyer, R., Wheatley, J., Relyea, H., Rimkus, S., and van der Donk, W. A. (2005) Site-directed mutagenesis of active site residues of phosphite dehydrogenase, *Biochemistry 44*, 4765-4774.
4. Fogle, E. J., and van der Donk, W. A. (2007) Pre-steady-state studies of phosphite dehydrogenase demonstrate that hydride transfer is fully rate limiting, *Biochemistry 46*, 13101-13108.
5. Hung, J. E., Fogle, E. J., Christman, H. D., Johannes, T. W., Zhao, H. M., Metcalf, W. W., and van der Donk, W. A. (2012) Investigation of the role of Arg301 identified in the X-ray structure of phosphite dehydrogenase, *Biochemistry 51*, 4254-4262.
6. Webb, M. R., and Trentham, D. R. (1980) Analysis of chiral inorganic [16O, 17O, 18O]thiophosphate and the stereochemistry of the 3-phosphoglycerate kinase reaction, *J. Biol. Chem. 255*, 1775-1778.
7. Arnold, J. R., and Lowe, G. (1986) Synthesis and stereochemical analysis of chiral inorganic [16O, 17O, 18O] thiophosphate, *J. Chem. Soc., Chem. Commun.*, 865-867.
8. Gerlt, J. A., Coderre, J. A., and Mehdi, S. (1983) Oxygen chiral phosphate esters, *Adv. Enzymol. Relat. Areas Mol. Biol. 55*, 291-380.
9. Knowles, J. R. (1980) Enzyme-catalyzed phosphoryl transfer reactions, *Annu. Rev. Biochem. 49*, 877-919.

10. Knowles, J. R. (1982) Phospho transfer enzymes: lessons from stereochemistry, *Fed. Proc. 41*, 2424-2431.

11. Chlebowski, J. F., and Coleman, J. E. (1974) Mechanisms of hydrolysis of O-phosphorothioates and inorganic thiophosphate by Escherichia coli alkaline phosphatase, *J. Biol. Chem. 249*, 7192-7202.

12. Woodyer, R., van der Donk, W. A., and Zhao, H. (2003) Relaxing the nicotinamide cofactor specificity of phosphite dehydrogenase by rational design, *Biochemistry 42*, 11604-11614.

13. Johannes, T. W., Woodyer, R., and Zhao, H. (2005) Directed evolution of a thermostable phosphite dehydrogenase for NAD(P)H regeneration, *Appl. Environ. Microbiol. 71*, 5728-5734.

14. Johannes, T. W., Woodyer, R., and Zhao, H. (2007) Efficient regeneration of NADPH using an engineered phosphite dehydrogenase, *Biotechnol. Bioeng. 96*, 18-26.

15. Woodyer, R., van der Donk, W. A., and Zhao, H. (2006) Optimizing a biocatalyst for improved NAD(P)H regeneration: Directed evolution of phosphite dehydrogenase, *Comb. Chem. High Throughput Screen. 9*, 237-245.

16. Piettre, S. R., and Raboisson, P. (1996) Easy and general access to α,α-difluoromethylene phosphonothioic acids. A new class of compounds, *Tetrahedron Lett. 37*, 2229-2232.

17. Cirino, P., Mayer, K., and Umeno, D. (2003) Generating mutant libraries using error-prone PCR, In *Directed Evolution Library Creation* (Arnold, F., and Georgiou, G., Eds.), pp 3-9, Humana Press.

18. Fromant, M., Blanquet, S., and Plateau, P. (1995) Direct random mutagenesis of gene-sized DNA fragments using polymerase chain reaction, *Anal. Biochem. 224*, 347-353.

19. Metcalf, W. W., and Wolfe, R. S. (1998) Molecular genetic analysis of phosphite and hypophosphite oxidation by Pseudomonas stutzeri WM88, *J. Bacteriol. 180*, 5547-5558.

20. Liu, D.-F., Ding, H.-T., Du, Y.-Q., Zhao, Y.-H., and Jia, X.-M. (2012) Cloning, expression, and characterization of a wide-pH-range stable phosphite dehydrogenase from *Pseudomonas* sp. K in *Escherichia coli*, *Appl. Biochem. Biotech. 166*, 1301-1313.

21. Hirota, R., Yamane, S., Fujibuchi, T., Motomura, K., Ishida, T., Ikeda, T., and Kuroda, A. (2012) Isolation and characterization of a soluble and thermostable phosphite dehydrogenase from Ralstonia sp. strain 4506, *J. Biosci. Bioeng. 113*, 445-450.

22. Hengge, A. C., and Cleland, W. W. (1991) Phosphoryl-transfer reactions of phosphodiesters: characterization of transition states by heavy-atom isotope effects, *J. Am. Chem. Soc. 113*, 5835-5841.

23. Wanner, B. L., and Gottesman, M. (1983) Overlapping and separate controls on the phosphate regulon in Escherichia coli K12, *J. Mol. Biol. 166*, 283-308.

24. Neidhardt, F. C., Bloch, P. L., and Smith, D. F. (1974) Culture medium for Enterobacteria, *J. Bacteriol. 119*, 736-747.

APPENDIX A: INVESTIGATION INTO POSSIBLE COVALENT CATALYSIS BY PTDH

A.1 Introduction

Protein phosphorylation events are very common in all domains of life. Serine/threonine and tyrosine kinases are well characterized and are commonly used in signal transduction pathways (*1*). Another common post-translational modification that is frequently overlooked is phosphorylation of histidine residues, which can occur at both the Nε2 and Nδ1 nitrogen sites (Figure A.1) (*2*). It is estimated that this type of phosphorylation may make up as much as 6% of total phosphorylation in eukaryotes (*3*), and that it is as much as 10- to 100-fold more abundant than tyrosine phosphorylation (*4*). They are also common in two-component signaling pathways in prokaryotic systems, which consist of a histidine kinase and a regulator protein which receives the phosphate. This family of proteins encodes ~1% of encoded proteins in eubacteria (*5*). A number of crystal structures of enzymes containing these phosphorylated histidines have been published (*6-8*), and the phosphohistidine adduct is observed in the X-ray structures. However, this adduct is highly acid labile, and as such mass spectrometric (MS) analysis, the standard tool in proteomic detection, is difficult (*2, 9, 10*). Recently, however, methods to detect the presence of phosphohistidine through mass spectrometric (*9, 11*) and NMR (*12*) methods have been developed.

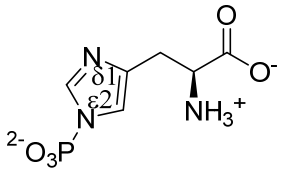

Figure A.1. Histidine phosphorylated at the Nε2 nitrogen, the likely modification site in PTDH, if the enzyme uses a covalent modification

An alternative mechanism in PTDH catalysis to the direct nucleophilic attack of water or hydroxide onto phosphite (regardless of whether this occurs through a concerted, associative, or dissociative mechanism) is a covalent catalysis mechanism. In such a case, a residue in the PTDH active site would covalently attack the phosphite substrate, yielding a covalent phosphohistidine intermediate following hydride transfer to NAD^+ (Figure A.2). This intermediate would then be hydrolyzed, with the enzyme utilizing another residue to act as the base to deprotonate the water nucleophile, yielding the free enzyme and final products. In the crystal structure, His292 could potentially act in this fashion, as the ε2 nitrogen on the imidazole ring is 3.7 Å from the sulfur of sulfite in the ternary complex (see Figure 2.2). In an attempt to determine if a covalent catalysis mechanism is being utilized by PTDH, the presence of a phosphohistidine intermediate was investigated using mass spectrometric analysis.

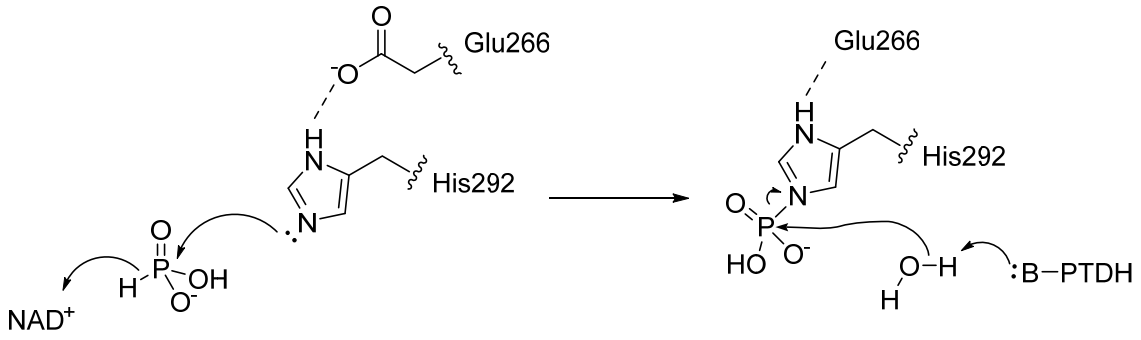

Figure A.2. A covalent catalysis mechanism for PTDH, with His292 as the nucleophile.

A.2 Results and Discussion

A.2.1 Investigating Formation of a Phosphohistidine Covalent Adduct

The possibility of a covalent catalysis mechanism was investigated by probing for a phosphohistidine intermediate. Although the phosphohistidine adduct is highly acid labile, methods have been developed to detect its presence through MS by iodinating all the unprotected

histidines, leaving only the phosphorylated histidine unmodified (*9*). Following *in vitro* reaction of PTDH with saturating amounts of NAD^+ and phosphite, the enzyme was denatured by exposure to guanidinium hydrochloride while excess substrate was still present (i.e. the enzyme remained under k_{cat} conditions). The mixture was then digested by trypsin and iodinated to covalently modify accessible tyrosine and histidine residues. If present, the phosphohistidine intermediate would protect histidine from iodination by occupying its lone pair electrons, and acidification prior to mass spectrometric analysis would lead to an unmodified residue, as the adduct is acid labile (*9*). For both 17X-PTDH and R301A-PTDH, however, the MS of the samples with and without phosphite added (a negative control incapable of forming the phosphohistidine adduct) were almost identical by MALDI-MS (Figure A.3 shows the data for 17X-PTDH, the spectra for the R301A mutant are similar) The expected tryptic peptide 271–ADRPQQIDPALLA**H**PNTLFTP**H**IGSAVR–298 has two sites capable of being iodinated, both histidines as indicated in bold. The expected mass for the singly- and doubly-iodinated species are M+H = 3161 and 3287. Very low intensity ions for single iodination are observed in both the experimental and negative controls, which likely correspond to incomplete iodination unrelated to the presence of the adduct. MS spectra of the reaction mixture prior to iodination (where the phosphohistidine adduct would be the expected modification at M+H = 3116, umodified M+H = 3035) also failed to yield ions that would indicate the presence of a phosphohistidine adduct.

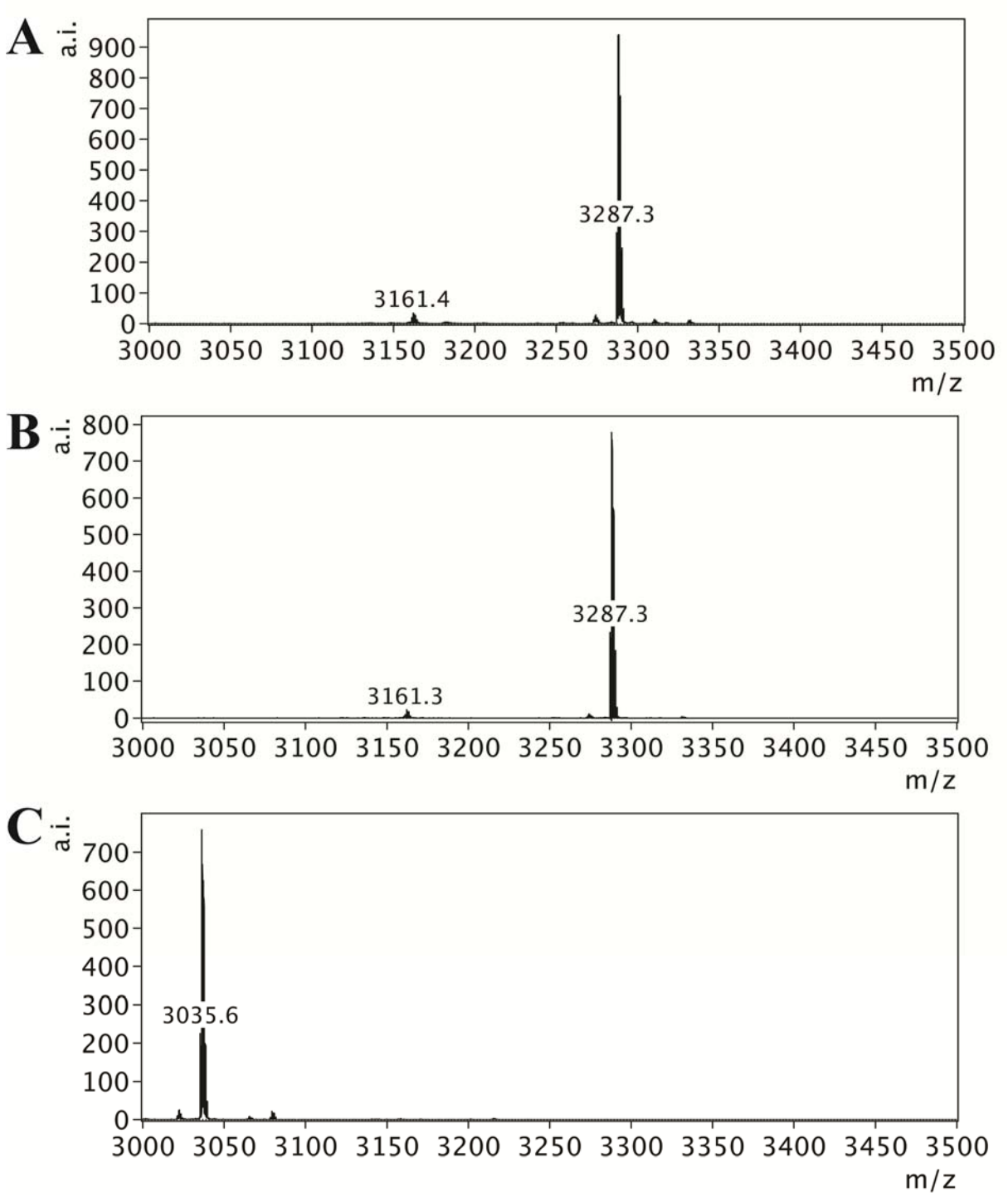

Figure A.3. MALDI-MS spectra of the tryptic fragment of 17X-PTDH containing His292. (A) 17X-PTDH with phosphite, (B) negative control of 17X-PTDH without phosphite, and (C) reaction mixture without iodination.

In the case of covalent catalysis by His292, Arg301 would be the most likely candidate for the catalytic base to deprotonate water for attack on the phosphoryl group. Thus, removal of the arginine functional group, as in R301A, would likely lead to slower turnover of the phosphohistidine adduct and therefore a greater likelihood to observe the intermediate. However, for both 17X-PTDH and R301A, the trypsin-digested peptide fragments containing His292 were observed to be predominantly iodinated and identical to the negative control reactions performed without phosphite, suggesting that phosphohistidine was not present to protect the residue from iodination. This data suggests that a covalent catalysis mechanism does not occur, although it cannot be ruled out that the phosphohistidine intermediate was formed in amounts too small to be accurately detected by mass spectrometry and differentiated from the negative control using this method.

A.3 Conclusions

Overall, the mass spectrometry data shows that phosphohistidine not was present in the PTDH sample, suggesting that a covalent catalysis mechanism using His292 as the nucleophile is unlikely. Although the enzyme was fully saturated in substrate and acting under k_{cat} conditions and therefore should have had the maximum possible occupancy in the intermediate state, it remains possible that the catalytic amount of intermediate may be below the detection limit of this method. As such, the possibility that PTDH utilizes a covalent catalysis mechanism cannot be completely ruled out.

At present, no direct experimental evidence is available to suggest that PTDH utilizes a covalent catalysis mechanism. PTDH has no sequence homology with known histidine kinases, and available data suggests that His292 acts as a base rather than a catalytic nucleophile (see Chapter 2). Furthermore, since Arg301 appears to act in electrostatic catalysis as a positively

charged residue, no other obvious conserved residues in the active site could act as the catalytic base (see Figure 2.2). Therefore, it is more likely that His292 acts as the catalytic base in the reaction, as opposed to the PTDH reaction occurring through covalent catalysis.

A.4 Materials and Methods

A.4.1 Investigation of the Phosphohistidine Adduct

The method was adapted from (*9*). The PTDH reaction was allowed to proceed for 2 min under saturating conditions of both substrates at room temperature to allow for potential phosphohistidine formation (Conditions: 100 mM Tris pH 7.3, 4 mM NAD, 100 mM phosphite, 7.3 nmol 17X-PTDH or R301A-PTDH in 200 μL). The reaction was quenched by addition of 2 mL denaturing solution (12 M guanidinium hydrochloride, 50 mM Tris pH 8.5, 10 mM DTT) and incubated at 55 °C for 1 h. Then 3 equivalents of iodoacetamide were added (175 nmol, to label the 8 Cys residues in PTDH) and the reaction was incubated in the dark at 55 °C for 1 h. The mixture was then diluted to 10 mL with water to dilute the denaturant, and trypsin was added (1:50 ratio of protease to protein). The reaction mixture was incubated at 37 °C overnight. The sample was then desalted with a C4 solid phase extraction column (Vydac) using the supplied protocol, with the exception that trifluoroacetic acid (TFA) concentration was reduced to 0.01% to slow phosphohistidine decomposition (*4*). The sample was immediately lyophilized (overnight) to remove TFA. The samples were then reconstituted to 50 mM Tris pH 9.2, 2 mM NaI (1 mL).

A fresh I_2 solution was prepared by addition of Chloramine T solution (330 nmol, a 2.5 stoichiometric excess of the iodable His and Tyr residues on PTDH, 1 mL) to the NaI solution (1320 nmol, 4-fold excess to Chloramine T, 2 mL) followed by mixing for 10 min. The resulting

I_2 solution was added to the digested PTDH solution in the dark (6 aliquots of 0.5 mL, added every 10 min). The reaction was allowed to proceed for an extra 30 min and was mixed with 1.5 equivalents $Na_2S_2O_5$ to quench the excess I_2. The reaction mixture was desalted by C4 SPE column and then analyzed by MALDI mass spectrometry (Bruker Ultraflex). (JEH-6-15)

A.5 References

1. Pawson, T., and Scott, J. D. (2005) Protein phosphorylation in signaling – 50 years and counting, *Trends Biochem. Sci. 30*, 286-290.
2. Puttick, J., Baker, E. N., and Delbaere, L. T. J. (2008) Histidine phosphorylation in biological systems, *Biochim. Biophys. Acta 1784*, 100-105.
3. Matthews, H. R. (1995) Protein kinases and phosphatases that act on histidine, lysine, or arginine residues in eukaryotic proteins: A possible regulator of the mitogen-activated protein kinase cascade, *Pharmacol. Ther. 67*, 323-350.
4. Klumpp, S., and Krieglstein, J. (2002) Phosphorylation and dephosphorylation of histidine residues in proteins, *Eur. J. Biochem. 269*, 1067-1071.
5. West, A. H., and Stock, A. M. (2001) Histidine kinases and response regulator proteins in two-component signaling systems, *Trends Biochem. Sci. 26*, 369-376.
6. Oberholzer, A. E., Schneider, P., Siebold, C., Baumann, U., and Erni, B. (2009) Crystal structure of Enzyme I of the phosphoenolpyruvate sugar phosphotransferase system in the dephosphorylated state, *J. Biol. Chem. 284*, 33169-33176.
7. Bond, C. S., White, M. F., and Hunter, W. N. (2001) High resolution structure of the phosphohistidine-activated form of Escherichia coli cofactor-dependent phosphoglycerate mutase, *J. Biol. Chem. 276*, 3247-3253.

8. Lott, J. S., Paget, B., Johnston, J. M., Delbaere, L. T. J., Sigrell-Simon, J. A., Banfield, M. J., and Baker, E. N. (2006) The Structure of an Ancient Conserved Domain Establishes a Structural Basis for Stable Histidine Phosphorylation and Identifies a New Family of Adenosine-specific Kinases, *J. Biol. Chem. 281*, 22131-22141.

9. Sun, Q., and Julian, R. R. (2011) Probing sites of histidine phosphorylation with iodination and tandem mass spectrometry, *Rapid Commun. Mass Spectrom. 25*, 2240-2246.

10. Besant, P., and Attwood, P. (2009) Detection and analysis of protein histidine phosphorylation, *Mol Cell Biochem 329*, 93-106.

11. Kleinnijenhuis, A. J., Kjeldsen, F., Kallipolitis, B., Haselmann, K. F., and Jensen, O. N. (2007) Analysis of histidine phosphorylation using tandem MS and ion−electron reactions, *Anal. Chem. 79*, 7450-7456.

12. Himmel, S., Wolff, S., Becker, S., Lee, D., and Griesinger, C. (2010) Detection and Identification of Protein-Phosphorylation Sites in Histidines through HNP Correlation Patterns, *Angew. Chem. Int. Ed. 49*, 8971-8974.